Republic of Iraq

Ministry of Higher Education and Scientific Research

University of Babylon

College of Materials Engineering

Department of Metallurgical Engineering

Influence of Tungsten Carbide Powder Recovered by Electrochemical Process on Coating Performance for Tribological Applications

A Dissertation

Submitted to the Department of Metallurgical Engineering/ College of Materials Engineering/ University of Babylon in Partial Fulfillment of the Requirements for the Degree Doctor of Philosophy in Materials Engineering/ Metallurgy

By

Lubna Muneer Hadi Qaddoori

(B.SC. Materials Engineering 2012)

(M.Sc Metallurgical Engineering 2015)

Supervised by

Prof. Dr. Haydar Al-Ethari

2023 A.D 1444A.H

بِسْمِ اللَّهِ الرَّحْمَنِ الرَّحِيمِ

۞ وَيَسئلُونَكَ عَنِ الرُّوحِ قُلِ الرُّوحُ مِنْ أَمْرِ رَبِّي وَمَا أُوتِيتُم مِّن الْعِلْمِ إِلاَّ قَلِيلاً ۞

صدق الله العليّ العظيم

{سورة الاسراء / آية 58}

Dedication

To my father, my first teacher in life. I learned great things from you, Thanks for being there for us.

To my beloved mother, my sweety, my inspiration, who will always take my hand and never leave it. Thank you for being my mother, for being there for me.

To those who did not skimp on helping me...

My husband Mohammed

To my brothers (Haider, Ali, Karar), you are my source of support, happiness and encouragement. My world is full of smiles whenever you are with me.

Lubna

2023

Acknowledgments

Great thanks to Almighty Allah, my Creator and inspirational for being merciful to me and gave me health, strength and protection. I cannot express enough thanks and gratitude to my supervisor, Prof. Dr. Haydar A.H. Al-Ethari who support, helped, encouraged, and gave me all the acknowledgement I need to finish my research. It was a great privilege and honor to work and study under his guidance

Iam extremly grateful to my family and my husband for their love, prayers, caring and continuing support made this work possible. I am also extremely thankful to my friends for their kind support

Lubna

2023

Supervisor Certificate

We certify that this thesis entitled ***"Recovery of Metallic Powders From Carbide Cutting Insert by Electrochemical Process"*** was Prepared by (***Lubna Muneer Taj-Aldeen***) had been carried out under our supervision at the University of Babylon / College of Materials Engineering/ Department of Metallurgical Engineering in partial fulfillment of the requirements for the degree of doctor of Philosophy in Material's Engineering/Metallurgical Engineering.

Signature :

Prof. Dr. Haydar Al-Ethari

(supervisor)

Date : / / 2023

Abstract

Hard metal industries have extensively used tungsten carbide to manufacture cutting inserts and high-wear resistant parts. When these parts and pieces of tools are scrapped, they should be gathered and recycled.

In this study, carbide cutting inserts type P10 were recycled to obtain tungsten carbide powder. The obtained powder was deposited as coating layers on the surface of the stainless steel to enhance its wear resistance. The recycling process was performed in three steps, firstly by the use of an electrochemical process, a pure tungstic acid (H_2WO_4) was obtained. The effect of four variables was studied in this process. These variables are the type of the cathode (graphite and aluminium plate), the concentration of the electrolyte (nitric acid), the current density, and the cell temperature. The optimum values of these variables were obtained using Grey Relational Analysis based on the Taguchi method by using mintab17 software. These values were a current density of 4000A/m^2; a solution concentration of 1.8M, a cell temperature equals 70°C and an Al-cathode. According to this optimum condition, the responses resulted were a power consumption of 3.702 kw.h/kg, and Weight loss/hour of 1.350g/hr. of a tungstic acid (H_2WO_4) with a particle size of 11.11μm.The acid was verified by using XRD and SEM. Secondly, the tungstic acid powder was converted to tungsten oxide powder (WO_3) with a particle size of 18.38μm by calcination at 800°C. Then, at the third step, carburization process was involved to obtain WC powder by reduction of WO_3 using its mixture with graphite mixtures according to (1:5) mole in vacuum furnace with argon at different temperatures (900, 1100 and 1200°C) with different times (45, 90 and 130 minutes).To produce pure quantities WC. The best temperature and time were 1100°C and 135min respectively.

In this work, thermal spraying process has been embraced to deposit a mixture of the recycled tungsten carbide with a known percentage of pure cobalt on the surface of stainless steel (SS316). Three weight percentages of cobalt (8, 12, and 16%) were considered, for each of which three velocities of the spraying (300,400 and 500 m/min) were employed. Characteristics and tribological behavior of the coating layer were investigated. X-ray diffraction revealed significant amount of WC, but did not reveal substantial amounts of cobalt containing subcarbides glassy Co-W-C phases, i.e., Co_6W_6C. The pattern for the coatings also indicates minimum decarburisation takes place in coating process.

Thermal spray coating, exceptionally flame thermal spray, improves the hardness and wear of metal. Coating parameters play a vital role in the properties of the coating. The quality of coating can be increased by selecting appropriate coating parameters. The most significant parameter is velocity of particles that directly influence on hardness, roughness and wear resistance of the coating. As a result of spraying at (400m/min) and incorporating a weight percentage of cobalt equals (8, 12 and 16%) the coating had a good homogeneous structure and no oxidation layer was formed. These three layers coating have high hardness (1480,1290 and 1085 Kg/mm^2 HV) respectively, surface roughness (2, 1.9 and 1.8 μm) respectively, and have lower wear rate. The specific wear rates of the coatings gradually decrease with the increase in the coating hardness.

Table of Contents

List of Tables

List of Figures

List of Abbreviations

Symbol	Meaning
Adj MS	*Adjust Mean Square*
Adj SS	*Adjust Sum Square*
ANOVA	*Analysis of Variance*
APS	*Atmospheric Plasma Spray*

Symbol	Meaning
APT	*Ammonium Paratungstate*
DOE	*Design of Experiments*
EDS	*Energy Dispersive Spectroscopy*
G	*Gibbs Free Energy*
GRA	*Grey Relational Analysis*
GRC	*Grey Relational Coefficient*
GRG	*Grey Relational Grades*
HVAF	*High-Velocity Air Fuel*
HVOF	*High Velocity Oxy- Fuel*
H_2WO_4	*Tungstic Acid*
P	*Power Consumption*
Seq SS	*Sum of Squares*
TGA	*Thermogravimetry Analysis (TGA)*
TM	*Taguchi method*
WC	*Tungsten Carbide*
Wt. /h	*Weight loss/Hour*
XRD	*X-Ray Diffraction*

List of Symbols

Symbol	Meaning	Units
A	*Area*	mm^2
I	*Applied Current*	*A*
t	*Time*	*min*
T	*Temperature*	℃
V_{cell}	*Cell Voltage*	*V*
W	*Weight*	*g*
$W_{act.}$	*Actual Weight of the Deposit*	*g*

CHAPTER ONE

INTRODUCTION

Chapter One

Introduction

1.1 General Introduction

Cemented carbides, often known as hard metals, are a form of composite materials made of hard carbide particles bonded by a metallic binder like cobalt Co, nickel Ni, nickel-chromium-cobalt Ni-Cr-Co, or, nickel-chromium Ni-Cr. Carbide particles include tungsten carbide WC, tantalum carbide (TaC), titanium carbide (TiC), vanadium carbide (VC), molybdenum carbide (Mo_2C) and other very hard carbides. Due to their many advantageous characteristics, including their high melting point, high mechanical strength, electrical and thermal conductivity, low thermal expansion and corrosion resistance. WC-based cemented carbides are commonly used for tools in the industrial production [1]. Such carbides have a wide range of applications especially as cutting tools for milling, turning and drilling processes, and as dies for drawing and extrusion processes [2].

During the production of the parts containing WC in their compositions or at the end of their useful lives, many forms of tungsten scrap are produced. Three different forms of scrap are produced throughout the production process; powder scrap from compaction; faulty solid product and machining scrap. Hard scrap and soft scrap are the two categories of WC scrap that are generally sold on the market. Hard scrap is typically created from used tools, such as cutting bits made of the hard tungsten carbide [3].

One of the major concerns with the technology is recycling tungsten carbide from its scrap. Recycling helps the environment by protecting it from pollution, preserving natural resources, consuming less energy and lowers costs [4].

There are a number of causes that have led to an increase in tungsten carbide recycling, including the fact that tungsten natural resources are quickly running out and that more cemented carbide is being scrapped from various manufacturing fields on a constant basis. It is important to recycle tungsten resources since doing so may help reduce the amount of tungsten-containing waste that is generated[5].

To recycle hard and soft scraps of hard metals, a variety of techniques have been developed, including zinc process, chemical method, coldstream process, melting metallurgy, bloating/crushing, hydrometallurgical processes and electrochemical/hydrothermal [6].

The electrochemical method, which is one-step process that uses little energy, has been identified as an interesting way among the various methods for processing WC tool bit scraps that are accessible in the literature [7]. There are several methods to producing WC powder, almost all of them based on either carbothermal reduction of tungsten oxide or direct carburization of tungsten[8].

Mechanical component can be subjected to corrosion, wear, oxidation, abrasion, adhesion and radiation. These surface phenomena cause a great damage to the parts. The extent of deformation and wear depends on the surrounding media. Wear, friction and corrosion are surface phenomena and cause great damage to the parts. All industries including automobile, aerospace and biomedical receive the highest impact of these phenomena. The primary requirement of surface engineering is modification of surface properties through various processes, the essential at which is the surface coating [9].

Stainless steel type (316) having good mechanical and chemical properties and being easy to fabricate, has a wide application in chemical, mining, steam generating plant as piping, superheater tubing, petroleum and nuclear industry. In all these applications, this steel is subjected to serious problems of wear. So, there is a need to high performance of coating. This can be obtained using suitable coating materials and coating method that are capable of fulfilling these. Tungsten carbide one of the materials that are used in this field[10].

Thermal spray is a coating process by which the coating material in metal or non-metal form is deposited on the surface of a formulated substrate in a molten or semi-molten state. The material to be coated can be deposited in various states, particularly wire, powders, rods, suspension, or molten form. The coating material heated during combustion or plasma generation converts to a molten or semi-molten state and is propelled by the high velocity and high-temperature gas stream to the substrate. Figure (1.1) shows the thermal spray coating process [11].

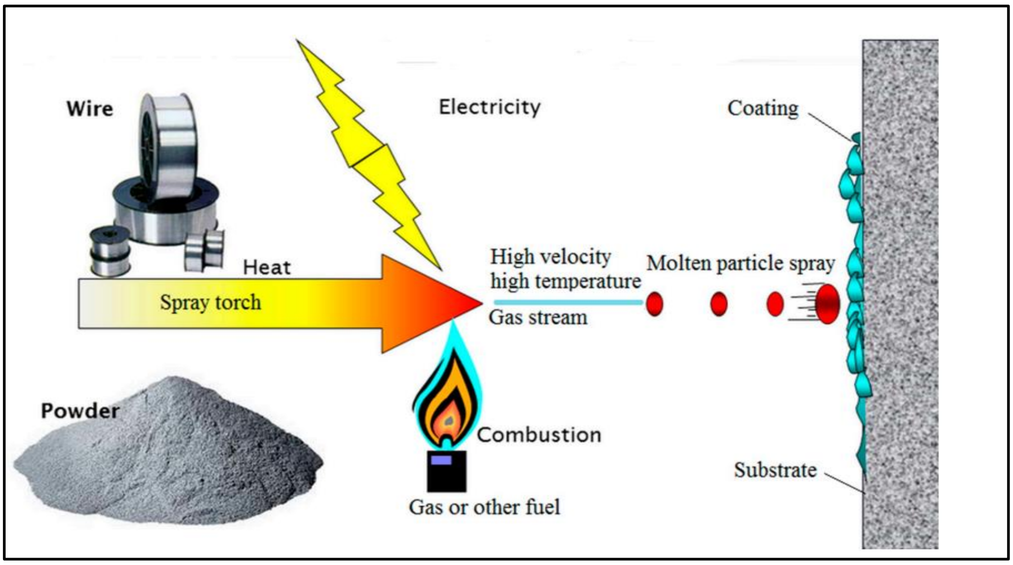

Figure (1.1) Thermal Spray Process[11].

The coating particles flatten and solidify quickly to develop a splat. The physical characteristics of the deposited coatings is depend upon the shape of the splat. However, the shape of splat is based on many factors such as velocity, topology, size, thermo-physical characteristics of the powder particles and physical characteristics of base material (substrate). Although, in all the thermal spray coating, the successive impingement of coating material particles forms splats layer-by layer to develop a laminar structure [12].

Flame spraying is a simple and inexpensive form of thermal spraying. It uses less heat and velocities than other technologies, resulting in porous coatings with less density and adhesive strength. Flame spray feedstock may be wire or powder, but the behaviour in the flame spray cannon is the same for both. All metals that melt under a flame's temperature of 3000-4000^{O}C may be sprayed with flame spray[13].

The velocity of particles sprayed on the surface determines coating porosity and binding strength. There are two stages to a thermally distributed cermet coating. One phase is nickel chrome, which provides exceptional corrosion resistance, while the other is chrome carbide, which protects against wear, hence in applications where parts are exposed to corrosion[14].

The WC-Co coating combines the ceramical abrasion resistance and high temperature resistance with the metallic ductility. Because of its superior mix of hardness and toughness, WC-Co coatings are employed for a variety of applications where great resistance to abrasion, sliding, fretting, and erosion is needed, turbine blades in hydroelectric plants, airplane, diesel engines, landing gear, and paper mill rollers are all good examples [15, 16].

1.2 Objectives of the Work

This work is focused to recover the tungsten carbide from tungsten carbide scrap. Due to the great need for tungsten carbide in industry made tungsten carbide a strategic commodity of worldwide importance. the sustainability of tungsten carbide over the long term is of prime concern to all users. It is essential, therefore, that as the concept of sustainable development gains ever-increasing importance in the world's future, more efficient and economical recovery and re-use of the world's finite resources of tungsten carbide be achieved. The recycled powder can thus totally compete with conventional powders, opening avenues for the recycling of cemented carbide tools. Optimum condition for the oxidation and reduction of (WC-Co) scrap was investigated for a low-cost and environmentally friendly recycling process. The recycled WC was used as a coating layer on the stainless steel 316 to enhance its wear resistance.

CHAPTER TWO

THEORETICAL PART& LITERATURE REVIEW

Chapter Two

Theoretical Part and Literature Review

2.1 Introduction

This chapter is divided into four sections, the first deals with composite tungsten carbide cutting tool and its properties, chemical composition, sources and recycling methods of tungsten carbide (WC) scrap and focused on electrochemical method for the recovery of WC. The second section discusses optimization of recovery conditions by the electrochemical method. The third section deals with coating, type of thermal coating suitable for tungsten carbide. The forth section contains a literature review from several approaches for recovery of (WC) and its use as a coating material.

2.2 Cemented Carbide

Cemented carbides are formed from one or more carbide compounds that have been joined together in a metallic matrix. The most often used cemented carbides are constructed with chromium carbide (Cr_3C_2), titanium carbide (TiC), and tungsten carbide (WC). Other compounds, less often used, include tantalum carbide (TaC). Nickel and cobalt are the main metallic binders [17]. Tungsten carbide, a very hard ceramic material, is utilized as the primary component in cemented carbides. Because Co has good mechanical qualities and enables excellent wetting on the tungsten carbide grains, it is the most suitable binder [18].

Cemented carbides using tungsten carbide (WC) as main raw materials with high hardness and excellent wear resistance are widely used in drill, mold, needle and cutting tool. Due to the high bonding strength and fine microstructure between ultrafine WC particles and metal binder phase, ultrafine-grain cemented carbide combines the characteristics of ceramics and metal at the same time, which has high toughness, good strength and excellent hardness [19].

Possibly the widest utilised cutting tool materials are the cemented carbide family of tooling, of which the group derived from tungsten carbide is most readily employed. In Figure (2.1), a comparison of some of the tooling materials is highlighted, here, fracture toughness is plotted against hardness to indicate the range of influence of each tool material[20].

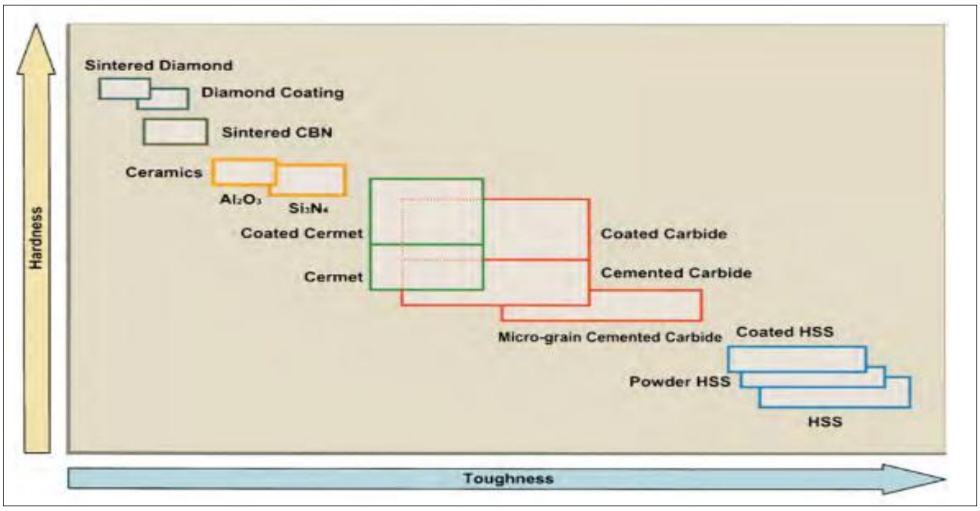

Figure (2.1): Cutting Tool Materials Comparison[20].

2.3 Properties and Applications of Tungsten Carbide

Due to its unique properties, tungsten carbide is commonly utilized in industry. The WC particle size, WC size distribution, and cobalt concentration all play a significant role in determining the mechanical properties. For instance, a smaller grain size increases hardness, while a greater amount of binder increases toughness [21].

There are only two phases in the basic form, prismatic face-centered cubic (fcc) Co with some W and C in solid solution (black) and WC grains (grey) , as depicted in Figure (2.2) [22].

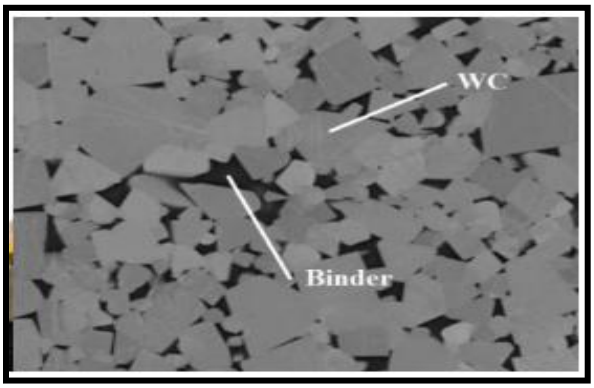

Figure (2.2): WC-Co Cemented Carbides[22].

A hard metal's strength is determined by the properties of its softer metallic binder, hard phases, carbide-carbide contacts, and carbide-binder interfaces. Table (2.1) provides a comparisons' of some hard materials' typical properties [23].

Table (2.1): Important Properties of Hard Materials [23].

Properties	High-speed steel	WC-Co cemented carbides	TiC-based cermets
Density, g/cm^3	8.0-9.0	9.0-15.0	5.0-9.0
Vickers hardness, HV	750-800	800-1900	1500-2200
Transverse rupture strength, N/mm^2	3000-4000	1000-3000	900-1800
Hot transverse rupture strength (1000 °C), N/mm^2	500	900-1500	600-1500
Compressive strength, N/mm^2	3500-4000	4000-7000	3000-5000
Modulus of elasticity, kN/mm^2	210	400-680	300-450
Thermal expansion coefficient, $10^{-6}/K^{-1}$	12	5.0-7.0	6.0-8.0

The excellent mechanical properties of WC-Co make it highly useful in the production of cutting tools [24]. Cemented carbides capture one half of the market, followed by high speed steel. The two important ingredients of the carbide tools mentioned above namely tungsten and cobalt-were earlier identified (in 2011) as being among the list of the 14 critical raw materials. Figure (2.3) shows the distribution of the type cutting material [25].

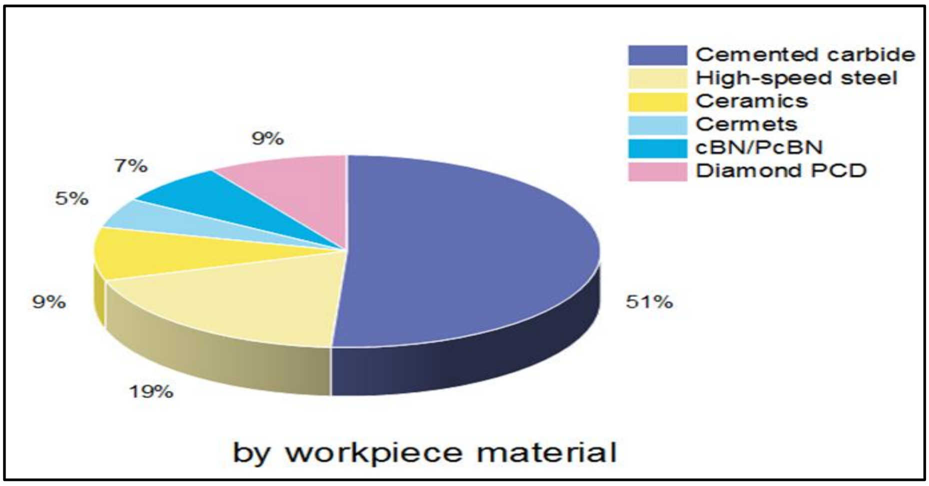

Figure (2.3): Distribution of the Global Market for Cutting Tools by Type of Work piece [25].

Figure (2.4) shows the distribution of applications of WC materials in various industries due to its incredible wear resistance and excellent corrosion resistance properties. WC-Co cutting tools show very high abrasion resistant, compressive strength and also withstand higher temperatures than standard high speed steel tools. WC-Co has produced a better surface finish, and its high-temperature stability allows the faster machining. WC is also used for making the projectile, and various anti-aircraft and anti-missile warheads[26].

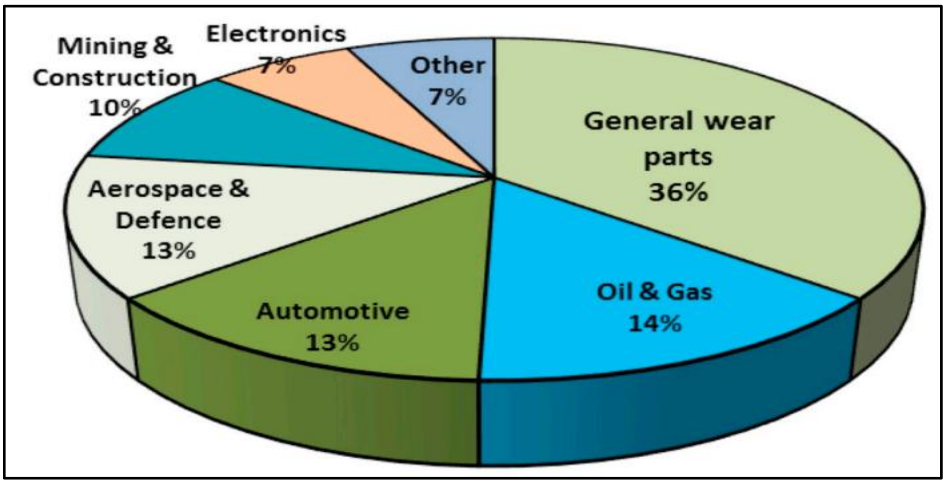

Figure (2.4): Distribution of Tungsten Carbide material uses in various areas [26].

2.4 Structure of Tungsten Carbides

Tungsten carbides are widely used in the production of structural and tool materials capable of working at high temperatures, in aggressive environments, and under high loads [27].

The tungsten carbides have hexagonal structures, whereas the most significant others are cubic. In contrast to steels, which may be soften by annealing and hardened by quick cooling, these stiff and tightly bonded compounds do not experience significant structural changes up to their melting temperatures, and as a result, their properties are stable and unaffected by heat treatment [28].

The two main forms of tungsten carbide are tungsten carbide (WC) and tungsten semi-carbide (W_2C). Due to the combination of its extremely high melting point (2700℃) and excellent microhardness (23GPa), tungsten mono carbide (WC) is regarded as a wonderful ceramic material [29]. In table (2.2), tungsten carbides' characteristics and properties are listed, WC It's also known as (δ-WC). Two more carbides can be formed by tungsten: The first form, $WC_{0.5}$ (often known as β-W_2C), has a hexagonal compact (HCP); the second form, (γ-WC1-x), has a faced center cubic (FCC) [30].

Table(2.2): Properties and Characteristics of WC [31].

Phases	**WC (also called δ-WC)** **W_2C (subcarbide β-WC)**
Crystal structure and lattice parameters (nm)	WC: hexagonal, a= 0.2907, c= 0.2837, c/a-0.976 W_2C: hexagonal, a= 0.3001, c= 0.4736, c/a- 1.578
Composition	Narrow range of homogeneity, δ-$WC_{0.98}$-$WC_{1.00}$
Molecular weight	WC: 195.86 g/mol W_2C: 379.71 g/mol
Color	WC: Gray
X-ray density	WC 15.8 g/cm^3 W_2C: 17.2 g/cm^3
Melting point	WC: 2785°C W_2C: 2715°C
Specific Heat (C_P)	WC: 39.8 J/mol K
Heat of Formation ($-\Delta H^\circ_f$)	WC: 37.7 kJ/g-atom metal at 298 K
Thermal expansion	WC: a=5.2x10^{-6} °C^{-1}, c=7.3 x 10^{-6} °C^{-1}
Vickers Hardness	WC: 22 GPa
Young's Modulus of Elasticity	WC: 620-720 GPa
Poisson's Ratio	WC: 0.18
Transverse rupture strength	WC: 550 MPa
Oxidation resistance	WC: Oxidation in air starts at 500-600 °C
Chemical resistance	WC is resistant to acids and not attacked at room temperature by mixtures of HF and HNO_3, but attacked by these acids at elevated temperature. Attacked by chlorine above 400 °C and by fluorine at room temperature. Stable in dry hydrogen until the melting point. W_2C is less stable than WC and reacts with Murakami's n* reagent.
Test temperature is 20 °C unless otherwise is stated.	

2.5 The Importance of Scrap's Recycling

In addition to having the highest melting point and the lowest thermal expansion coefficient of all metals, tungsten also comes into prominence with its high density, good electrical and thermal conductivity, and good high temperature mechanical properties. Due to these characteristics, it is impossible to replace the powder of tungsten in several technological fields, including the electronics manufacturers, industry for heavy metal alloys, cutting tool, chemical applications, cannon shells, grenades, light bulbs, high energy radiation shields, X-ray targets, cathode ray tubes heating devices, pigment, and more [32]. Due to increasing raw material costs, limited tungsten sources worldwide, and stringent energy conservation rules, recycling research and the industrialisation of cemented carbides have rapidly increased in recent years [33]. It is essential to recycle the scrapes containing high percentage of tungsten.

As illustrated in Figure (2.5), about 1/3 of the total tungsten demand is supplied by cemented carbide scrap, which is a clear indication of its importance in the manufacture of WC products[34].

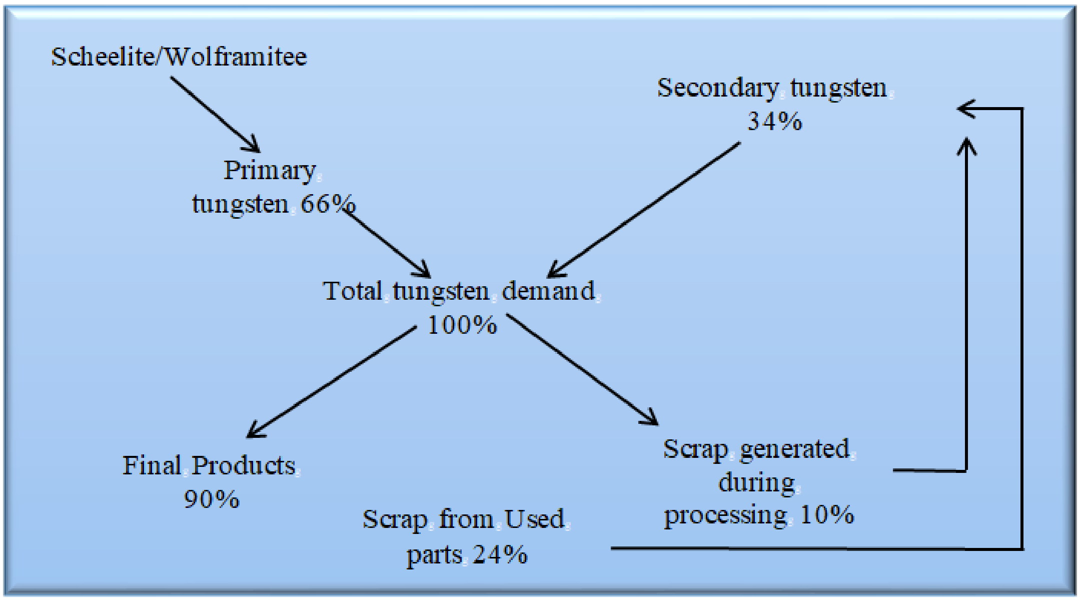

Figure (2.5): Tungsten Flow Sheet[34].

2.6 Sourcing of Scrap

When a product is no longer useful, it is referred to as scrap. The drill head might become worn out and the hard metal drill could break. When this occurs to an end product, the scrap that results is known as old scrap as shown in Figure (2.6) [35].

Figure (2.6): Examples of Old Scrap Cemented Carbide [35].

The scrap is known as new scrap when it involves a first-use product which sometimes known production scrap or primary scrap. Grinding sludge from hard metal drill manufacturing, hard metal sintered rods or drill bits (or even the created end products) that fail quality inspections for a variety of reasons, such as failure, metallurgy, dimensional porosity, etc. are examples of new scrap as shown in Figure (2.7)[35].

Figure (2.7): Examples of New Scrap Tungsten Carbide [35].

2.7 Recycling Methods of Cemented Carbides

The recycling processes can be divided into three types according to the kind of cemented carbide conversion processes used. These type are: direct processes; indirect processes; semi-direct processes [34].

2.7.1 Direct Recycling Method

Direct recycling involves either chemical, physical or a mix of both processes to transform the input material to powder of the same composition. Direct recycling has several requirements, including [36]:

• The final product's composition must match that of the scrap.

• The scrap must be highly pure; both in terms of quality and foreign contaminants (e.g., WC-Co hardmetal scrap shouldn't include TaC-TiC bearing qualities in addition to maintaining a small range for the WC grain size). The procedure must allow for the transformation of the scrap into a metallurgically suitable form of powder.

• No foreign materials were introduced during processing. Examples include the zinc process, the cold stream recycling method for cemented carbide waste and the oxidizing and later reduction of tungsten heavy metal turnings. Table (2.3) lists the many forms of direct recycling.

Table (2.3):Direct Recycling of Tungsten Scrap[36].

Process	product	Scrap
Zinc Bloating/crushing Coldstream	Hard metal powder	Sorted hard metal pieces Heavy metal turnings
Oxidation/reduction	Heavy metal powder Tungsten powder	Tungsten pieces, turnings, powder

2.7.2 Indirect Recycling Method

Indirect recycling involves recovering single element from scrap and purifying them using several chemical methods. WC-Co can be indirectly recycled through leach milling with total cobalt removal, chlorination, nitrate-carbonate fusion and oxidation-sodium hydroxide leaching [37].

2.7.3 Semidirect Recycling Method

The semi-direct recycling technique involves the chemical dissolution of a particular component while leaving the others unaltered. A variety of semi-direct recycling techniques are illustrated in table (2.4) [38].

Table(2.4): Semidirect Recycling [38].

Scrap	Principle	Method
Hardmetal pieces	Selective dissolution of the Co binder	Attack by acid (H_3PO_4) Leach milling (mixed chemical and mechanical attack) Electrolysis (acidic solution)
WC or WC + mixed carbides can be recycled to hardmetal grade powder preparation.		
Heavy metal pieces	selective dissolution of the Ni – Fe binder	Attack by acqueous $FeCl_3$ solution
Powder consists of approximately 40-µm tungsten spheres and be used in plasma spraying.		

2.8 Electrochemical Systems

An electrochemical system contains at least: electrodes, electrolyte and outer circuit. The external electric circuit is connected to electrodes, and the electrolyte acts as a medium that bridges the two electrodes via ionic conduction. A simple illustration of such system is shown in Figure (2.8) [39].

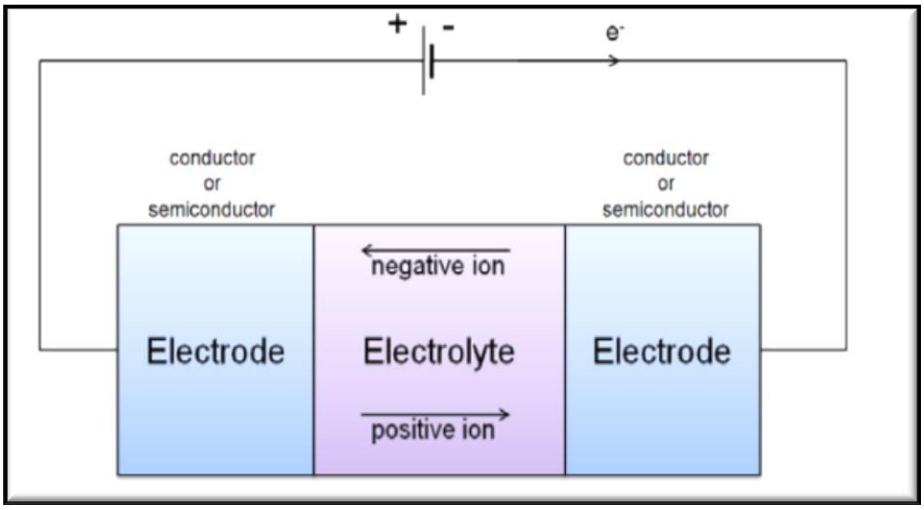

Figure(2.8): Simple Electrochemical System Structure[39].

Chemical processes are usually important, however in order to dissolve metallic materials, the metallic element must be oxidized in order for it to become soluble in a liquid phase. For corrosion to occur, there are four requirements: anodes (where oxidation occurs), cathodes (where reduction occurs), path of electrolytic for ionic conduction between the two places of reaction and the path of electrical for electron conduction between the two places of reaction [40]. A metal or a semiconductor may act as an electrode's electronic conductor, while fused salt, aqueous solution, solid or gaseous electrolyte (gaseous plasma) may act as the electrode's electrolyte [41]. Several factors affect the conductivity of electrolytic solutions, such as the composition of the electrolyte, ions' ability to dissolve in the solvent, the solvent's viscosity, temperature and the solution's concentration or dilution [39]. Charge transport between electrodes (electric conductors) and electrolytes (ionic conductors) in electrochemical systems depends largely on a variety of factors including ions concentration, temperature, electrolytes homogeneity, pressure, surface roughness of the electrode, magnitude of electric current (I) and potential electricity (E)[42]. Current densities (i) are preferred because it is related to the rate of corrosion or oxidation on an electrode contact surface (As) in an electrolyte [43]. Thus,

$$i = I/A_s \qquad (2.1)$$

Where I=electric current, A_s= electrode contact surface area

The cathodic reaction occurs when a particle of negative charge, such as an electron or an anion, moves from an electrode to an electrolyte (such as an aqueous solution), and the anodic reaction occurs when a particle of positive charge, such as a hole or cation, moves from an electrode to an electrolyte [44]. Cathodic and anodic reactions are shown in equations (2.2),(2.3) respectively [45].

$$X^{X+} + xe \rightarrow X \tag{2.2}$$

$$M \rightarrow M^{m+} + me \tag{2.3}$$

In an electrochemical cell, the difference in electric potential between the electrodes may be measured. Usually, a high impedance voltmeter is used for this. This cell potential is a measurement of the energy available to move charge externally between the electrodes. It is expressed in volts (V), where 1 V = 1 joule/coulomb (J/C) [46].

Galvanic and electrolytic cells are the two subtypes of electrochemical cells. A galvanic cell is one with spontaneous reactions (Gibbs free energy (G) < 0), which consists of converting chemical energy into electron movement, which is electrical energy, as seen in Figure (2.9A), While an electrolytic cell needs a potential applied that is greater than its open-circuit potential to drive an electrochemical process (e.g., non-spontaneous, G $>$ 0), which refers to converting electrical energy into chemical energy as illustrated in Figure (2.9B)[47].

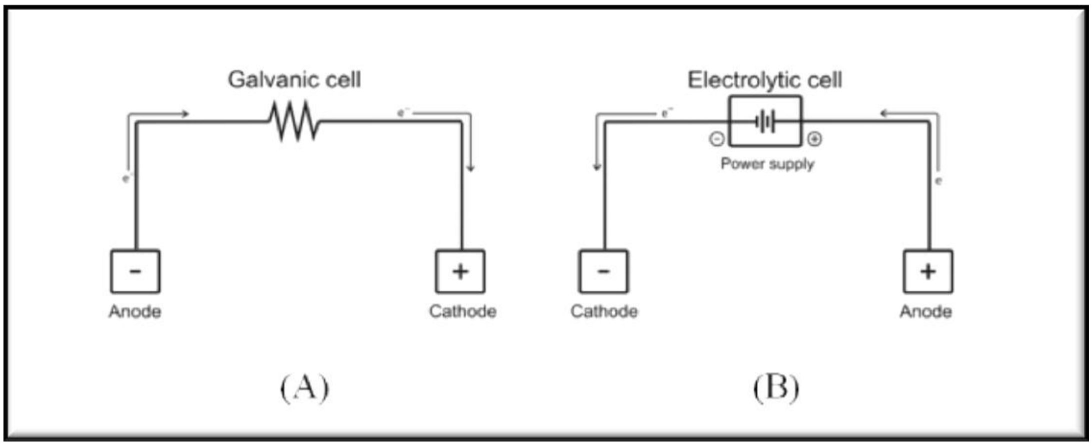

Figure(2.9): Schematic Representation of (A) Galvanic Cell and (B) Electrolytic Cell [47].

2.9 Electrochemical Recovery Process

The fundamental idea behind this technique is that, with cemented carbides acting as the anodes and applied of suitable voltage and current conditions, the carbide phases may be oxidized, causing the cobalt binder to dissolve. The cobalt binder dissolves to create cobalt ions in acidic electrolytes, but tungsten is oxidized to its maximum oxidation state and remains undissolved in the state of tungstic acid. The tungstic acid is then either reduced to tungsten metal or recovered by extraction. Precipitations with the addition of oxalic acid or electrolysis are two methods for recovering cobalt. The reaction can be described as [48, 49]:

$$WC + 6H_2O \longrightarrow H_2WO_4 + CO_2 + 10H + 10\,e^- \quad (2.4)$$

And

$$Co \longrightarrow Co^{+2} + 2e^- \quad (2.5)$$

The primary benefits of this process are low energy consumption, protection of the environment, no pollution, economic and, in most cases, technological benefits, direct recovery of tungsten carbide, high purity of the recovered product, and simplicity of use of the equipment and procedure for recovery [50].

The most recent method for processing WC scrap involves oxidizing tungsten to WO_3 and selective electrochemical dissolution of cobalt binder in acid electrolytes. Table (2.5) provides a summary of a few electrochemical studies for the dissolution of WC. WC is efficiently dissolved by H_3PO_4, H_2SO_4, HCl, and HNO_3-based electrolytes [51].

Table (2.5): Recycling of WC Scrap By Electrochemical Processing [51].

	Electrolyte	Input Waste	Process Output
1	**NaOH**	Tungsten Alloys	W suspension
		Tungsten	Tungstate
		Tungsten Alloys	APT
		Sintered WC	WC Powder and Co
2	**H_2SO_4**	WC-Ni	tungsten trioxide
		Tool grade WC	tungstic acid
3	**HNO_3**	Hard alloys	tungsten trioxide
		Sintered WC	W, Co
		Cemented WC	W, Co
		WC scrap	tungsten trioxide
4	**H_3PO_4**	WC-Co	WC, Co
		WC-Co	W, Co
		WC-Co	WC, Co
		WC-Co	WC, Co
5	**HCl**	WC-Co	W, Co
		Cemented WC	WC, Co
		WC-15wt%Co	W, Co
6	**NH_4OH**	Heavy metal alloys	APT
		Cemented WC	APT
		WC scrap	WO_3, Co

2.10 Tungsten- Oxygen System

There are a number of stable oxide phases, which complicates the tungsten-oxygen system. Four oxide phases presents, they are WO_2 (brown), $W_{18}O_{49}$ (purple), $W_{20}O_{58}$ (blue), and WO_3 well-known to exist (yellow). Another oxide, β - tungsten (W_3O), is known to exist, although there is no evidence to support it as an equilibrium phase in the literature. Depending on the temperature, the highest oxide, WO_3, can exist in at least three different forms. The homogeneity range of the lowest oxide, W_3O, reaches to the β-Wphase. Figure (2.10) provides the tungsten-oxygen phase diagram at 1 atm pressure .The different oxides are listed in table (2.6), crystalline structure, along with their range of existence, density, and colour. If the composition was stoichiometric, the highest oxide is yellow, but a slight reduction causes the colour change to grey or blue [52].

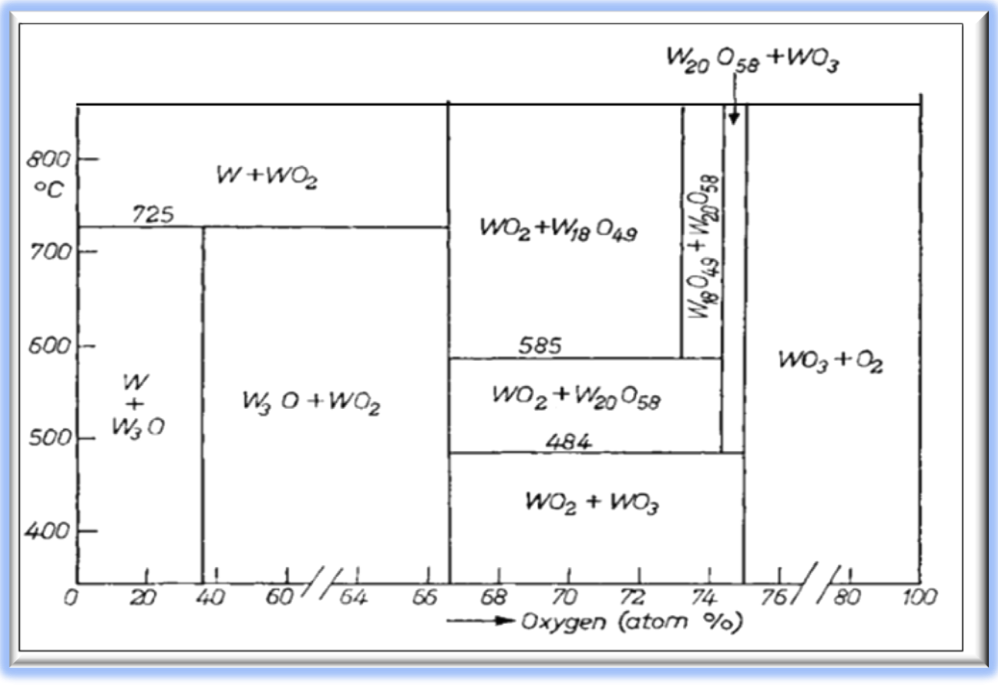

Figure(2.10): At 1 atm Total Pressure, the W-O Phase Equilibrium[52].

Table (2.6): Tungsten Oxides [52].

Type of oxide	Formula	Crystal structure cell dimensions (A)	Density g/cm³	Color
(β-W)	W_3O	cubic	14-19	grey
δ	WO_2	monoclinic	11	brown
γ	$W_{28}O_{49}$	monoclinic	7.7	Reddish-violet
β	$W_{20}O_{58}$	monoclinic	7.15	blue-violet
α	WO_3	below 320° monoclinic above 320°C orthorhombic above 720°C tetragonal	7.33	Yellow(green-blue)

Tungstic acids with the formula ($WO_3.nH_2O$) are materials important for many industrial goods, screens, and passive and active sensing devices. The classic tungstic acid, with the formula H_2WO_4 ($WO_3.nH_2O$, n=1), is now mostly used for the formation of tungsten carbide in hard metals and used as an alloying component in heavy metals. It was initially used to manufacture tungsten filaments for incandescent lamps [53]. It has been widely recognized that WO_3 and $WO_3.nH_2O$ are of great interest for their potential applications in photocatalysis, electro-chromic, and photochromic devices. A number of studies have found that $WO_3.nH_2O$ is very attractive materials for use as photocatalysts in the decontamination of contaminated water. These materials are also equally effective for the detection of hazardous gases, Lithium-ion batteries, supercapacitors, adsorbents, dye-sensitized solar cells, electrochromic devices, and electronic devices [54, 55].

2.11 Calcination

The traditional calcination-reduction-carburization (CRC) method has the capacity to create commercial tungsten carbide powders having mean grain sizes under 0.5 μm (ultrafine grades)[56].

The tungstic acid was calcined in order to produce stable monoclinic WO_3. The particle's surface area decreased with increasing calcination temperature. The heating rate was also an important parameter [57]. The reaction occurs as shown in Eq.(2.6) [58].

$$H_2WO_4 \longrightarrow WO_3 + H_2O \qquad (2.6)$$

There are several crystallographic phases of tungsten oxide (WO_3), including monoclinic, hexagonal, cubic, and orthorhombic. This material is largely considered for use in a variety of applications, including flat-panel displays, writing-reading-erasing devices, optical memory, gas sensors, energy storage devices, field-emission devices and notably in photocatalysis because its activity in visible light. It is also thermally stable and resistant to photo-corrosion [59].

2.12 Reduction of Tungsten Oxides Powder by Using Carbon

In general, the reduction of metal oxides with carbon is of great practical importance, and is an integral part of the extraction of many metals from their ores. The reduction does not occur primarily by the reaction of solid carbon with the solid oxide, that is, by so-called "direct" reduction [60]:

$$MO_{x(s)} + C_{(s)} \longleftrightarrow Moy_{(s)} + CO_{(g)}/CO_{2(g)}$$

Where x > y. Reaction (2.7) would occur at the points of contact between the reactants, followed by diffusion of the reactants across the product layer. Such a process is expected to be limited by the rate of diffusion of the reactants. In carbothermal reduction, however, the contribution of reaction (2.7) to the overall process is probably small. Rather, the interaction between the solids is predominantly indirect and takes place via intermediate gases. This involves two gas-solid reactions:

$$MO_{x(s)} + CO_{(s)} \longleftrightarrow Mo_{y(s)} + CO_2 \qquad (2.8)$$

And the reaction:

$$C_{(s)} + CO_{2(g)} \longleftrightarrow 2CO_{(g)} \qquad (2.9)$$

The formation of $CO_{(g)}$ is a necessary first step in the process, and might result from direct reduction (reaction (2.7)), or from the reaction of carbon with oxygen (either residual oxygen or oxygen from the dissociation of the metal oxide). The process terminates when CO and CO_2 are removed from the specimen [60].

Carbon reduction of WO_3 in the solid state has obtained technical importance and interest when tungsten carbide is desired as the final product, this process is known as "Direct Carburization," and the following equation encapsulates the fundamental reaction [61]:

$$WO_{3(s)} + 4C_{(s)} \longleftrightarrow WC_{(s)} + 3CO_{(g)} \qquad (2.10)$$

addition to the primary reaction; the following reactions also take place:

$$WO_{3(s)} + 5/2C_{(s)} \longleftrightarrow WC_{(s)} + 3/2CO_{2(g)} \qquad (2.11)$$

$$C_{(s)} + CO_{2(s)} \longleftrightarrow CO_{(g)} \qquad (2.12)$$

2.13 Surface Modification by Coatings

Surface coatings technology allows the engineer to improve the performance, extend the life, and enhance the appearance of materials used for engineering components. This technology has been developed because the interactions of manufactured components with other components, liquid, and/or gaseous environments can result in component degradation and failure[62].

Coatings have been utilized to enhance tribological performance, extend component durability. The main advantages of coatings are very high flexibility concerning alloy selection and optimization for specific resistance to corrosion, oxidation, erosion and wear. Surface coating may be one layer, multi layer or functionally graded material on the substrate. The materials used for coating may be polymeric, metallic, ceramic or a mix of these materials depending on the environment and the using conditions of the substrate. Figure (2.11) shows the types of coating [63].

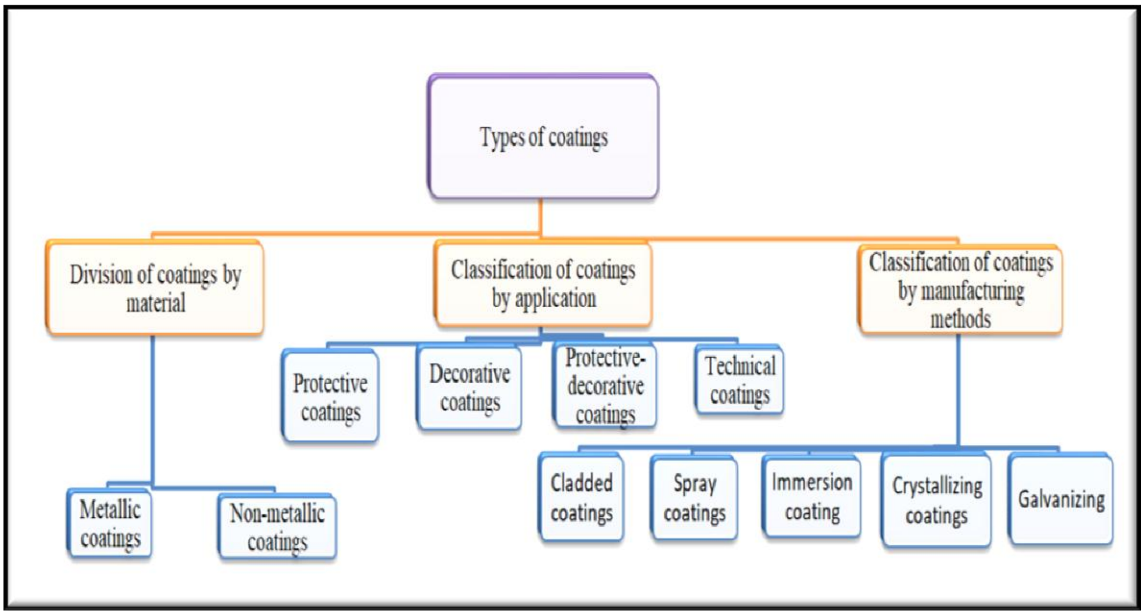

Figure(2.11): Types of Coating[63].

2.14 Thermal Spray Coatings

Thermal spraying is used in a wide range of applications including automotive systems, boiler components, and power generation equipment, chemical process equipment, aircraft engines, pulp and paper processing equipment, bridges, rollers and concrete reinforcements, orthopedics and dental, land-based and marine turbines, and ships[64].

Thermal spraying encompasses a family of coating deposition techniques that involve the same basic steps. As shown in Figure (2.12), thermal spray equipment generally consists of heat source, feed, and flow. The feedstock forms include powder, wire, solution and suspension[65].

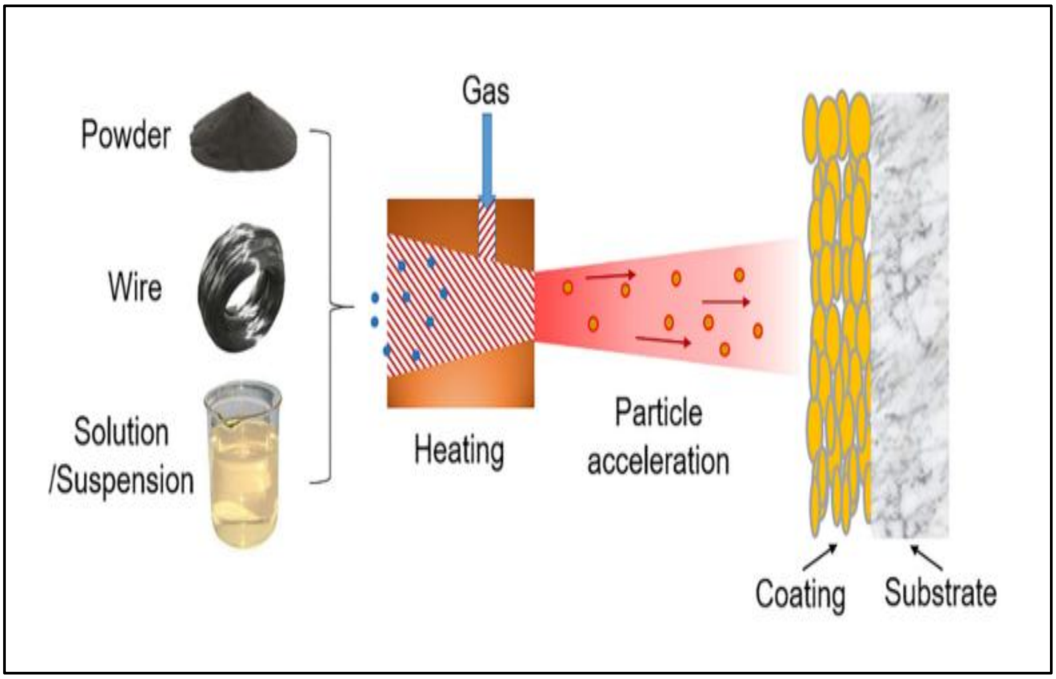

Figure(2.12): Schematic Diagram of A Thermal Spray Process [65].

Thermal spraying is a technique that helps to provide exceptional resilience to wear, erosion, and corrosion by placing metallic and nonmetallic materials on the surface of the medium in a liquefied or semi-liquefied condition. By applying an electrical arc or combustible gas, the coating by thermal spray method entails melting material. The coating by thermal spray method includes applying electrical (plasma or arc) or chemical means to melt the coating substance to a molten or semi-molten state (combustion flame)[66]. Thermally sprayed coatings have some distinct advantages over other methods as they can be deposited over a wide thickness range (from tens to hundreds of microns), onto components with complex geometries without the constraints typical of in-chamber processes, and at comparatively lower costs[67]. Thermal spraying inputs a relatively low amount of heat to the substrate. This minimizes thermal distortion of the substrate and allows for deposition on heat-treated components. Another advantage of thermal spray processes is the ability to deposit an extremely wide range of materials. Virtually any material that has a stable molten phase can be deposited with one or more traditional thermal spray processes. This includes virtually all metals and metal alloys, many ceramics and glasses, as well as some polymers. Even some materials that do not melt, such as graphite and many carbide or boride ceramics, can often be co-deposited with another spray able material to create a composite coating material[68].

Since thermal spraying is often a deposition technique that does not significantly raise the substrate temperature during processing, it may be used with a wide variety of substrate materials, including polymers and their composites, in addition to metals and alloys. Table (2.7) summarizes the use of different materials as substrates in thermal spray coating [69].

Table(2.7): Suitability of Various Substrate Materials in Thermal Spray Coating Processing [69].

Substrate material group	Suitability to thermal spraying; remarks
Mild steels, low alloyed, and steel alloys	Excellent materials to be coated, prevent oxidation by avoiding heating above 150 °C
Hardened steels	Can be coated, high substrate hardness lowers efficiency of grit blasting, for steels <50 HRC
Stainless steels, nickel-based alloys	Can be thermally spray coated, high thermal expansion coefficient must be noted, preheat to max. 100°C
Copper and Cu alloys	Can be coated, high thermal expansion coefficient must be noted, no preheating due to oxidation sensitivity
Aluminium and Al alloys	Can be coated, high thermal expansion coefficient must be noted, no preheating due to oxidation sensitivity
Titanium and magnesium	Can be coated, no preheating
Polymers and polymer composites	Can be coated but requires low heat input, low temperature resistance, low bond strength, buffer/intermediate layers recommended

2.15 Microstructure of Thermal Spray

Coating produced by thermal spray is characterized by lamellar structure embedded with solid particles, oxide and inclusions. Molten or semi-molten particles are accelerated towards the substrate and solidify rapidly on contact with the substrate surface, forming a strong bond. The adhesion between substrate and coating is predominantly by mechanical interlocking further impact of droplets or 'splats' build up the coating to the required thickness. A schematic of the type of structure built up by thermal spray coating is shown in Figure (2.13) [70].

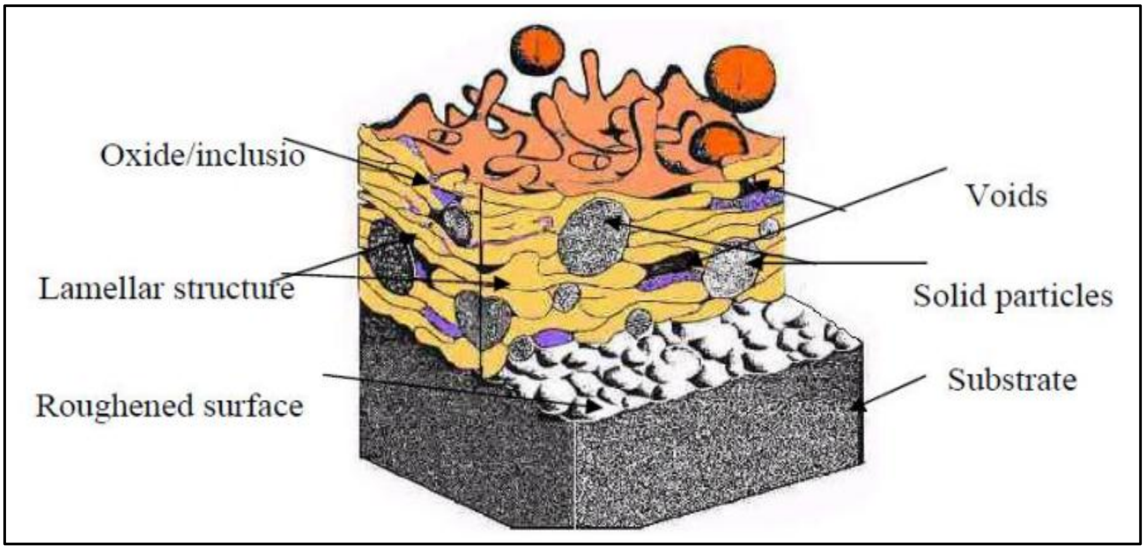

Figure (2.13): Schematic Showing Typical Microstructure of Thermal Spray Coating [70].

A lamellar structure is created when the coating is built up through numerous "splat" collisions with the surface; as the individual splats settle, the lamellar is formed. Within the impact, columnar granules will develop if the cooling rate is high enough. The process does not produce a perfect coating; oxides formed on the surface of a molten droplet will become inclusions in the coating along with unmelted particles. As a general rule the inclusion of oxides, unmelted particles and foreign objects is detrimental to coating properties [71].

Powder particles move towards the substrate they melt but also react with air. The particles oxidize over their surface forming an oxide shell. The turbulent flow of the molten particles causes oxide shell crack so that the oxide is redistributed along the whole volume of the molten particle. While flattening on the substrate surface the upper parts of the particles are exposed to the atmosphere rich in oxygen so that oxidation occurs even after the particles impact onto the substrate surface[72]. Inclusion content in the coating may be reduced by (a) proper inert gas shrouding; (b) reducing the average temperature of particles; (c) reducing the dwell time of the particles by minimizing spray distances or increasing velocities; (d) reducing substrate/coating surface temperature using cooling air jets or increasing the speed of the thermal spray deposition, thus minimizing oxidation at the coating surface; and (e) using the proper feedstock powder particle size. Larger particles have a lower surface area to volume ratio, which minimizes overall oxide content[73].

However, a dense coating with less porosity and good inter-splat bonding significantly reduces the extent of such a degradation . In order to achieve such a dense coating, the process parameters have to be optimized for each coating composition to be deposited. Heat flux/oxy-fuel volume ratio, standoff distance (distance between component to be coated and gun exit), powder feed rate are the major parameters to influence the coating properties. Therefore, proper optimization of process parameters to obtain dense coating is very essential for depositing coatings by thermal spray techniques. Since the interface bonding being provided by mechanical interlocking, cleaning of the component surface from oil, dirt and roughening of surface by grit blasting before coating deposition is the key to produce well-adherent coatings[74].

Porosities are often produced when a high number of unmelted or resolidified particles are trapped in the coating (Figure 2.14), which reduces the coating's ability to resist wear and corrosion. Additionally, the following causes might lead to porosities developing: (1) small particles that have not completely melted, have only partly melted, or have resolidified are trapped and cause voids to develop; (2) material shrinks as it cools from a liquid state; (3) high deposition angles that cause shadowing or "snow drifting"; (4) cracking that occurs between or inside splats; and (5) inherent porosities of the feedstock powder production process. The porosities present in the thermal spray deposited structure may be modified by adjusting the particle morphology, particle size and distribution, particle thermal characteristics, jet temperature, particle dwell duration and enthalpy distribution. The coating defects caused by the thermal spray deposited coating are schematically shown in Figure (2.15) [75].

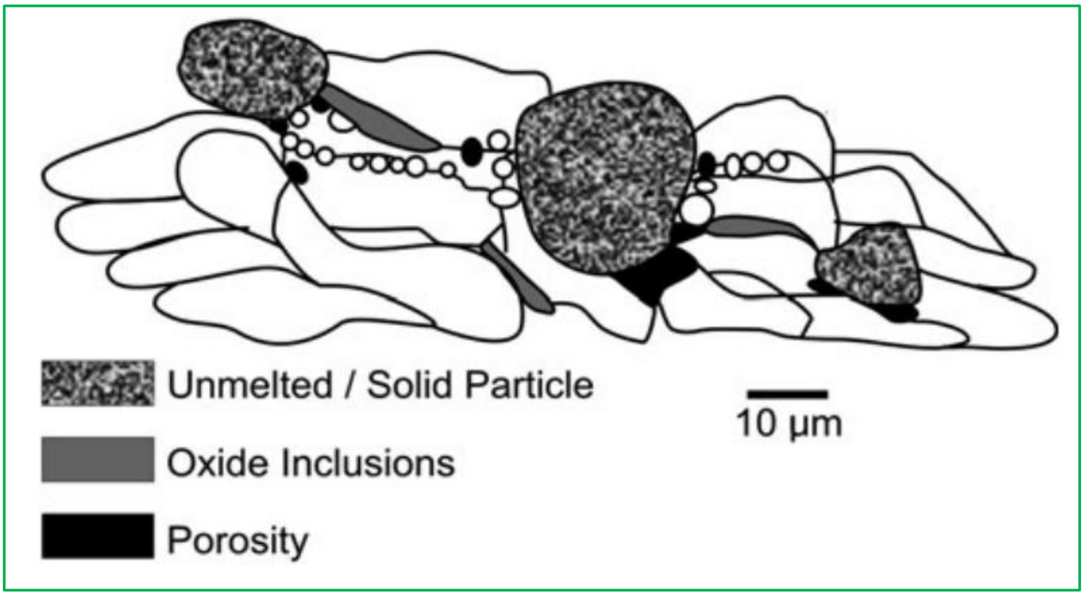

Figure (2.14): Defects Generated in Thermal Spray Deposition [75].

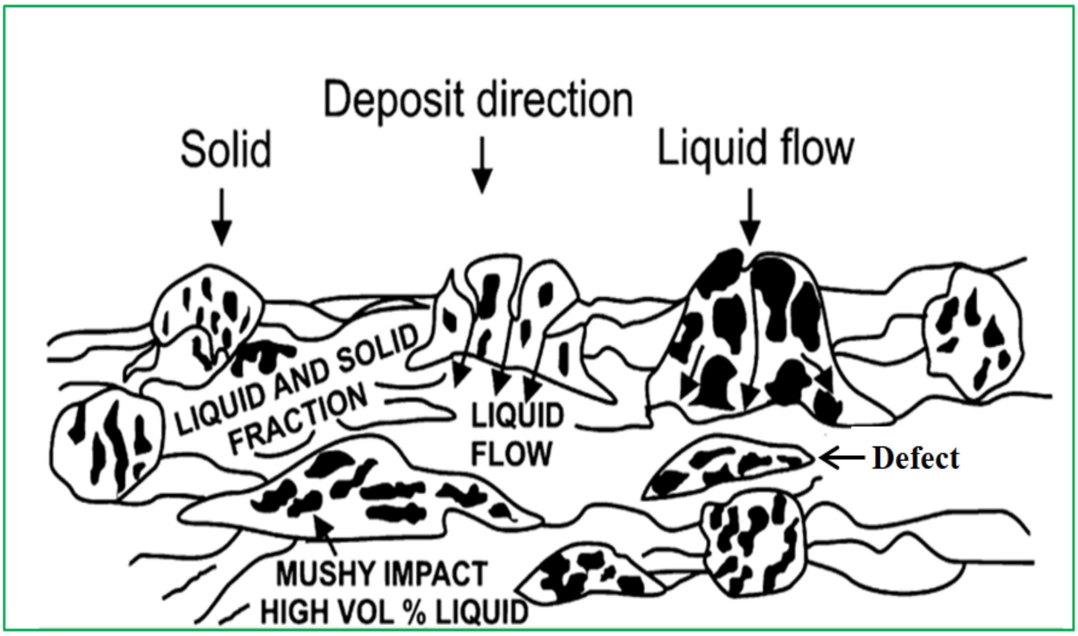

Figure (2.15): Genesis of Porosity Development in Thermal Spray Deposition [75].

2.16 Classification of Thermal Spray Deposition

The primary categorization of the thermal spray deposition method is shown in Figure (2.16). The four major coating methods for thermal spray deposition include flame spraying, plasma -arc spraying, electric-arc spraying , and kinetic spraying, along with numerous subcategories of each. Many more groups are included in each of these processes. Each procedure has its own characteristics, which leads to the development of a covering with those characteristics. For the particular application, the best coating method must be chosen based on the intended coating qualities [76].

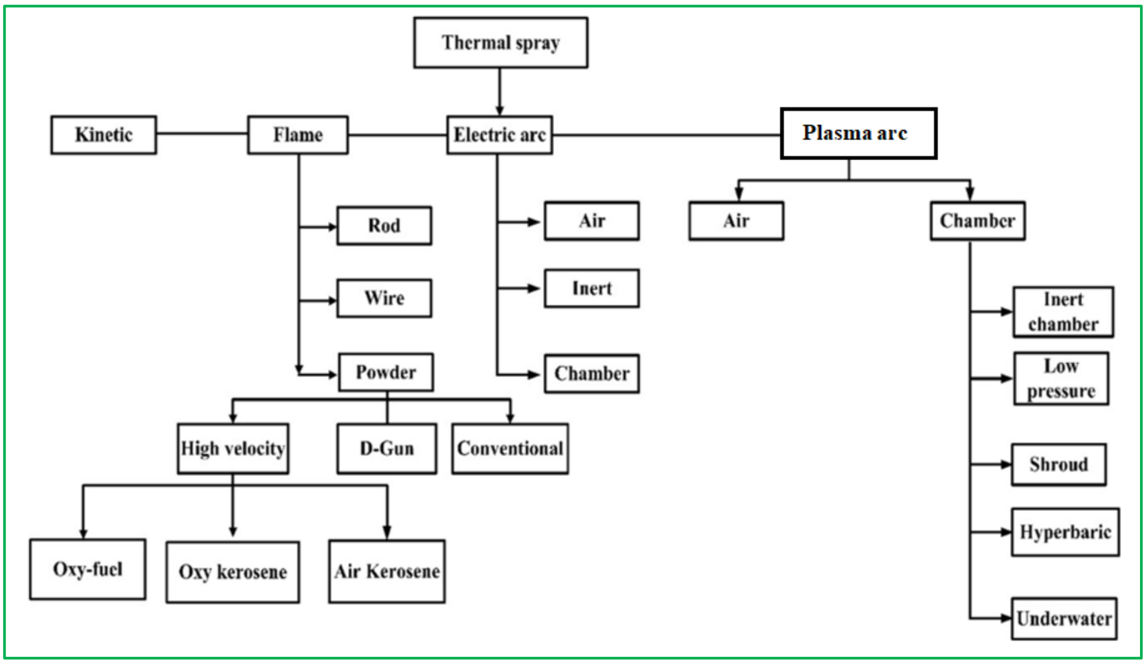

Figure (2.16): Classification of Thermal Spray Deposition Techniques [76].

Most advantages of thermal spraying are: virtually any coating material can be used (metals, ceramics, cermets, plastics); low thermal stress on substrate parts; local and reinforced coatings possible; nearly any substrate material can be coated; high deposition rates (coating thickness from 20 µm to several millimetres) [77]. The most suitable materials to be sprayed strongly depend on the flame's temperature. Ceramic coatings are often created using the atmospheric plasma spray technique, although temperature-sensitive materials like ceramics are better sprayed using techniques that use a lower flame temperature. The usual operation ranges for different spray devices are shown in Figure (2.17) [78].

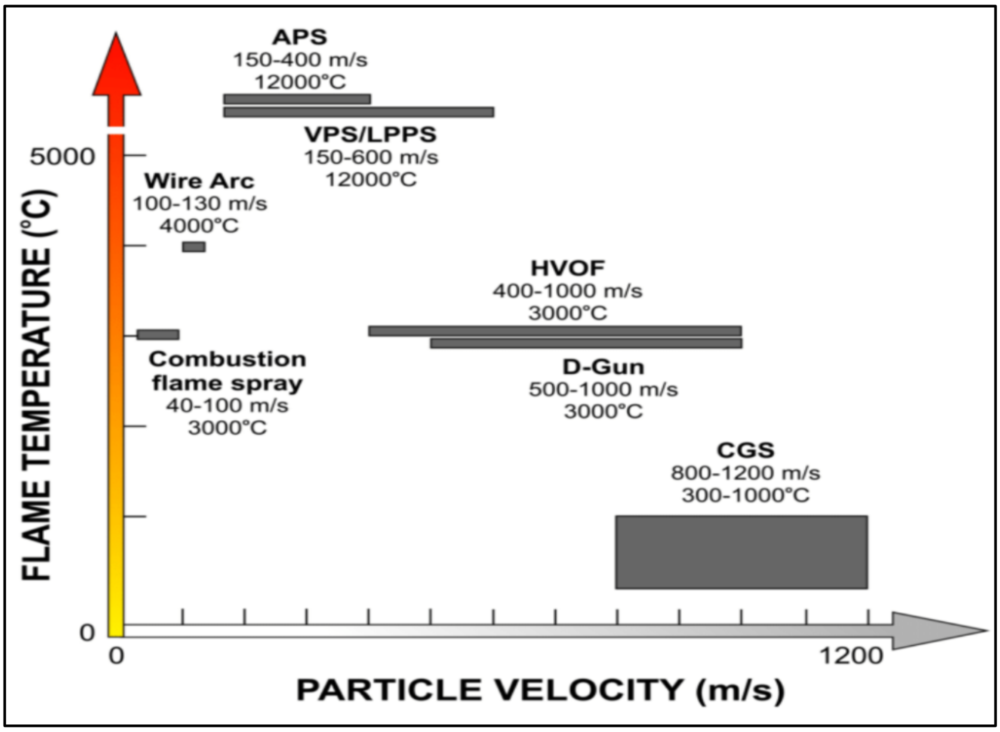

Figure (2.17): Typical Flame Temperature And Particle Velocity Operation Ranges For Various Thermal Spray Systems [78].

* APS: Atmospheric Plasma Spray, VPS: Vacuum Plasma Spray, LPPS: Low Pressure Plasma Spray, HVOF: High-Velocity Oxy-Fuel, CGS: Cold Gas Spray.

Table (2.8) shows comparative process parameters of different thermal spray systems[79].

Table (2.8): Comparison of Thermal Spray Processes [79].

Features	Flame spray	Electric arc	APS	HVOF	HVAF	Cold spray
Jet						
Jet temperature (°C)	3000	4000	15,000	2800	2000	200-1000
Jet velocities (m/s)	50-100	50-100	300-1000	500-900	800-1400	400-1200
Gas flow (slpm)	100-200	500-3000	100-200	400-1300	300	1000-2000
Gas nature	O_2, C_2H_2	Air, N_2, Ar	Ar, He, H_2, N_2	CH_4, C_3H_6, H_2 + O_2	C_3H_6 (+Air)	He, N_2
Power input (kW)	20	2-5	40-150	150-300	300	40-100
Particle feed						
Particle temperature (°C)	2500	>3800	>3800	3000	<1600	<600
Particle velocities (m/s)	50-100	50-200	200-600	600-1000	800-1200	800-1000
Feed rate (g/min)	30-50	150-2000	50-150	20-100	50-500	20-200
Deposit/coating						
Density range (%)	85-90	80-95	90-95	95	98	95
Bond strength (MPa)	7-18	10-40	40-70	70-100	100-200	80-100
Oxide level	High	Moderate to high	Moderate to coarse	Moderate to low	low	None
Hardness (WC coating) (HRC)	45-55	…	50-65	55-72	65-75	55-65

***** HVAF: High-Velocity Air Fuel.

2.16.1 Flame Thermal Spray

Flame spraying is the oldest of the thermal spraying processes, characterized by low capital investment, high deposition rates and efficiencies, and relative ease of operation and cost of equipment maintenance. Flame spray uses combustible gas as a heat source to melt the coating material[80].

Feedstock components for flame spraying are available in rod or wire and powder shape. Figures (2.18) and (2.19), which show the wire or rod shape technique and powder feedstock materials, respectively. In order to create a heat source, the process depends on the molecular interaction between air and a fuel of combustion (acetylene, hydrogen). A vapor stream is produced by this heat source. Compressed air is used to atomize the molten metal and propel the metal particulates onto the substrate after the feed stock material for the spray is delivered into the flame. Materials with greater melting points than the flame can provide or materials that break down when heated restrict the use of the flame spray process. Because of the low flame temperature and particulate velocity, coatings are frequently porous, and the binding and shear strength between the covering and the base are also generally low[81, 82].

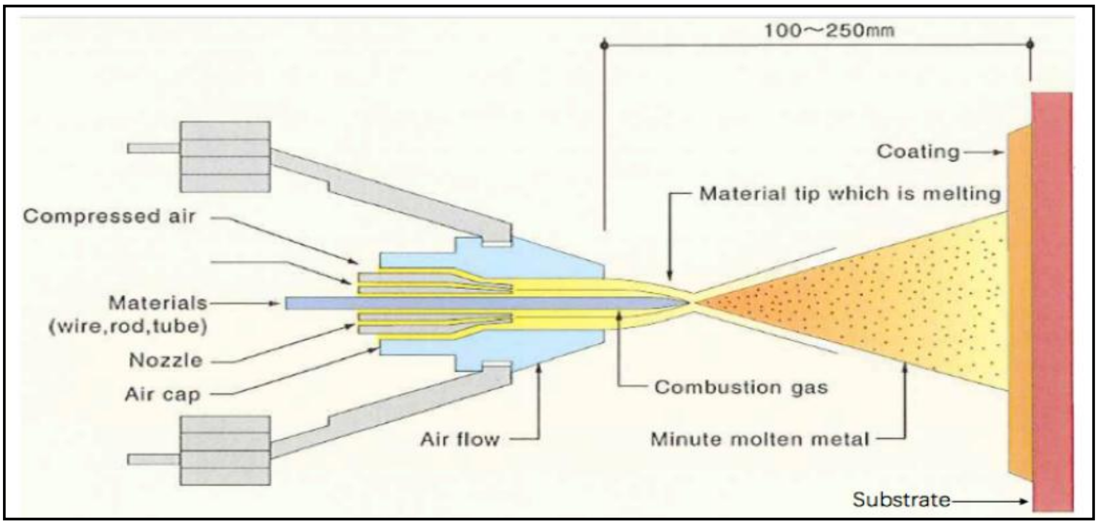

Figure (2.18): Schematic for flame spray with wire or rod form feedstock materials [81].

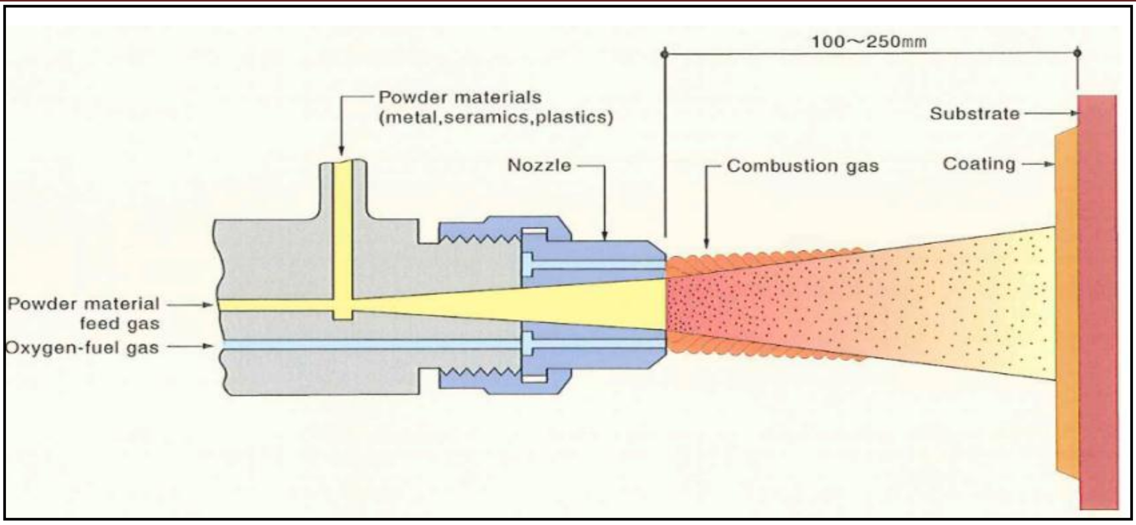

Figure (2.19): Schematic for flame spray with powder form feedstock materials [81].

2.17 Spray Parameters of Flam Thermal Process

The spray parameters are summarized in Figure (2.20) [83]. The first group of these parameters are related to ***substrate***. This group includes: the temperature control of the substrate during the preheating, spraying, and cooling; substrate shape, size, roughness and its thickness. The second group includes parameters related to the ***coating.*** This group includes: the powder composition, its velocity and temperature, size distribution, and particle morphologies depending on the manufacturing process or the cord composition and post-treatment[83].

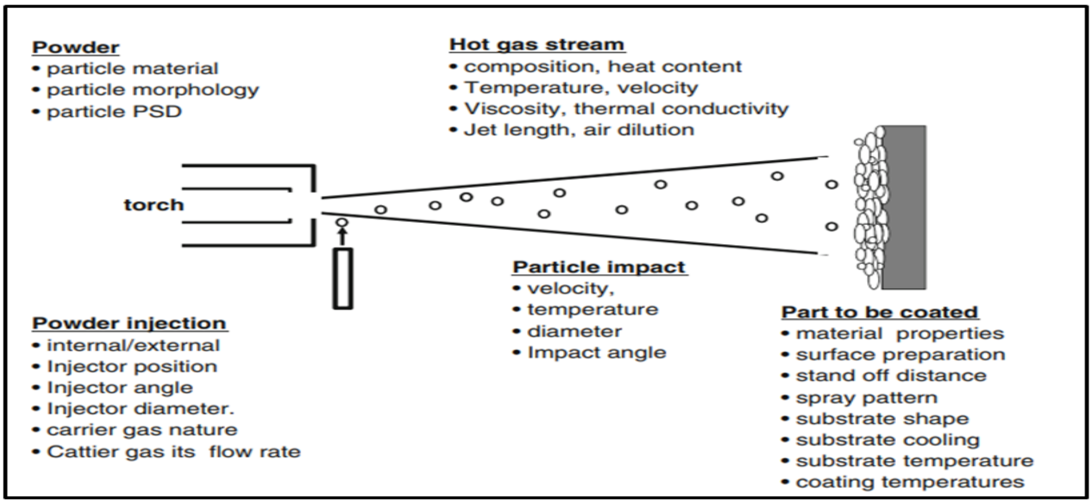

Figure (2.20): Different Spray Parameters[83].

The feedstock characteristics (particle form, size distribution, density and chemistry) have an effect on deposit evolution and process efficiency by change in thickness per pass, and to other properties, such as thermal conductivity and elastic modulus. Powder properties and characteristics depend on the detailed powder manufacturing method, i.e., crushing and milling, water and gas atomization, spray drying, agglomeration and sintering [84].

Moisture on the substrate surface may be removed by exposing the surface to a high temperature, a process known as pre-heat treating. Thermal stresses occur when there is a difference in the thermal expansion coefficient between the substrate and the deposited material [85]. Residual stresses developed in thermal spray can be attributed to two main contributions: quenching stresses, always tensile in nature and generated as the impacting splat contracts during cooling to the substrate temperature, and differential thermal contraction stresses, generated due to differences in thermal expansivity as the splat/substrate system cools-down to ambient temperature. The residual stress developed in coating may be controlled by a proper preheating and postheating operation prior to and after deposition, respectively. Figure (2.21) illustrates the residual stress generation process schematically [73, 86].

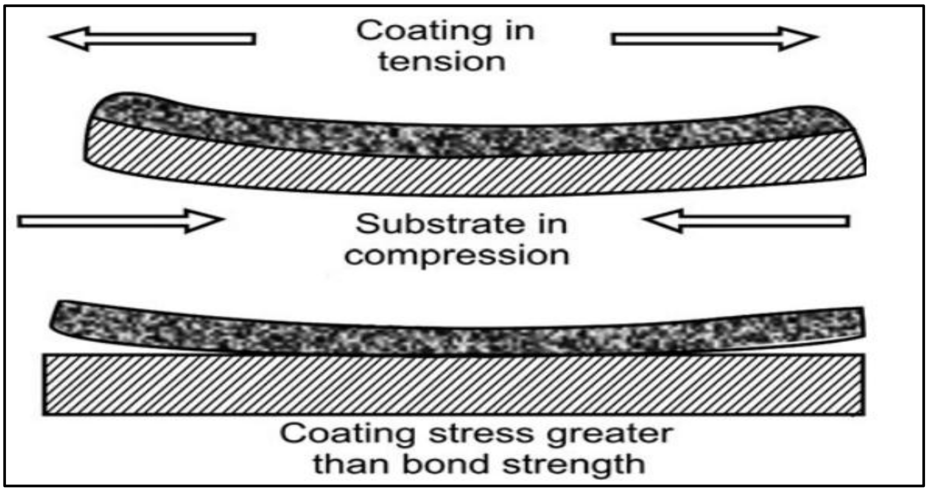

Figure (2.21): Schematic Showing How Residual Stress is Made [73].

Different flame spray systems can use a wide range of fuel gases, such as acetylene, hydrogen, propylene, ethylene and propane. Because each of them has distinct dissociation energy, the thermal conductivity of the flame changes, affecting the quantity of heat transfers to the powder particles. The fuel gas to oxygen ratio, changes the temperature of the flame, allowing the spraying conditions to be changed from a low temperature flame with a reducing environment to a higher temperature with an oxidising atmosphere [87].

The particle temperature usually correlates to the particle's surface temperature prior to reaching the substrate. The particles are heated to a molten or semi-molten state by the thermal energy of the flame, with the particle surface temperature influenced by the following factors: flame temperature, particle density, in-flight duration, feedstock rate, particle size, and particle thermal conductivity. It is usually undesirable for the particles to reach the fully molten state as the feedstock will decarburize and sub carbide phases will become dominant, making the coating behave in a brittle nature [88].

The increased kinetic energy supports particle splat flattening and has been shown to reduce the coating porosity which is typically in the range of 1% by volume. The increased particle velocity reduces the particle dwell time within the flame and thus the particle temperature and oxidation content. The particle velocity can also be affected by the fuel/oxygen ratio where it has been found that increasing the fuel/oxygen ratio the temperature decreases and the particle velocity increases [89, 90].

Thermal treatment of coatings involves various heating procedures such as remelting, fusing, sintering and annealing. The goals can be listed as elimination of pores and splat boundaries to improve cohesion strength and enhancing in bonding strength by creation of metallurgical bonding between coating and substrate; improvement in thermal shock resistance or fracture toughness due to microstructural refinement and metallurgical bonding; microstructural modifications such as stress relieving; to complete the reaction between elements; for example, formation of final compounds likes intermetallic; crystallization of amorphous coatings and to enhance wear and corrosion resistance by eliminating open pores. Along with a reduction of residual stresses the wear resistance of WC-Co coatings has been shown to be improved by heat treatment, due to the increase of carbide content through recrystallization of the amorphous phase into one of the eta carbides (M_6C or $M_{12}C$) [91].

2.18 Thermal Spray Processing

The flame thermal spray comprises four basic stages as shown in Figure (2.22) [92].

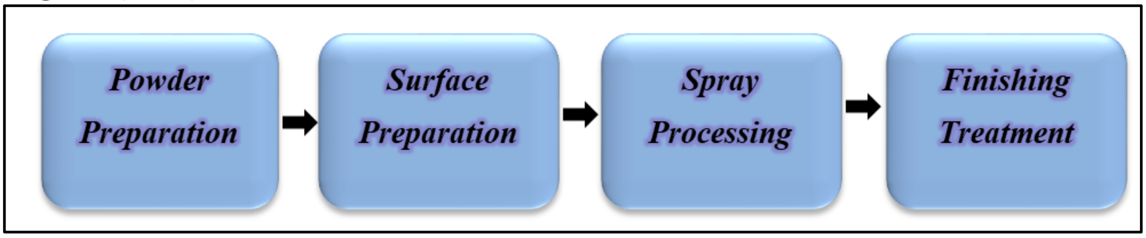

Figure (2.22): Principal Stages in Flame Thermal Spray Processing [92].

The powders of metals and alloys are usually prepared by atomisation methods or sometimes sintering. Carbide and oxide ceramics are generally manufactured by fusing followed by crushing [92].

Coating adhesion is related to the cleanliness and roughness. The preparation of the surface is the most critical step in the thermal spraying operation. The first step in the preparation is to remove all surface contaminants, such as scale, oil, and paint, by different techniques: scraping, wire brushing, machining, vapor degreasing, vapor blasting, acid pickling, or oven backing. These techniques must be adapted to the substrate material and contaminants. After the latter have been removed, the cleanliness must be maintained until spraying is completed: no finger prints, clean fixtures and materials, and no airborne debris especially during spraying. After cleaning, the substrate surface is generally roughened to promote adhesion. In most cases, this is achieved by grit blasting [93].

After spraying coatings are treated to achieve the final dimension and obtain a smooth surface, machining (Turning, Milling) for metal coatings turning and milling can be easily used to establish the final dimension and remove the as-deposited coating roughness, grinding for ceramic coatings and abrasive belt grinding and polishing can be ground and polished metal, cermet, and ceramic-sprayed coatings with coated abrasive belts. The main advantages of these belts are that they cut without overheating [94].

2.19 Applications of Sprayed WC-Co

Tungsten carbide-cobalt based spray coatings are widely used in industry for applications requiring abrasion, sliding, fretting and erosion resistance. The hard WC particles in the coatings lead to high coating hardness and high wear resistance, while the metal binder (Co, Ni, or CoCr) supplies the necessary coating toughness[96]. Cermet coatings are often used on metals when high surface hardness and wear resistance are demanded. Figures (2.23) and (2.24) show the multitude of parts that are coated using thermal spray technology in a jet engine and in an automobile[83].

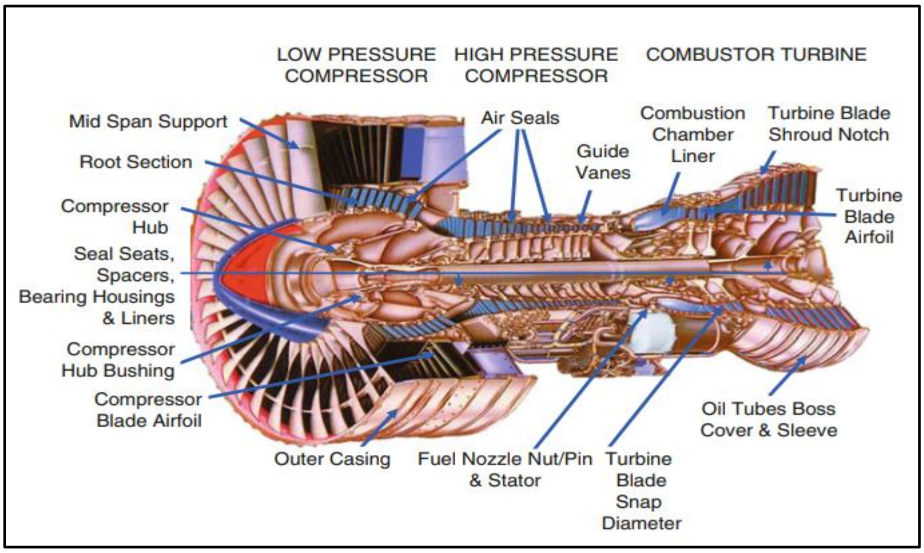

Figure (2.23): Thermal-Sprayed Coatings on Aircraft Turbine Engine Parts [83].

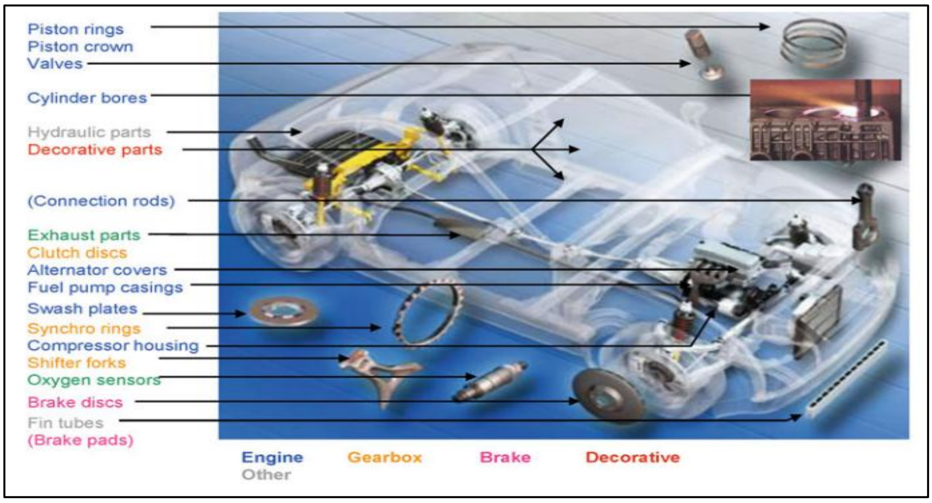

Figure (2.24): Thermal Spray Components In The Automotive Industry [83].

Today, applications in the aero-engine industry represent an important part of the market for thermal spray coating. WC–Co coating by high-velocity combustion spraying for adhesive wear application as shown in Figure (2.25) [95].

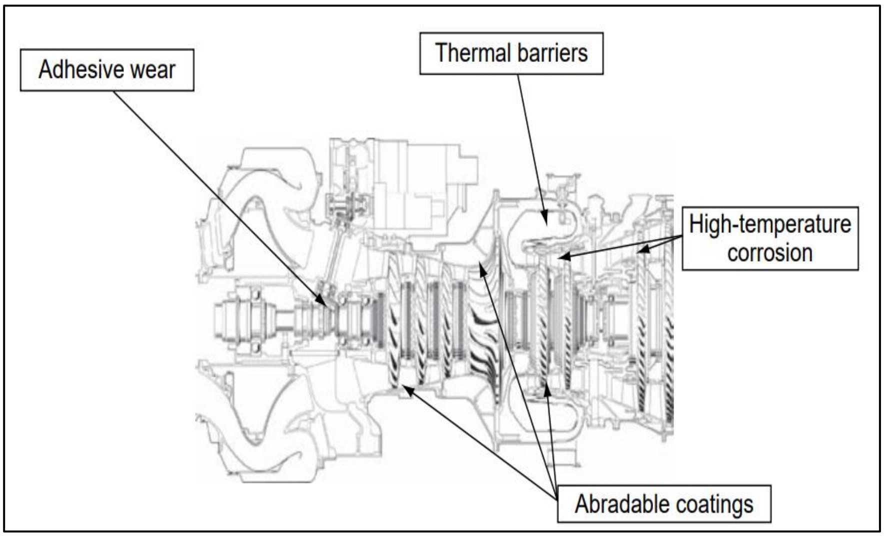

Figure (2.25): Section of An Aero-Engine Showing the Families of Thermally Sprayed Coatings and Their Places of Application[95].

Tungsten-carbide materials have been widely used historically to protect surfaces from adhesive and abrasive wear in many different applications (for aerospace, paper, and oil and gas industries). Functionally, the carbides have been used as sprayed coatings, composite coatings, and sintered cermets; all with different fundamental mechanical properties and behavior. For the aerospace application of replacing hard chrome electroplating, the beneficial wear properties of the carbides were very attractive as compared to other materials[96].

Thermal-sprayed WC-Co coating is extensively used in several places in the steel industries. Continuous casting moulds are coated with WC-Co coating. Briddle rolls are used to control the tension of steel strips as they passes through the continuous pickling, annealing and galvanizing lines. There are some coating materials which are used according to type of wear for thermal spray coating as shown in Table(2.9) [97]:

Table(2.9): Different Coating Materials[97].

Type of wear	Application	Materials
Abrasive wear	Cutting Blades Glass Mould Pump	WC-CO NiCr-Cr_3C_2 Cobalt based hardfacing alloy Nickel/Cobalt self-fluxing alloy
Sliding wear	Piston Rings Impeller Shafts Cylinder Bores	WC-CO Cast iron-molybdenum molybdenum based self-fluxing alloy Cobalt Chromium
Erosion/Cavitation wear	Steam turbine Blades Water turbine	WC-CO WC-CO-Cr NiCr-Cr_3C_2

2.20 Design of Experiments

Experimental techniques are very complex and required a wide number of experiments as the number of process parameter rises. The Taguchi design is widely accepted and used in engineering analysis and optimization. This approach has been built based on the design of experiment (DOE), which is employed to study the influence of multiple variables simultaneously. The method is useful in reducing the number of experiments dramatically by using orthogonal arrays and also tries to minimize the effects of the factors out of control [98].

The Taguchi method (TM) defines two main groups affecting the products: control factors and noise factors. The noise factors are used to designate all factors that cause variations, while the control factors are used to select the best (optimum) conditions for manufacturing or design stability. DOE is employed concurrently to study the influence of multiple variables. Taguchi’s technique is a form of DOE which has special application bases. Taguchi realized that the manufacturing process stage and the design of the product stage are the best opportunity period in order to minimize variation. Achieving performance consistency is necessary to improve quality by lowering variability around the objective. One method for influencing each of these performance characteristics is experiment design [99].

2.21 Optimization by Grey Relational Analysis

Deng Julong's proposed Grey Relational Analysis (GRA) can be joint with the Taguchi system. The multi-response problem in GRA, is reduced to a problem with a single response, and the best possible answers to that issue are assessed. This method employs a trial-and-error approach based on Grey Relational Grades (GRG) to determine the level of approximation between sequences. By employing GRG as a performance metric, the Taguchi method may determine the optimal configuration for the method factors being optimized [100]. The following steps are part of the Grey Relational method using the Taguchi technique:

Step A: To estimate the quality and determine the factors, the signal to noise (S/N) ratio is determined. A higher S/N ratio value signifies better performance of the factor. The S/N ratio can be defined via Eq. (2.13) and Eq. (2.14). Equation (2.13) represents the higher- better S/N ratio type and can be utilized when a maximization of response is intended, while equations(2.14) denotes the lower-better type [101].

$$S/_N\, ratio\ (Y_{ij}) = -10\, Log_{10}\left[\left(\frac{1}{n}\right)\left(\sum_{i=1}^{n}\frac{1}{y_{ij}^2}\right)\right] \tag{2.13}$$

$$S/_N\, ratio\ (Y_{ij}) = -10\, Log_{10}\left[\left(\frac{1}{n}\right)\left(\sum_{i=1}^{n}\ y_{ij}^2\right)\right] \tag{2.14}$$

Where, n = number of repetitions; yij = the response, i = 1, 2. . . n; n is the number of the test in the orthogonal array; j = 1, 2,. . ., m. m is the number of the process response.

Step B: The second step of GRA is to normalize S/N ratio, in the range between 0 and 1, using formulations (2.15) and (2.16) to maximize and minimize the quality properties respectively[101].

$$X_{ij} = \frac{(Y_{ij}) - Min(Y_{ij})}{Max(Y_{ij}) - Min(Y_{ij})} \tag{2.15}$$

$$X_{ij} = \frac{Max(Y_{ij}) - (Y_{ij})}{Max(Y_{ij}) - Min(Y_{ij})} \tag{2.16}$$

Step C: Calculation of deviation utilizing the formula, $\Delta = 1 - x_{ij}$, where x_{ij} = Normalized S/N ratio

Step D: After treating the results, Grey Relation Coefficients (GRC) for the j^{th} response in the i^{th} experiment can be stated as follows [102]:

$$GRC = \frac{\Delta min + \gamma \Delta max}{\Delta + \gamma \Delta max} \tag{2.17}$$

Where Δ is the deviation of the response; Δmin is the minimum value of Δ; Δmax is the maximum value of Δ; γ is the distinguishing factor (0.5 is widely accepted).

Step E: After computing GRC, Grey Relational Grades (GRG) can be calculated via the next formulation:

$$GRG = \frac{1}{m}\sum_{i=1}^{m} GRC \tag{2.18}$$

Where m represents the number of responses. The GRC and GRG have been determined for all experiments. For optimal method factors, the maximum value of GRG is near to the product quality. An order of 1 is assigned to the maximum GRG value and ranking is performed in a decreasing order [102].

Step 6: To classify the significant variables, perform ANOVA. The main purpose of the analysis of variance ANOVA is the application of a statistical method to identify the influence of individual factors. Results from ANOVA can determine very clearly the effect of each factor on the method results. The whole sum of the squared deviations SST is decomposed to two sources: the sum of the squared deviations because of each method factor and the sum of the squared error. The percentage contribution via each of the method factors in the total sum of the squared deviations SST can be utilizeded to evaluate the importance of the method-factor change on the performance characteristics. Usually, the change of the method factor has an important influence on the performance characteristic when the F value is high[103].

2.22 Literature Review

A preview of the recent studies about recovery of metallic powders from carbide cutting insert by electrochemical process will be discussed in the following items.

2.22.1 Studies Related to Recovery of Tungsten Carbide

Latha and Venkatachalam, 1989[104] investigated tungsten recovery from scrap by using electrochemical method with nitric acid electrolyte. In this method, insoluble tungstic acid powder (H_2WO_4) is produced and the ions of cobalt go to the solution, at the anode, carbide material is oxidized. Studied nitric acid concentration, temperature, time and current density, as the variables, the factors causing tungsten carbide to material oxidize and dissolving of cobalt. The ideal conditions for concurrent cobalt dissolution and tungsten carbide oxidation are 10% nitric acid, the temperature between 55-60℃ and 10 kAm^{-2} current density. The investigation's findings also showed that, in contrast to other conventional methods, electrochemical process can lead to the recovery of component metals with a high purity level.

Ashrafizadeh, et al., 2003 [105] studied recovery of hard carbides from scrap species by using electrolysis process that was carried out under various conditions while the optimal conditions were (current density of 1500 A/m^2 , an acid concentration of 1.5 M, and a cell temperature in the vicinity of 60 to 80°C). The result that was obtained is a pure tungstic oxide after calcination the precipitate of tungstic acid at 800℃. The rate of collapse of the anodic pieces remains constant until the completion of the recovery process, the cell voltage, and consequently the consumed energy, decreased with increasing the nitric acid concentration in the electrolyte solution while maintaining the current density. Increasing the nitric acid concentration up to 15 wt% (l.5M) decreased the amount of consumed specific energy about 20% in comparison to that of 5wt%, the mass of the submerged carbide pieces, the surface area of the anode, and the mode and extent of agitation do not affect the rate of collapse of the carbide pieces.

Nogueira, et al., 2004 [106] prepared tungsten trioxide by calcination of the tungstic acids, in air, at 500℃ over one hour ,the research prepared different specimens of $WO_3.H_2O$ each specimen with specific hydration number then these specimens were analysed morphologically by using SEM that show each specimen has specific morphology($WO_3.H_2O$ particles shows ‘‘square plates’’, $WO_3.2H_2O$ particles: ‘‘round plates’’ in specimens, $WO_3.1/3H_2O$ agglomerated particles with undefined shape in the amorphous specimen).

Abdullah, et al., 2007 [107] showed that at different calcination temperatures with several phase transitions of WO_3 occurred. The crystallization temperature for WO_3 nanoparticles was found to be above 300°C, no diffraction peaks were found in the X-Ray diffraction at 300°C.The result from XRD and thermogravimetric-differential thermal analysis (TG-DTA) show that the formation of polymorphs WO_3 nanoparticles have the following sequence: orthorhombic (β- WO_3) $\rightarrow$ monoclinic (γ-WO_3) $\rightarrow$ triclinic (δ-WO_3) $\rightarrow$ monoclinic (ε-WO_3) with respect to the calcination temperature of 400, 500, 600 and 700°C. It is also found that the X-Ray diffraction measurements produced an average diameter of (30$\pm$5), (50$\pm$5), (150$\pm$10) and (200$\pm$10) nm at calcination temperatures of 400, 500, 600 and 700 C respectively by using Debye-Scherrer formula. The TG curve revealed that the WO3 particles is purely anhydrous since the weight loss is insignificant (0.3-1.4)% from 30 until 600 C for the WO3 particles calcined at 400 C. Finally, the composition and the purity of the WO3 particles examined by X-Ray photoelectron spectroscopy (XPS). The results indicate no significant changes to the composition and the purity of the WO_3 particle produced due to the temperature variations.

Kumar, et al., 2009 [108] synthesized WC-nanoparticles from WO_3 using Thermo-chemical reaction rout. Specimens were placed in furnace and using acetone, and ethanol as carbon source. The temperature of the furnace increased from room temperature to $600^{O}C$ with heating rate of 5 ^{O}C/min. The acid-treated samples were washed with distilled water, first followed by ethanol to eliminate the water absorbed in the powders. The dried powders were characterized to investigate the formation of WC phase. The results indicate that reduction of WO_3 to WC takes place by the adsorption of carbon at the surface of WO_3 forming porous structure at the defect sites through which carbon diffuses.

Ma and Zhu, 2010[109] calcined WO_3 solid-state thermally to nano WC particles mechanically by mixture of WO_3 and graphite at 1215° C in a vacuum. The precise planning procedure was as follows: Raw materials WO_3 and graphite powders were combined at a molecular weight of 1:4, and then ball milled for 10 hours in an Ar environment. The composite powder was put into a ceramic vessel, heated in a vacuum tube furnace to 741° C, then raised to 1215° C at a rate of 10° C/min, and maintained at that temperature for one hour. Based on a rise in homogeneity and its corresponding decline during the diffusion phase of mechanical milling, ultrafine WC particles were produced. The effective creation of WC powders is also due to the generation of certain intermediates, including $WO_{2.72}$ and WO_2. WO_3 is converted to various lower-valence WO_3 kinds, such as $WO_{2.72}$ and WO_2, when the calcination temperature rises. Magneli-phase WO_3 is the name given to these low valence WO_3 forms (meta-stable phase WO_3).

Katiyar, et al., 2014 [110] researched recovery of valuable metals (W, Co) from cemented tungsten carbide scrap materials by using different processes. In electrochemical process, scrap material acts as anode and graphite or stainless steel or platinum foil is used as the cathode, electrolytes that has been used either acid or alkali, in acid type of electrolyte (nitric acid) Co is deposited on the cathode and small amount of Co also goes into the solution leaving behind the WC skeleton. Co is removed from the solution by electro winning process. WC materials are obtained from bottom of the cell after drying in a furnace.

Ahmadi, et al., 2014 [111] investigated preparation of tungsten oxide (WO_3) by annealing tungstate ($WO_3.H_2O$). It was fully examined by annealing a number of specimens in air at temperature between 500℃ to 800℃, the results showed that the morphology of the specimens significantly changed as a result of the heat treatment in air with a change from a 2D to a 3D structure of the product for temperatures in excess of 600℃, additionally, the product that was heated to 300℃ required many days to settle to the bottom of the containers, but product that was heated to 500℃ or higher sank in only a few hours, directly correlated to their sintering

Wongsisa, et al., 2015 [112] researched a sustainable industry manufacturing method for direct recycling cemented carbide tool scraps combining a hydrothermal and electrolysis process (CHEP). The research methodology was performed by studying the current recycling carbide tools, scraps industry and associated recycling technologies. The results of this research indicated that this recycling process was effective in recycling cemented carbide from industrial cutting tools scraps and can be used to purify the recovered WC rate to near virgin material, resulting in a more environmentally friendly process and reducing natural tungsten material usage.

Xiao, et al., 2017 [113] studied the effect of applied voltage, electrolysis current, and electrolysis times on the composition of the product by recovered cobalt, tungsten, and tungsten carbide powders from cemented carbide scrap using molten NaCl − KCl salt electrolysis. Results showed that pure cobalt powder can be obtained when the electrolysis potential is lower than 0.6 V or during low current and short times and obtained pure tungsten carbide powder. Scanning electron microscope results show that the diameters of tungsten, tungsten carbide, and cobalt powder were smaller than 100, 200, and 200 nm, respectively.

Behnami, et al., 2017[114] studied the development of a simple, easy, and inexpensive process for W_2C-free tungsten carbide preparation through microwave heating of WO_3-C mixtures. In the results, for the synthesis of WC, the use of over stoichiometric amount of C together with a specially assembled experimental setup (which effectively retains heat in the system) is necessary. In this study using different ratio of carbon with WO_3 when the optimum ratio of this mixture was WO_3:4C .The WC powder was successfully obtained by heating WO_3-C mixture with temperature range (300 to 1800 k) in a domestic microwave oven at time starting from 40s to several minutes. Although thermodynamic evaluations show that WC is the stable carbide phase under the conditions used in this study, the W_2C phase is formed in the specimen and the presence of W_2C is attributed to the favourable kinetics of its formation as well as to the carbon insufficiency (i.e., carbon burn) in the system so the using of adequate amounts of excess carbon to prevent this from occurring and also to avoid excessive heat loss from the system.

Sun, et al., 2019 [115] Studied selective dissolution method to recycled WC and Co from cemented carbide scrap. The anodic passivation slows down oxidation and leads to inefficiency during electrolysis. The porosity of the WC coat is the main impact factor for passivation. Types of

WC-Co scraps (YG8/YG15/YG20) obtained under a current density of 10 mA cm^{-2} in 1 M HCl. The thickness of the coat was measured, and the diffusion coefficients (Di) were calculated by Ficks first law of diffusion. The Di of cation was $0.088 * 10^{-10}$, $0.61*10^{-10}$, $0.70*10^{-10}$ $m^2\ s^{-1}$ for YG8, YG15, YG20, respectively. The inferior diffusion coefficient resulting from the dense coat was believed to be the main reason for the low dissolving rate.

2.22.2 Studies Related to Coating

Kahraman and Gulenc, 2002 [116] investigated wear behaviour of powder flame sprayed coatings on steel substrates. Coating was carried out onto both hot and cold substrates. The results show the heating of the substrates prior to the coating led to the decrease in the hardness of the coating layers and wear resistance. This may be attributed to the softening of coating layer as a result of heating after the powder deposition. Wear resistance of flame sprayed coatings was seen to be dependent on the chemical composition and characteristics of coating materials and coating condition. The common behaviour observed from the curves is that weight losses decreased with increasing time. However, decrease in weight losses or increase in total weight losses took place rapidly in the initial period of the tests whereas after a while a decrease in wear rates were observed. This can be attributed to the effect of surface roughness of the coating layer after being machined. Samples with higher R_a values showed less wear resistance than those with lower R_a values. Additionally, the decreasing slope of the weight loss curves can also be attributed to the work hardening during the tests. The tests hardness measurements were carried out on the specimens and some increase in hardness was observed therefore improved wear resistance.

Krishna et al., 2002 [117] studied oxy-acetylene spray system with various oxygen to fuel ratios using two different tungsten carbide powders and powder feeding methods. Carbon content of the powders and coatings were determined to study the decarburisation of the material during spraying process. Coatings were also characterised by their hardness and abrasive wear. The effects of metallurgical transformation and phase content are related to wear performance. The results demonstrate that the powders exhibit various degree of phase transformation during the spray process depending on the type of powder, powder feeding and spray parameters. The carbon loss during the spray process in excess of 45% resulted in reduced hardness and wear resistance of the coatings. Coatings with high amount of WC and W_2C along with FeW_3C showed higher wear resistance.

Nahvi and Jafari,2016 [118] investigated different WC-based coatings with steel substrate, measuring their microhardness, porosity and fracture toughness. The total volume fraction of carbides in WC-FeCrAl and WC-N was almost the same, but NiMoCrFeCo displayed a much lower microhardness (1254 HV). The authors attributed this result to the higher W_2C content (W_2C/WC ratio equal to 40.42). Even though W_2C has a higher hardness than WC, the W_2C phase surrounding the WC grains decreases the cohesion of the grains with the matrix, deteriorating both the hardness and the fracture toughness. The WC-Co coating, which had the lowest fraction of carbides, showed the highest fracture toughness value and an intermediate value of hardness (1305 HV).

Kıratlı,2017 [119] investigated of the wear and hardness behavior of carbon steel coated by the powder flame spraying method using three types of powders,(Ni-Cr-B-Si), (Ni) and (Ni, Cr- Si- B). As a result, it was found the wear resistance and hardness was improved for all coating. (Ni-Cr-B-Si) specimen has more resistant against wear and high hardiness. The reason for that hardness shows a tendency to thus be that Cr, Si, and B located in coating powders play an important role on coating layer. Another reason for the increase of hardness was that porosity oxide and non-melted particles have an effect on the hardness of coating layer. It was observed that wear resistance decreases by decreasing hardness in other specimens.

Ferrer et al., 2019 [120] studied projection parameters of a WC-18Co coating sprayed with a thermal flame spraying process from a commercial feedstock powder were determined to decide the conditions under which compact coatings are obtained with low porosity, avoiding dissociation of the tungsten carbide. The thermal spray by flame allows to obtain homogeneous coatings of WC-Co and to maintain the tungsten carbide phase. A neutral flame and a projection distance between 7.5 and 12 cm are the conditions under which coatings with low degradation of tungsten carbide are obtained.

Matthews et al., 2021[121] investigated the theoretical feasibility of employing a novel carbide composite processing technique involved generate nanostructured WC-Co composite coatings by flame thermal spray techniques. The variation in microstructure implied that at impact the molten particles contained two distinct liquid phases from; (i) the molten Co binder with dissolved carbide elements, and (ii) a W-based liquid generated by the peritectic decomposition of WC. The composition was dominated by an amorphous Co-based phase. A higher amount of metallic W (3.2 wt %) was formed relative to the coating. The agglomerated and sintered feedstock WC-17 wt%Co powder consisted of coarse WC particles agglomerated with Co particles. Only WC and Co were detected by XRD, although the carbon content of 4.96 wt% was slightly below the expected concentration of 5.1 wt%

2.23 Summary of the Literature Review

Researcher (s)	Recycling or Coating Process	Research Finding
Latha and Venkatachalam (1989)[104]	Electrochemical process	Pure tungstic acid (H_2WO_4) recovery from scrap
Ashrafizadeh, et al., (2003) [105]	Electrochemical process Calcination process	Pure tungstic acid (H_2WO_4) recovery from scrap pure tungstic trioxide after calcination the tungstic acid at 800℃
Nogueira, et al., (2004) [106]	Calcination process	tungstic trioxide after calcination the tungstic acid at 500℃
Abdullah, et al., (2007) [107]	Calcination process	Several phase transitions of WO_3 at different temperatures
Kumar, et al., (2009) [108]	Thermo-chemical reaction route	WC-nanoparticles obtain from reduction of WO_3

Ma and Zhu, (2010) [109]	Carburization Process	WC Powder
Katiyar, et al., (2014) [110]	Electrochemical process	Pure tungsten carbide was obtained from scrap materials by several steps firstly modification of tungsten oxide compenent secondly removal of binder medium from the matrix
Ahmadi, et al., (2014) [111]	Annealing process	Tungsten oxide (WO_3) nano-ribbons (NRs) were obtained by annealing tungstite ($WO_3.H_2O$) NRs.
Wongsisa, et al., (2015) [112]	utilizing both a hydrothermal and an electrolytic process	Pure tungsten carbide was obtained from several steps
Xiao, et al., (2017) [113]	Molten salt electrolysis process	Studied the effect of electrolysis current voltage and electrolysis time on the preparation of tungsten,cobalt , and tungsten carbide
Behnami, et al., (2017) [114]	microwave heating method	Homogeneously product (WC) under interaction of microwaves with magnetic and electric spins

Sun, et al., (2019) [115]	selective electro-dissolution process	Studied the effect of anodic passivation on cemented carbide scrap.
Kahraman and Gulenc,2002[116]	Flame thermal spray method	The heating of the substrates led to the decrease in the hardness and wear resistance of the coating layers
Krishna et al., 2002 [117]	Thermal spray method	The powders exhibit various degree of phase transformation during the spray process depending on the type of powder, powder feeding and spray parameters
Nahvi and Jafari,2016 [118]	Thermal spray method	When (WC/W_2C) ratio is high, microhardness and fracture toughness decreases
Kıratlı,2017 [119]	Thermal spray method	Wear resistance and hardness was improved by using flame thermal spray
Matthews,2021[121]	Flame thermal spray method	generate nanostructured WC-Co composite coatings

Through previous literature reviewed, we conclude:

1. Adopting the scrap carbide cutting insert and their recycling to obtain tungsten carbide and tungsten oxide with an optimal study of the influencing factors.

2. Adopting the recycled WC as a coating layer on the stainless steel 316 to enhance its wear resistance with a study of the influence of factors on the method used. Applications where component deterioration occurs due to wear are common places to find cemented tungsten carbide cermets. Ceramics are appealing as wear-resistant materials due to their great hardness; yet, their brittleness prevents them from being used in certain wear situations. High levels of hardness and toughness are often found in materials with excellent wear resistance. Cermets combine the toughness of metal with the abrasion resistance of ceramic. One kind of cermet combines the hardness of tungsten carbide (WC) with the malleability of a metal like cobalt.

CHAPTER THREE

EXPERIMENTAL PART

Chapter Three

Experimental Part

3.1 Introduction

This chapter is divided into two parts, the first part describes the techniques, experimental design, equipments and the materials used for preparation the tungsten carbide powder. In this part, several investigating tests were carried out: chemical composition, particle size analysis, XRD, SEM, EDS and thermogravimetric analysis (TGA). The second part describes specimen's preparation method for coatings and the materials used for the coating via the flame thermal spray method using (WC) powder recovered in the first part. Mechanical and physical tests carried out for the coating layer include: XRD, SEM, EDS, surface roughness, hardness and wear test.

3.2 Program of the Present Study

Figure (3.1) shows the experimental program utilized in this study.

3.3. Materials Used in the present study:

3.3.1. Materials Used for WC Recovery

●Uncoated tungsten cemented carbide tips grade P10 produced by Bader General Company/Iraq were used as a source for WC recovery. All the inserts have identical geometry designated by the American National Standard Institute (ANSI) as [TNMG 160408].

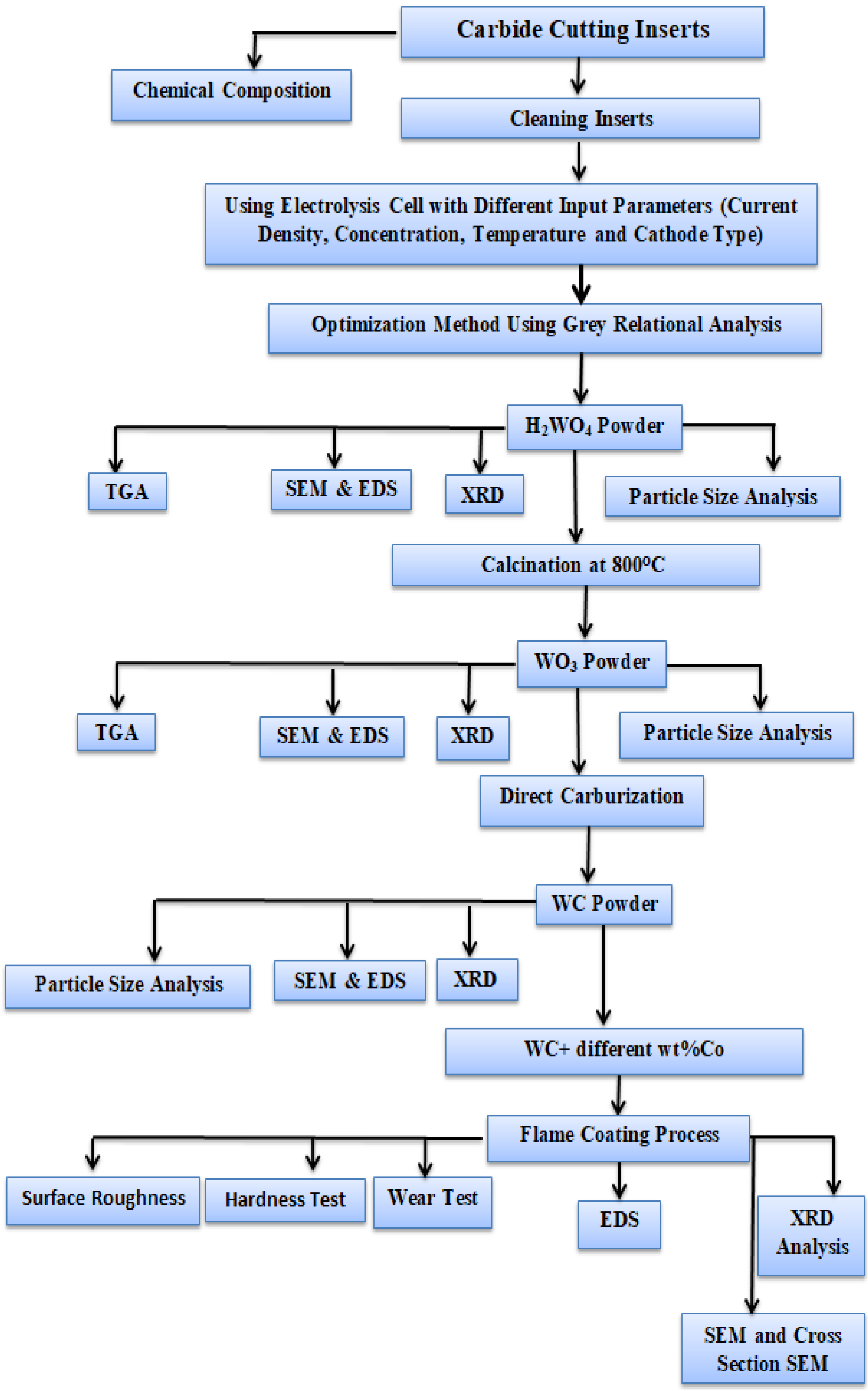

Figure (3.1): Experimental Program of the Present Work.

Table (3.1) shows the chemical composition of the used carbide cutting inserts. The analysis was carried out at the Faculty of sciences / X-Ray Lab, Tarbiat Modarres University/Iran. Calibrate the instrument using standards from Philips Analytical X-Ray.

Table (3.1) Chemical Composition of the Used Carbide Cutting Inserts.

Compositions	W	Co	C	Ti
wt.%	79	12	7	2

●Flat plates of aluminum or graphite with an area of $4cm^2$ were used as the cathode electrode according to the designed experiment.

● Nitric acid (HNO_3) from Central Drug House (P) Ltd. (CDH) was used as electrolyte solution. The concentration and molecular weight (M.W.) of this acid was 69% and 63.01g/mole respectively.

●Powder of graphite was used for reduction of the tungsten oxide WO_3 produced by the calcination of H_2WO_4. The purity of graphite powder was 99.6%.The source of this powder is Lemandou Chemicals Co., Ltd. China.

The powder's particle size of graphite was analyzed using a laser particle size instrument Type (Better size 2000). The tests were performed at Ceramics and Building Materials Labs, College of Materials Engineering, University of Babylon. Figure (3.2) displays the results. It is evident that the average particle size of the graphite powder is around 4.352 μm.

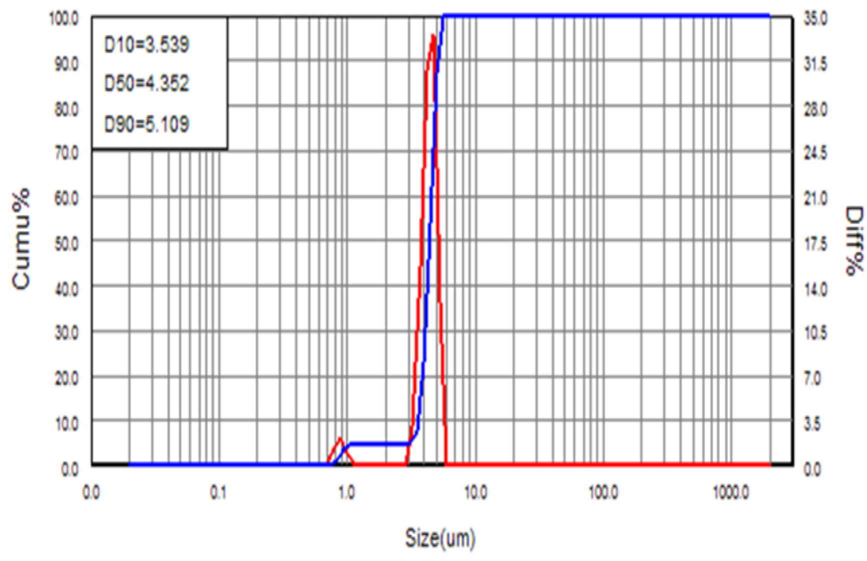

Diam um	Percent
0.100	0.00
0.200	0.00
0.500	0.00
1.000	4.08
2.000	4.66
5.000	87.81
10.000	100.00
20.000	100.00
45.000	100.00
75.000	100.00

Figure (3.2): Analysis of Particle Size for Graphite Powder.

3.3.2 Materials Used in the Coating Process

- Stainless steel type 316 with the hardness 256 Kg/mm^2 HV and chemical composition shown in table (3.2) was used as a substrate material.

Table (3.2): Chemical Composition of the Stainless Steel Used As the Substrate.

Compositions	C	Si	Cr	Mn	Ni	Mo	Fe
%	0.05	0.6	16	1.6	10.4	2.2	69.15

- Powder of cobalt was used after mixing with tungsten carbide. The purity and the average particle size of cobalt powder was 99.7% and 7.285 µm respectively. The source of this powder is Lemandou Chemicals Co., Ltd. China.

3.4 Experimental Procedure for WC Recovery

The process of preparing tungsten carbide powder includes three stages, the first stage is the preparation of tungstic acid powder by the electrochemical method, the second step, tungstic acid powder is converted to tungsten oxide powder (WO_3) by calcination. Finally, the third step, the tungsten carbide powder was obtained by reduction of tungsten oxides with graphite.

3.4.1 Preparation of Tungstic Acid Powder

This stage includes the preparation of tungstic acid powder by electrochemical method.

Experimental design is an essential tool for engineers and scientists. The wide range of (DOE) has improved the performance of processes and the development of the new process. Taguchi orthogonal array of Program (Minitab 17) was used to examine statistically the combined influence of electrochemical variables (current density, concentration, temperature and type of cathode) on the weight loss/hour and the power consumption. The specimens resulting from the experiment with the best readings was used in subsequent operations.

The electrolyte solutions were made with a 69 percent concentration of nitric acid (HNO_3). The acid was dilute with regular distilled water. Filter sheets were used to separate the created tungstic acid from the discarded electrolyte. Experimental cell is shown in Figure (3.3). The electrolysis cell was a glass beaker, with the cathode and anode electrodes being a plate of (aluminum or graphite) and a piece of carbide cutting tool, respectively. Before each experiment, the electrodes were polished with (220, 320, and 800) grit sandpaper to remove any contaminations on the surface, and then ethanol has been used to remove any grease. A digital DC power supply is connected to the cell in the electrical circuit, which is utilized to record the cell's electric current and voltage. The electrolyte solution was stirred with a magnetic stirrer.

To start the experiments, a desired concentration of nitric acid (0.4M to 1.8M) was generated and utilized as the electrolyte solution. The spacing between both electrodes was fixed at 5 cm, and the surface area of the cathode and anode was set at 4 cm^2. Electrolysis began at time zero and lasted for up to (1.5) hours.

The scrapped carbides are dissociated into tungstic acid, and CO_2 and H_2 gases according to the reaction bellow [110]:

$$WC + 6H_2O \longrightarrow H_2WO_4 + CO_2 + 5H_2 \qquad (3.1)$$

$$Co \longrightarrow Co^{2+} + 2e- \qquad (3.2)$$

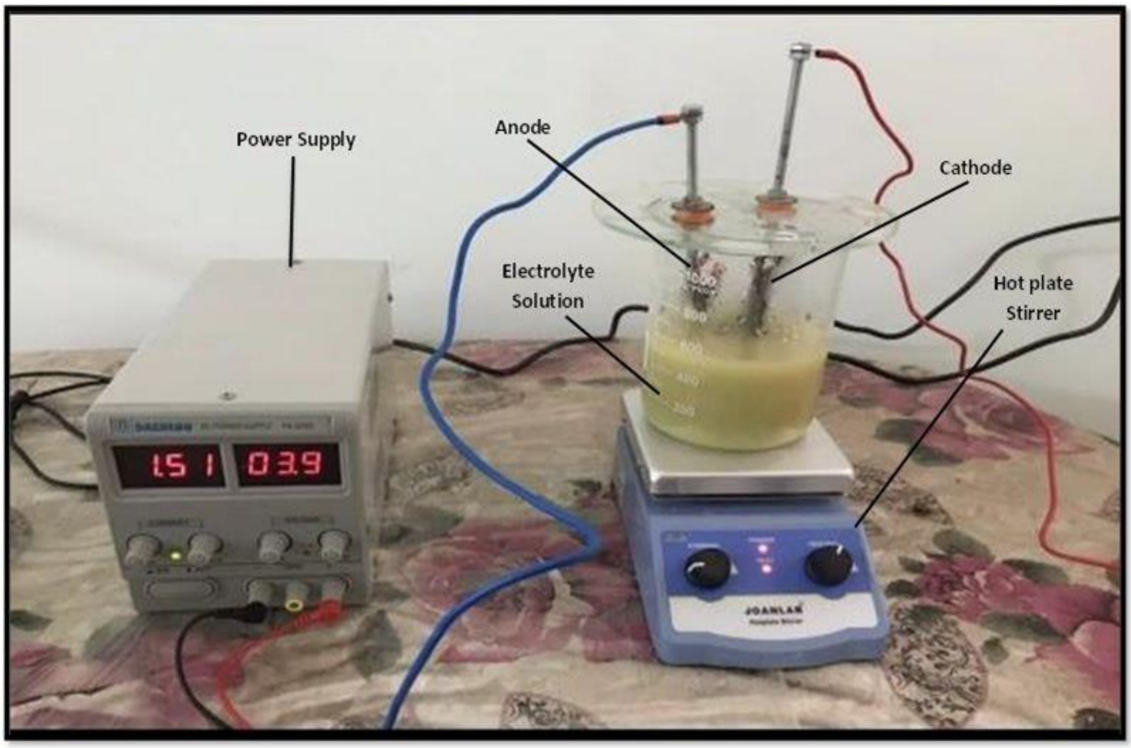

Figure (3.3): Electrolysis Cell.

The produced tungstic acid (H_2WO_4) shown in Figure (3.4), which is insoluble in the electrolyte solution precipitated in the bottom of the cell.

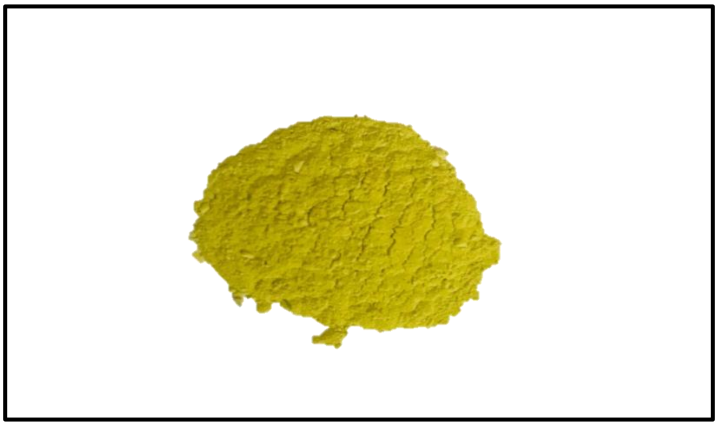

Figure (3.4): Tungstic Acid.

3.4.2. Preparation of WO_3 Powders

To get stable monoclinic WO_3, the tungstic acid obtained from the previous step was heated for 4 hour at 800℃ in an electric furnace type (Gallenkamp, British Made, Max. Temp. 1100℃) available at the University of Babylon/ college of Materials Engineering/ Metallurgical Laboratories. The specimens were charged by ceramic crucible and then heated at a rate of 10^{O}C/min until the desired temperature is reached. When the procedure ended, the specimens were left inside the furnace to cool to the room temperature.

3.4.3. Tungsten Carbide Powder Preparation

The prepared WO_3 powder from the previous step was mixed with the graphite powder. The process was achieved by electrical mixer, type STGQM-15⁄-2 so that powder particles are distributed perfectly and uniformly. The produced mixture shown in figure (3.5) was used for the next step.

Figure (3.5): Mixture of WO_3+ Graphite Powder.

The preparation of WC powders process was carried out using electrical tube furnace. According to the following experimental procedures: the specimens were accurately weighted (the weight of the specimen was 10g)using an electronic balance and then placed into ceramic crucible. The crucible was put into the reaction tube at a set distance while the reaction tube was fixed in place at a preset location in the furnace. For the reduction with graphite, argon was employed as the flushing gas. Before the furnace was heated, the system was flushed for (10-15) minutes. The specimens were then heated to different temperatures (900, 1100 and 1200) ^{O}C. The furnace was turned off at the end of the run; the specimens were allowed to cool in the furnace until their temperature reached the room temperature. The specimens removed from the furnace and their weights were recorded.

3.5 Coating Process

The coating process includes several steps as follows:

3.5.1 Substrate Preparation

Stainless steel (316) substrate has been cut by wire cutting machine with dimensions of (20×20×4 mm). The substrate preparation is the most critical step in the spraying operations. At first all surface contaminants including oil, paint and scale must be removed by acetone, because adhesion of coating is related to roughness and cleanliness of the surface. After cleaning the substrate surface is roughened prior to coating so as to increase the surface roughness of specimens, therefore a better adherent between substrate and applied layer. The specimens were roughed using the sand shoot a blast technique to produce a rough surface (equal to Ra=50µm) in accordance with (DIN) specification.

3.5.2 WC-Co Powder Coating Preparation

The specimens were coated with ceramic surface layer consisted of mixture of tungsten carbide powder (WC) and cobalt powder (Co) with three different compositions (WC-8wt%Co, WC-12wt%Co and WC-

16wt%Co). The process was achieved by electrical mixer, type STGQM-15⁄-2 for one hour so that powder particles are distributed perfectly and uniformly.

3.6 Flame Thermal Spray Process

This work used the flame thermal spraying method. The spray gun was linked to an automated control system for automatic spraying. To achieve uniform distribution of the deposited metal on the substrate surface, the amount of powder entering the spray gun was controlled using an electronic pulse technology system, which was mounted on a table moving with a bi coordinate system (X, Y), as shown in Figure (3.6).

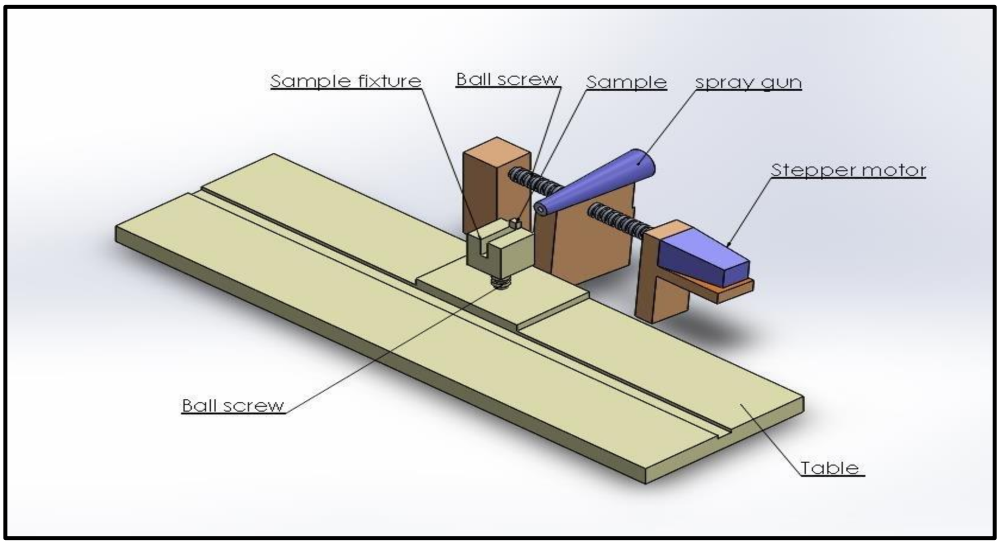

Figure (3.6): Sketch for Thermal Spray System.

Thermal spray coating was done in this work utilising an oxyacetylene thermal spray gun. On a flat surface, the specimens were placed in front of a spray gun. The specimens fixture was made consisting of a ball screw and a stepper motor that allowed for upward and downwards movement. Table (3.3) shows the parameters associated with the thermal spray method.

Table (3.3): Flame Thermal Spray Parameters [116,119,122]

Pressure of oxygen (bar)	0.5
Pressure of acetylene (bar)	1
Feeding of powder (g/min)	25
Distance of spray, mm	120

3.7 Conditions of Coating

The effect of the velocity of the powder's particles and the wt% of the added cobalt powder were studied. The layer thickness, microstructure, surface roughness, hardness and wear resistance were considered as the response parameters. Table (3.4) shows the code of each substrate specimen and the values of the choosed variables. The experiments were setted according to Taguchi orthogonal array design L(3*2) via the software minitabe17.

Table (3.4): Code of Each Parameter Used in Coating.

Code	Top Coat
A1	WC-8%Co ,velocity 300m/min
A2	WC-8%Co, velocity 400 m/min
A3	WC-8%Co, velocity 500 m/min
B1	WC-12%Co, velocity 300 m/min
B2	WC-12%Co, velocity 400 m/min
B3	WC-12%Co, velocity 500 m/min
C1	WC-16%Co, velocity 300 m/min
C2	WC-16%Co, velocity 400 m/min
C3	WC-16%Co, velocity 500m/min

3.8 Tests for the Produced Powders and the Coating Layers

3.8.1 SEM-EDS Analysis

Images of SEM were captured to investigate the microstructure clearly with high accuracy of the prepared powders. This analysis has been done using a Field Emission Scanning Electron Microscope inspect F50, made in Netherland.

SEM examination also is used to know the morphology of coated surface. Some of these specimens were used to attain the cross sectional to determine other features for instance microstructure of underneath surface and thickness of coating accordance with ASTM F1372. The microstructure analysis and the thickness measurement were performed. Figure (3.7) shows SEM apparatus that has been used.

Figure (3.7): Scanning electron microscope.

3.8.2 X-Ray Diffraction Analysis

X-ray diffraction analysis was carried out for H_2WO_4, WO_3 and WC powders in order to identify each powder separately.

X-ray diffraction analysis of fine powder formulations on a glass slide was performed to ensure the produced powder for the final specimens. The X-ray tube's target is copper with a wavelength of 1.540 A^{O}, voltage and current of 40kV and 30mA, and a scanning speed one degree/minute for a scanning range of ($2\theta^{\circ}$=20-80). To identify the phases found in the original powders, X-ray diffraction was used and to ensure that the tungsten carbide and cobalt is present in the coating and to specify if there is any chemical reaction between the coating materials and the substrate. Figure (3.8) shows XRD apparatus that has been used.

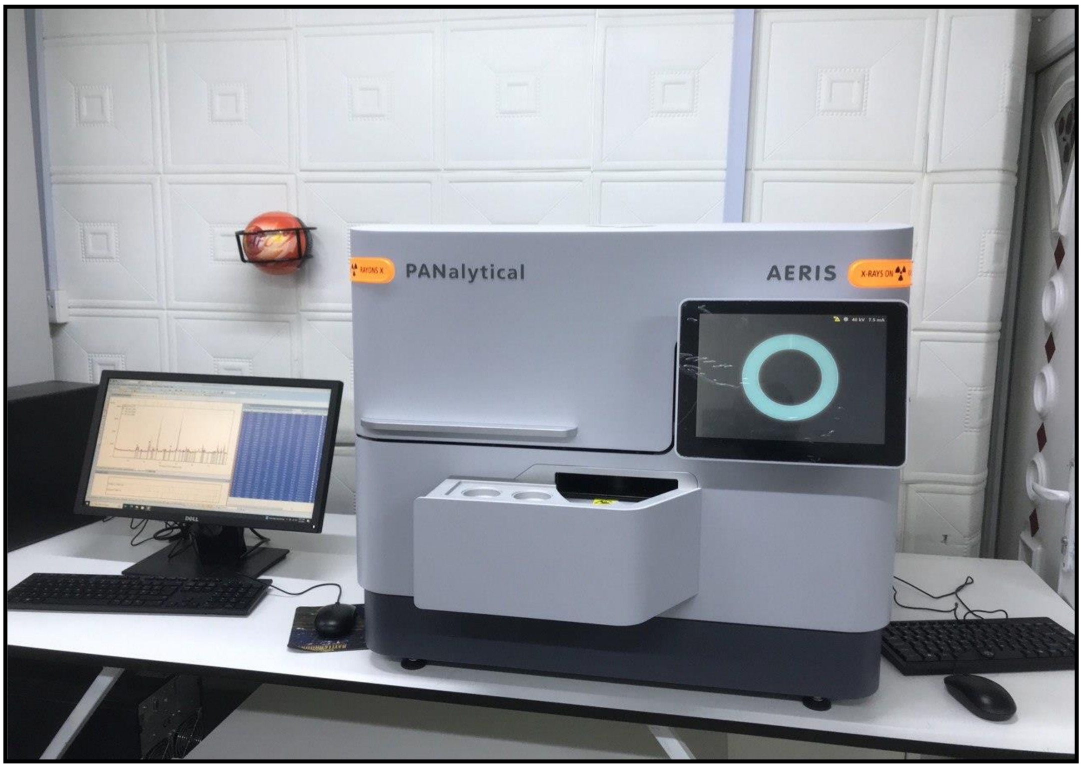

Figure (3.8): X-ray diffraction apparatus.

3.8.3 Thermogravimetric Analysis (TGA)

Investigations were performed using both isothermal and temperature-programmed thermogravimetry (TG). The Curie point method was used to check the temperature calibration of the TG furnace. When experiments were conducted in argon, the system was flushed with argon at 170 ml min^{-1} for at least 20 min before the experiment was started. Experiments at higher temperatures were carried out on a Setaram TGA 92 system. Specimens of 40 to 90 mg from WO_3 were held in an alumina crucible. The specimens were heated from 25 °C to 925 °C and at a heating rate of 10 °C/min. The analysis was carried out at the Tarbiat Modares University/Iran.

3.8.4 Wear Test

This test was carried out using the pin-on-disc method. The tester used for evaluating wear was of the MT4003 version 10.0 settings and data collection software. The experiment took place at room temperature for 25min with a 15N weight. The velocity of sliding was (0.5m/sec). The pin was a ball that is pressed against the revolving disc. Ceramic ball of alumina was used for testing. Weighing the specimens by a sensitive scale with an accuracy of four digits before and after the test to calculate the weight loss. The test was utilized in (the Lab of University of Babylon, Department of Metallurgical Engineering/College of Materials engineering). The wear instrument that was used in this work showed in Figure (3.9). The wear rate of the specimen is then calculated [123].

$$W.R = \Delta w / 2\pi rnt \qquad (3.1)$$

Where:-

W.R:- wear rate (g/mm)

ΔW:- weight loss (g) which is the difference in weight of the specimenss before and after the test.

t:- Sliding time (min.).

r:- The radius of the specimens to the center of the disc (3mm).

n:- Disk rotational speed (250 rev/min).

Figure (3.9): The Wear Machine.

3.8.5 Micro Hardness Measurement for Coating Specimens

The Vickers hardness test involves pressing a square pyramid indenter into a material with a defined amount of force to leave a square indentation. Under the microscope, the indentation's diagonals are measured. Vickers hardness is determined using the following formula (3.2). The indenter's force (F) in grammes and the average length of the diagonal indentation (d) are needed for this calculation[124].

$$HV = \frac{F}{A} \approx \frac{1.8544 * F}{d^2} \quad (3.2)$$

Digital micro hardness tester type (TH 715, Beijing times high technology Ltd) was used. Vickers hardness tests were carried out with a load of 300g with a holding time for 15 second. An average hardness value was determined based on ten indentations.

3.5.6 Surface Roughness Measurement

For all coating specimen, the surface roughness was measured. A surface roughness tester (TR200ohand-held roughness tester, model TA620Stann and Co, timeegroups Inc.) was used to measure the roughness accordance with ASTM D7127. In each case the specimens was mounted on a flat base then the distance to be tested was appointed and the probe of the measuring instruments was attached by special lever to the surface of the specimens, after that the instrument was switched on with continuous movement of the probe into front and behind. The instrument registration board gives the roughness value (Ra) directly and the maximum reading was recorded. Figure (3.10) shows surface roughness device. An average of five measurements was considered in this test. The test was utilized in (the Lab of University of Babylon, Department of Metallurgical Engineering/College of Materials engineering).

Figure (3.10): Surface Roughness Device.

CHAPTER
Four
RESULTS AND DISCUSSION

Chapter Four

Results and Discussions

4.1 Introduction

This chapter demonstrates and explores all the results of the tests conducted throughout this work. The chapter is divided into four parts. The first part contains the optimum electrochemical conditions by using Grey Relational Grades (GRG), based on the Taguchi Method. At this part, tungstic acid powder was obtained. In the second part, tungstic acid powder is converted to tungsten oxide powder (WO_3). In the third part, the tungsten carbide powder was obtained. Finaly, the forth part reveals the characterization, mechanical, and physical examinations of (WC-Co) coating layers.

4.2 Electrochemical Cell

Experimental program was designed according to Taguchi method. The current density, the electrolyte temperature, the electrolyte concentration and the material of the electrodes were considered as the affecting parameters, while the amount of produced material and the energy consumption were considered as the responses. Table (4.1) shows the code of each parameter, its levels and the value for each level. These levels were selected based on several previous experiments to determine the highest and lowest values for these parameters and then select the more affecting values. Table (4.2) shows the designed experiment according to Taguchi L16, and the resulted responses due to each experiment.

Table (4.1): Effected Parameters, Codes, Levels.

Parameter	Code	Levels			
		1	2	3	4
Current density(A/m^2)	A	1000	2000	3000	4000
Concentration (M)	B	0.4	0.8	1.4	1.8
Temperature (^{O}C)	C	25	40	55	70
Cathode	D	Aluminum	Graphite		

The power consumption was calculated for each experiment according to the following equation [125]:

$$\mathbf{P\ (kW.h/kg)} = \frac{V_{cell} * I * t}{W_{act.}} \qquad (4.1)$$

Where V_{cell}: the cell voltage (V); I: the current applied (A); t: the time of the deposit (hr); and $W_{act.}$: the actual weight of the deposit (kg).

Table (4.2): The Designed Electrochemical Experiments and the Resulted Responses.

Experiment	Coded Parameters				Experimental Results	
No.	A	B	C	D	Weight loss/Hour g/hr.	Power Consumption kW.h/kg
1	1	1	1	1	0.285	4.672
2	1	2	2	1	0.320	4.741
3	1	3	3	2	0.256	4.602
4	1	4	4	2	0.346	3.075
5	2	1	2	2	0.591	7.111
6	2	2	1	2	0.512	5.712
7	2	3	4	1	0.681	3.633
8	2	4	3	1	0.650	5.076
9	3	1	3	1	0.981	6.798
10	3	2	4	1	1.009	4.481
11	3	3	1	2	0.955	5.918
12	3	4	2	2	0.915	5.806
13	4	1	4	2	1.324	8.04
14	4	2	3	2	1.321	6.357
15	4	3	2	1	1.261	6.065
16	4	4	1	1	1.209	5.708

4.3 Parametric Analysis of the Responses

Analysis of variance by Minitab (Version 17) was done to all results to investigate the effect of the selected affecting parameters on each output parameter. Main effect plots were used to indicate the effects of the studied parameters on the responses.

4.3.1 Influence of the Effecting Parameters on the Weight loss/Hour

Figure (4.1) shows the plots of the major effects of the controllable factors on the Weight loss/Hour**.**

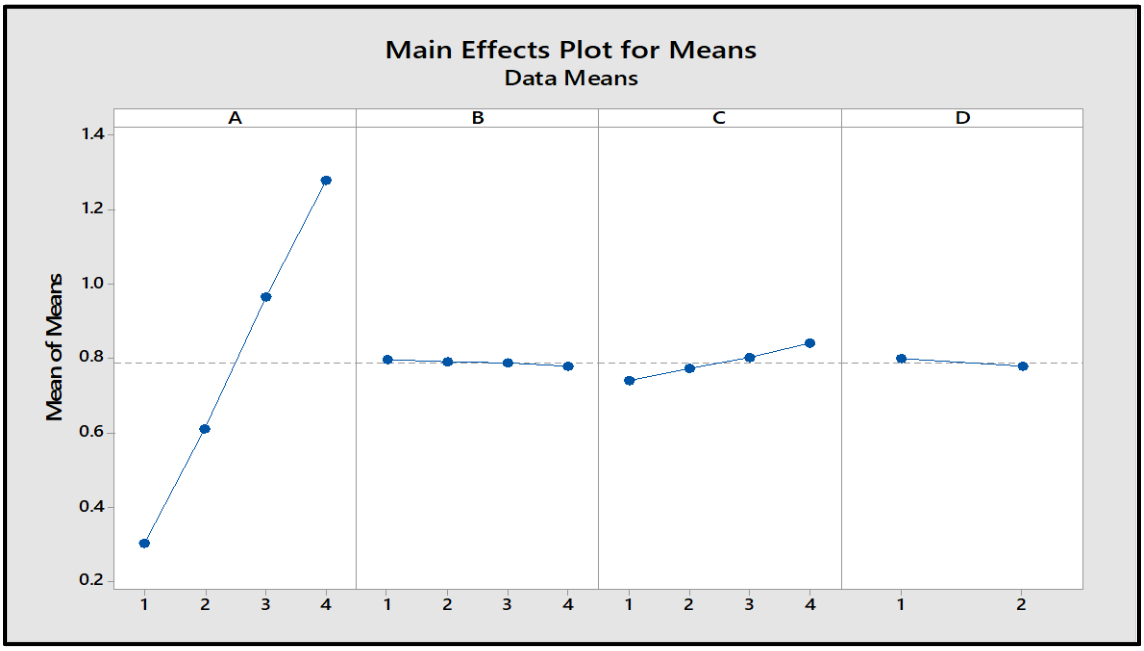

Figure (4.1): Effect of the Parameters on the Weight loss/Hour.

The plot shows the amount of weight loss of carbide pieces for four different current densities. As shown, the weight loss of the anode linearly increased with time for each particular current density, and no passivation occurred during the process. This is according to First law of Faraday: (the amount of electricity passing through an electrolyte directly proportionately determines the chemical deposition caused by the passage of current across it). The weight loss is more significant for higher current densities. It was also seen that in the case of the lower current densities 1000 A/m^2 , the rate of decomposition of anode was very low, and, therefore, a very long time would have been required to reach complete destruction of the carbide pieces. On the other hand, the current densities higher than 4000 A/m^2 may produce some operational difficulties including heating and evaporation of the electrolyte solution.

The effect of electrolyte concentration on weight loss of carbide pieces was another variable which was studied. Various sets of experiments were conducted at current densities of 1000, 2000, 3000 and 4000 A/m^2 while the electrolyte concentration was kept at (0.4, 0.8, 1.4 and 1.8%). This observation verifies that the anode weight loss has a weak dependence on the electrolyte concentration. But is strongly dependent on the current density of the electrolysis cell. These results agree well with those reported in [105]. The polarization of the anode and cathode is reduced and the electrolyte conductivity is increased as the electrolyte temperature rises and this leads to increase of the weight loss. This is according to Arrhenius Equation. The results indicated that the anode weight loss with the graphite electrode is lesser than that when the aluminum electrode is used due to the conductivity of aluminum is higher than that of graphite, so the efficiency of the electrode is higher.

4.3.2 Influence of the Effecting Parameters on the Power Consumption (kW.h/kg)

Figure (4.2) shows the main effects plot of each inputs parameters on the power consumption. By using equation (4.1), the power consumption, i.e., the power consumed per kilogram of tungstic acid produced, was calculated.

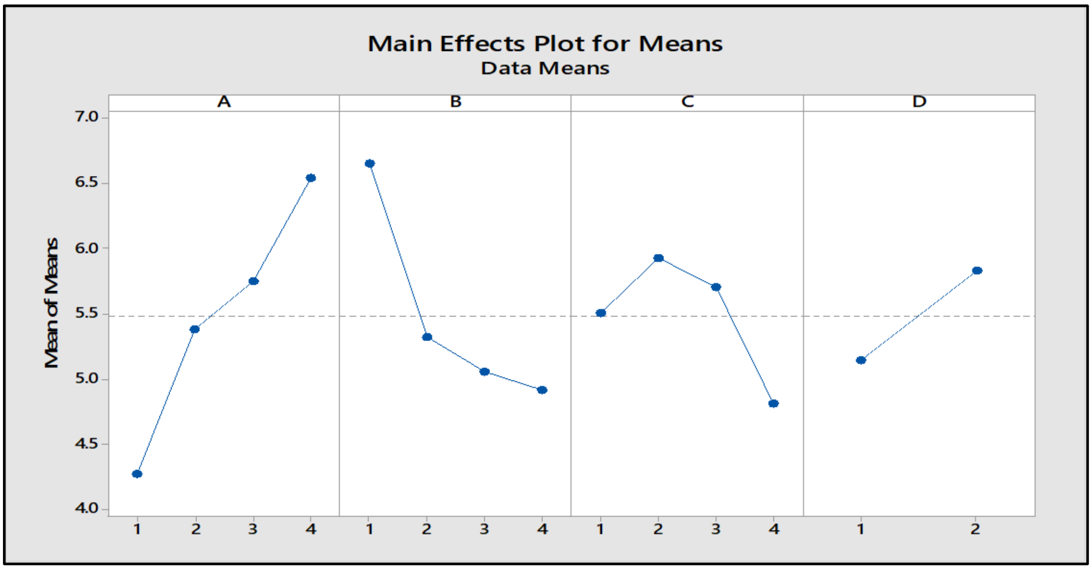

Figure (4.2): Effect of the Parameters on the Power Consumption.

As shown in figure (4.2) the consumed power increased when current density of the cell increased. Apparently, this observation is attributable to the lower efficiency of the system at higher current densities. In other words, although the higher current densities would advance the process more quickly, the efficiency of the power usage decreased due partly to the conversion of power to heat. On the other hand, as can be seen from this figure the consumed power decreased when the concentration of the electrolyte increased. This observation might be attributed to the decline in the resistance of the electrolyte solution which takes place at higher ionic concentrations. Results indicate that the power consumption decrease with increasing temperature. This is the result of a solution viscosity drop which leads to an increase in the mobility and diffusivity of ions, thus enhancing mass transfer phenomena. The results indicate that the power consumption with the aluminum electrode is lesser than that when the graphite electrode is used due to the conductivity of aluminum is higher than that of graphite, so the wasted energy is less.

4.4 GRA Optimization Method

The dynamic problems of multi-objective optimization can be reduced to a single target problem using the Taguchi system-aligned grey relational analyses (GRA). In GRA, the average of the experiment's grey relational coefficients (GRCs) is determined. Grey relational grade (GRG) is the name given to this average that corresponds to each response. Higher GRG indicates that the reaction is getting close to its ideal value. According to the equations (2.13 to 2.18) and application of (GRA), the results are shown in table (4.3).

Table (4.3): The Result of Grey Relational Analysis.

Exp No.	Normalized Value		Sequences of Deviations		GRC		GRG	Rank
	Wt./h	Kw. h/kg	Wt./h	Kw. h/kg	Wt./h	Kw. h/kg		
1	0.027	0.678	0.973	0.322	0.339	0.609	0.474	13
2	0.060	0.664	0.940	0.336	0.347	0.598	0.473	14
3	0.000	0.692	1.000	0.308	0.333	0.619	0.476	12
4	0.084	1.000	0.916	0.000	0.353	1.000	0.677	2
5	0.314	0.187	0.686	0.813	0.421	0.381	0.401	16
6	0.240	0.469	0.760	0.531	0.397	0.485	0.441	15
7	0.398	0.888	0.602	0.112	0.454	0.816	0.635	6
8	0.369	0.597	0.631	0.403	0.442	0.554	0.498	11
9	0.679	0.250	0.321	0.750	0.609	0.400	0.504	10
10	0.705	0.717	0.295	0.283	0.629	0.638	0.634	7
11	0.654	0.427	0.346	0.573	0.591	0.466	0.529	8
12	0.617	0.450	0.383	0.550	0.566	0.476	0.521	9
13	1.000	0.000	0.000	1.000	1.000	0.333	0.667	4
14	0.997	0.339	0.003	0.661	0.994	0.431	0.713	1
15	0.941	0.398	0.059	0.602	0.894	0.454	0.674	3
16	0.892	0.470	0.108	0.530	0.823	0.485	0.654	5

During the electrochemical method of the prepared specimen s, the optimum process parameter level is (current density 4000 A/m^2, solution concentration 1.8%, temperature 70°C and cathode electrode Al) as shown in figure (4.3) and table (4.4).

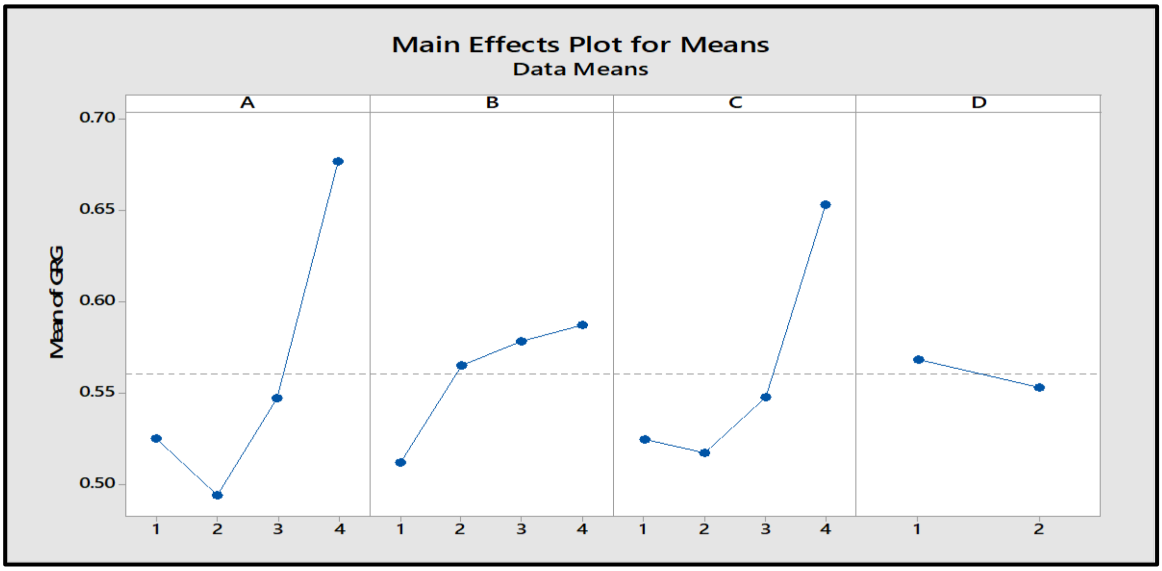

Figure (4.3): Grey Relational Grade Graph.

Table (4.4) demonstrates the delta value, which is the difference between the average GRG's maximum and minimum values.

Table (4.4): Mean GRG for the Affecting Parameters

Level	A	B	C	D
1	0.5249	0.5116	0.5244	0.5683*
2	0.4937	0.5650	0.5173	0.5530
3	0.5470	0.5785	0.5478	---
4	0.6768*	0.5874*	0.6530*	---
Delta(Max-Min)	0.1831	0.0759	0.1357	0.0153
Rank	1	3	2	4
*Levels for optimum GRG				

It is clear from table (4.4) that the current density (Δ = 0.1831) has the highest influence on electrochemical process followed by temperature (Δ = 0.1357), electrolyte concentration (Δ = 0.0759) and type of cathode electrode (Δ = 0.0153) as listed in the table's last row.

4.5 Mathematical Models for the Responses

For predicting, regression models were developed the weight loss/Hour (g/hr) and power consumption (Kw.h/kg) under various electrochemical process via Datafit (Versions9.1) software. In order to identify mathematical models that genuinely express these elements, a variety of linear, exponential, power function, and non-linear quadratic polynomial equations were studied. The calculation was based on the coefficient of multiple determination coefficients (R^2). The models and its determination coefficients are presented in table (4.5).

The models in table (4.5) give a prediction for the metal weight loss /Hour and power consumption for the range of the experimentation that was done.

Table (4.5): Mathematical Models for Weight Loss/Hour and Power Consumption.

Electrode	Response	Mathematical Model	R^2
Al	weight loss/Hour, W	**W**$=3.1530*10^{-04}A-1.6309*10^{-02}B+2.1266*10^{-03}*C-7.3480*10^{-02}$	**99%**
	power consumption, P	$P=2.9393*10^{-3}A-2.1741B+0.1799C-4.6546*10^{-7}A^2+0.6821B^2-2.3255*10^{-3}C^2$	**99%**
Gr.	weight loss/Hour, W	**W**$=3.4895*10^{-04}*A+2.5952*10^{-02}B+2.2666*10^{-03}*C-0.2285$	**99%**
	power consumption, P	**P**$=6.4984*10^{-04}A-1.8950B-1.1676*10^{-02}C+6.6526$	**89%**

A: Current Density, B:Concentration, C:Temperature

The predicted and experimental values of the responses parameters are listed in table (4.6). The difference among the experimental and predicted responses values based on the developed models is shown in figure (4.4).

The scatter plot diagrams showed in the figure shows that models are able to describe responses in the experimental field.

Table (4.6): Experimental and Predicted Responses Values.

Exp. No.	Exp. W(Al)	Predicted W(Al)	Exp. P(Al)	Predicted P(Al)	Exp. No.	Exp. W(C)	Predicted W(C)	Exp. P(C)	Predicted P(C)
1	0.285	0.2884	4.672	4.7573	3	0.256	0.2814	4.602	4.0072
2	0.320	0.3138	4.741	4.6463	4	0.346	0.3258	3.075	3.0741
7	0.681	0.6831	3.633	3.5079	5	0.591	0.5704	7.111	6.7272
8	0.650	0.6447	5.076	5.1732	6	0.512	0.5468	5.712	6.1443
9	0.981	0.9828	6.798	6.7281	11	0.955	0.9113	5.918	5.6572
10	1.009	1.0082	4.481	4.5240	12	0.915	0.9557	5.806	4.7240
15	1.261	1.2499	6.065	6.07821	13	1.324	1.3363	8.040	7.6766
16	1.209	1.2115	5.708	5.6505	14	1.321	1.3127	6.357	7.0937

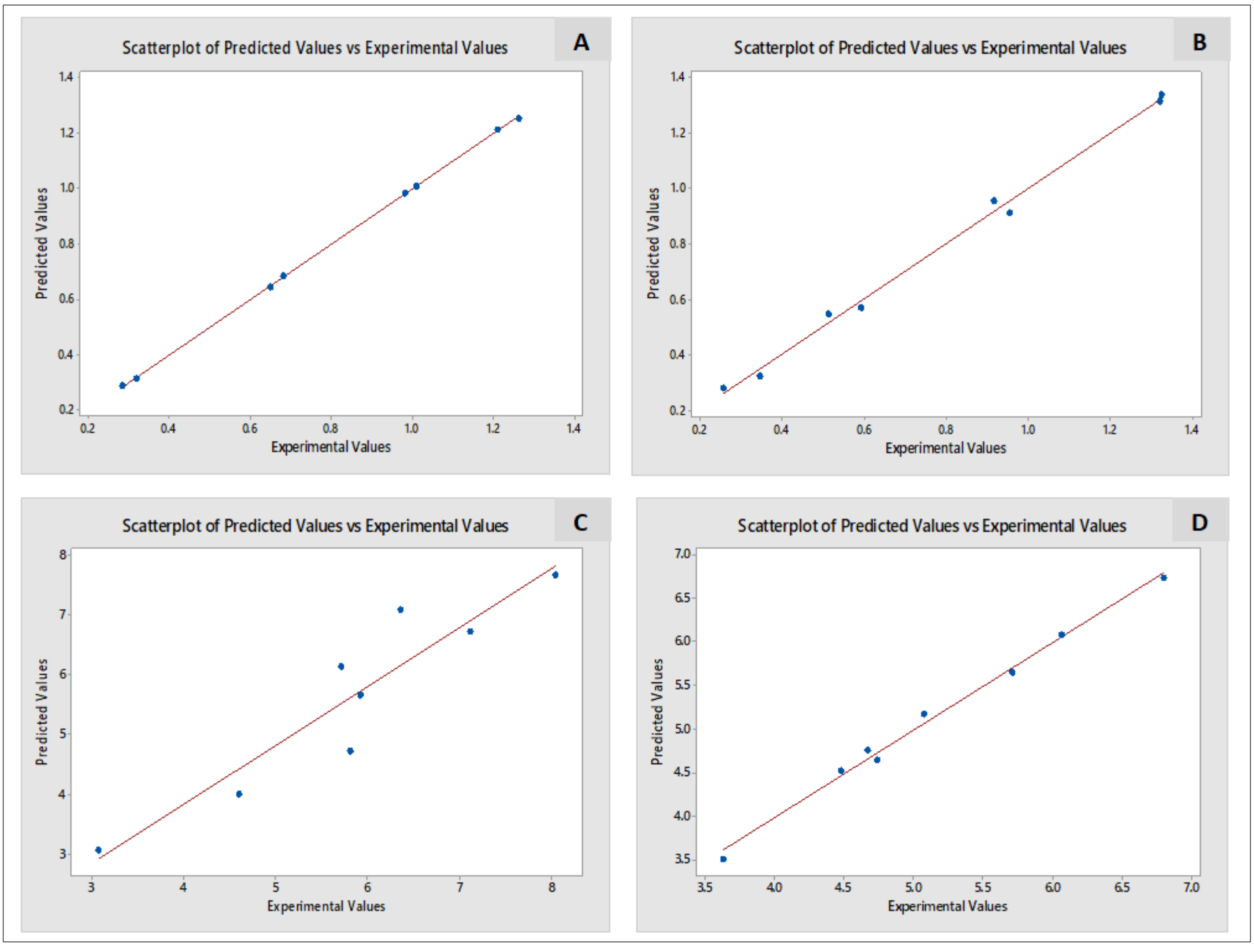

Figure (4.4): Scatter Plot Diagram for Experimental and Predicted Values, A) weighloss/Hour for Gr., B) weight loss/Hour for Al, C) Power Consumption for Gr., D) Power Consumption for Al.

4.6 Analysis of Variance (ANOVA)

Weight loss and power consumption have both been subjected to ANOVA. Tables (4.7) and (4.8) provide the results in separate tabulations so that each variable's effect on the responses can be determined. Degrees of freedom related with the specimen variance are two and three, which may be used to calculate the F-ratio of two specimen level of confidence (95%). The confidence level and parameter significance may be determined by comparing the F-value (the parameter is significant if $0 < P < 0.05$) [102].

Table (4.7): ANOVA Results for Weight Loss

Source	DF	Adj SS	ADj MS	F-Value	P-Value
i	3	2.16329	0.721097	331.68	0.000
Con.	3	0.00049	0.000162	0.07	0.971
Temp.	3	0.2177	0.007258	3.34	0.114
Electrode	1	0.00194	0.001936	0.89	0.389
Error	5	0.01087	0.002174		
Total	15	2.19836			

Table (4.7) indicates that the current density (A) has an effective influence on the output parameters (weight loss/Hour) because of P-value is lesser than 0.05. Concentration (B), temperature(C) and type of cathode (D) have an effective influence on (weight loss/Hour) but less influence because of (P value) greater than 0.05.

Table (4.8): ANOVA Results for Power Consumption.

Source	DF	Adj SS	ADj MS	F-Value	P-Value
i	3	10.678	3.5593	9.84	0.015
Con.	3	7.618	2.5395	7.02	0.031
Temp.	3	2.833	0.9442	2.61	0.164
Electrode	1	1.854	1.8544	5.13	0.073
Error	5	1.809	0.3617		
Total	15	24.792			

Table (4.8) indicates that the current density (A) and concentration (B) have an effective influence on the output parameters (Power Consumption) because of P-value is lesser than 0.05. Temperature (C) and type of cathode (D) have an effective influence on (Power Consumption) but less influence because of P-value more than 0.05.

4.7 Confirmation Test

Confirmation test has been carried out to verify the characteristics improvement for recovery of tungstic acid. The optimum results are selected for the confirmation test as presented in table (4.9) which shows the comparison of the experimental and predicted results of the Weight loss/Hour and the power consumption for the optimal process parameters obtained using equations presented in table (4.5).

Table (4.9): Result of the Confirmation Test for the Optimum Results.

Level of The Coded Parameters				**Response Parameters**					
A	B	C	D	Weight loss/Hour g/hr.			Power consumption kW.h/kg		
4	4	4	1	Predicted	Experimental	Error%	Predicted	Experimental	Error%
				1.307	1.350	3%	3.804	3.702	2.6%

4.8 X-Ray Diffraction (XRD)

The produced specimen based on the optimum values of the affecting parameters was subjected to an XRD test. Figure (4.5) shows the appearance of peaks for tungstic acid H_2WO_4 according to the international card (ICDD: 00-018-1418). The figure also shows that the highest intensity peak corresponding to the site ($2\theta^{\circ}=25.41176$). This indicates that the material obtained is tungstic acid.

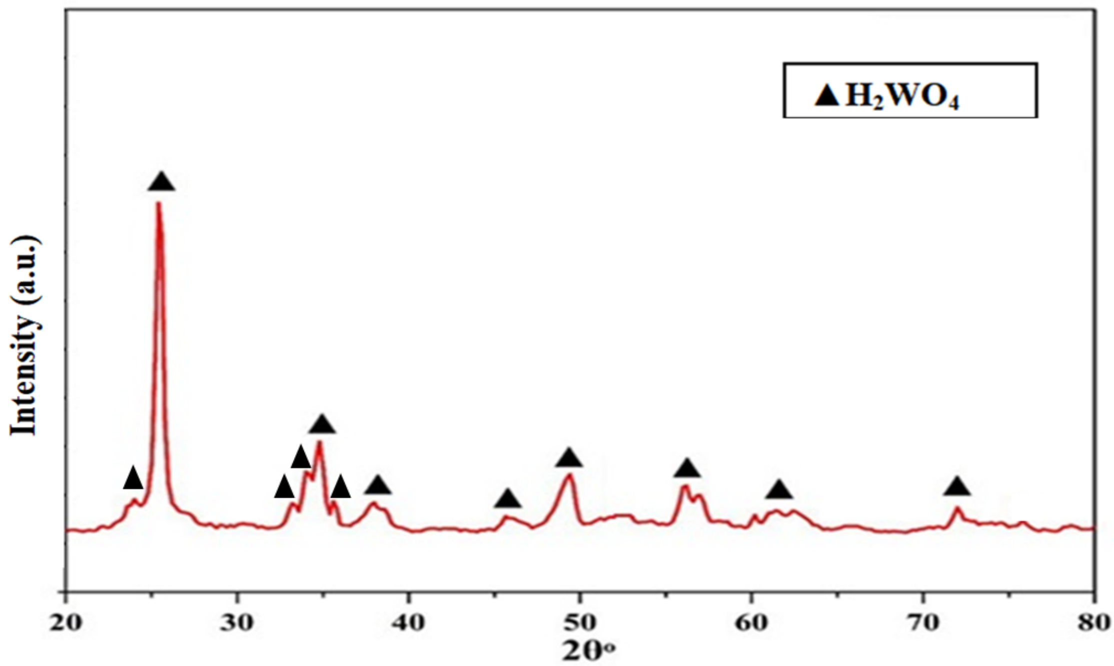

Figure (4.5): XRD Patterns of Tungstic Acid.

4.9 SEM Analysis

Figure (4.6) represents SEM test for the morphologies of tungstic acid obtained from optimal process parameters. The morphologies of tungstic acid show that the particle size distribution is relatively uniform regular spheres.

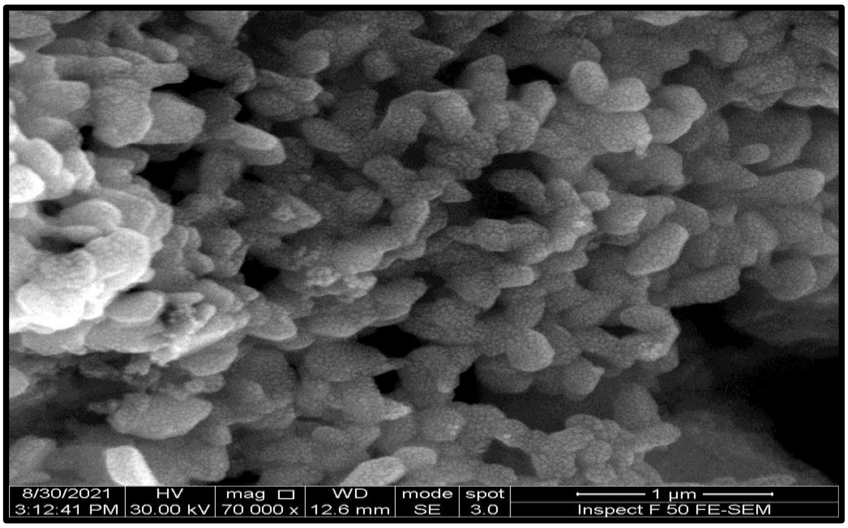

Figures (4.6): SEM for Tungstic Acid.

4.10 Particle Size Analysis

The particles size of H_2WO_4 powder has been analysed. The results are shown in figure (4.7). It is clear that the H_2WO_4 powder have an average particle size of about 11.11 μm.

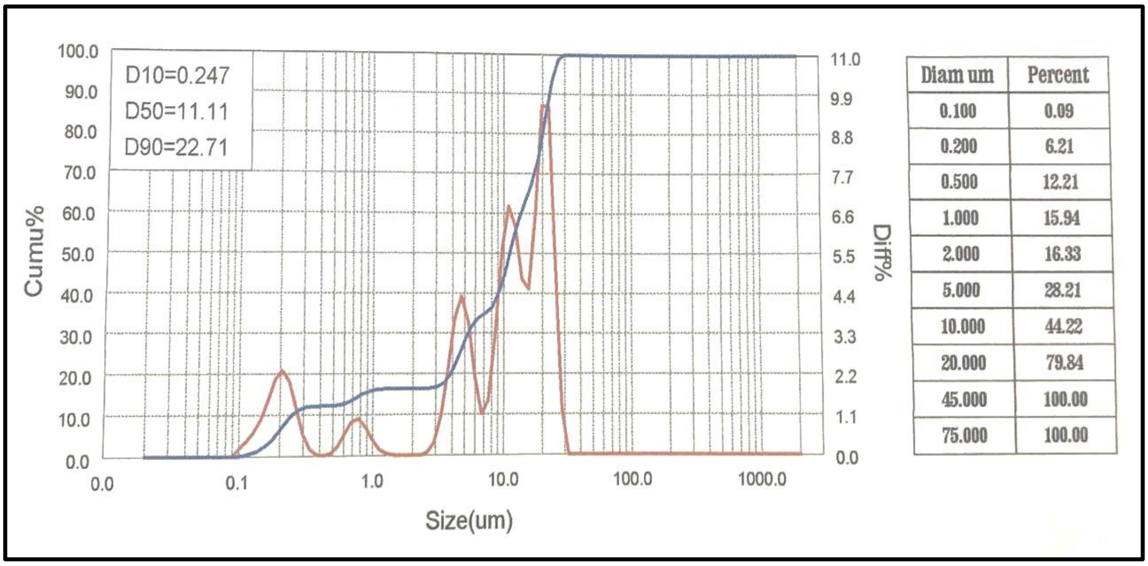

Figure (4.7): Particle Size Analysis for H_2WO_4 Powder.

4.11 Preparation of WO_3 Powders (Calcination)

For the fabrication of tungsten carbide WC, anhydrous tungsten trioxide WO_3 may be required. Tungsten trioxide was prepared by calcination of the tungstic acids ($WO_3.nH_2O$). Tungstic acids was calcined at $800^{O}C$ for 4h in an oxygen rich atmosphere to drive water from the crystal lattice

This process eliminated the structural water and the physically adsorbed water. Additionally, the rate of heating was an important parameter. The water-filled particles agglomerated as a result of the rapid heating rate. The specimens were heated at a rate of $10^{O}C$ per minute and then they were cooled to room temperature.

4.12 Thermogravimetric Analysis (TGA)

The main principle of thermogravimetric analysis (TGA) is that the mass change of a specimen can be studied under programmed conditions. The TG curve in figure (4.8) shows that the specimen is hydrous since the weight loss is insignificant from 30 up to about 200^{O}C with almost no further weight loss observed until 800^{O}C. This means that the aqueous tungsten oxide has been converted into tungsten oxide, and this is the temperature of the conversion to tungsten oxide.

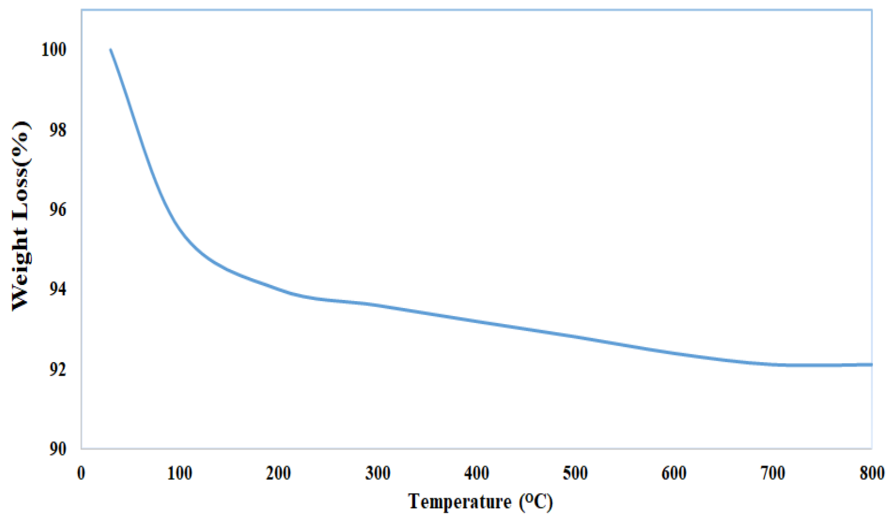

Figure (4.8): The TG curves of thermal decomposition of WO_3 powder.

4.13 X-Ray Diffraction (XRD) for WO_3 Powder

Figure (4.9) show (XRD) patterns of the WO_3 powders as a result of calcination at 800°C. Calcination as deposited specimens in an oxygen rich atmosphere, which was in good agreement with monoclinic WO_3 (ICCD 00-043-1035).

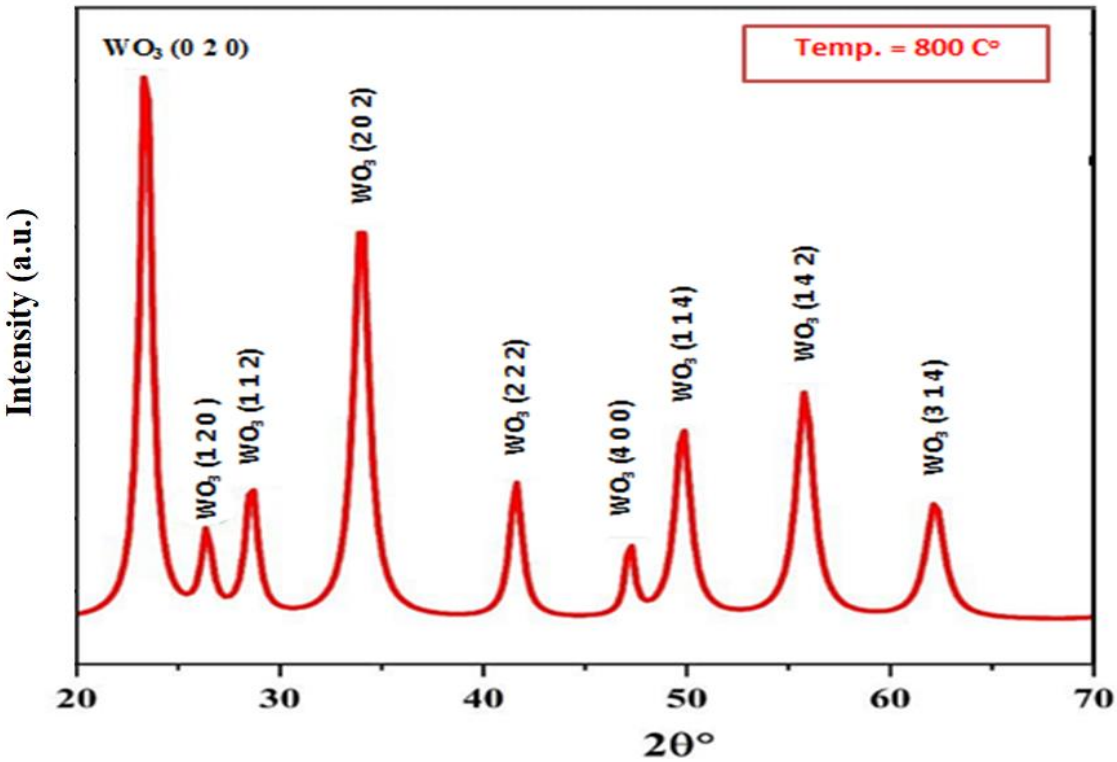

Figure (4.9): XRD of WO_3 Powder Calcination at 800°C.

The resulting powder from this stage at 800°C is WO_3, as shown in the Figure (4.10).

Figure (4.10): WO_3 Powder.

4.14 SEM & EDS Analysis

Figure (4.11) shows some profound effect on the morphology of WO_3 particles produced by calcination of the tungstic acids at 800°C. It is believed with increasing temperature, the diffusion rate increased and this will speed up the coalescence process between neighbouring (grains) and hence producing larger structures.This figure shows the calcined WO_3 powder produced in crystalline form, which looks bars. This indicates a transformation from tungstic acid to WO_3. We can infer that there is a favored crystallographic orientation for the development of WO_3.

The energy dispersive spectroscopy analysis (EDS) of (WO_3) powder as shown in figure (4.12) reveals the presence of only tungsten and oxygen. This ensures the purity of the produced powder.

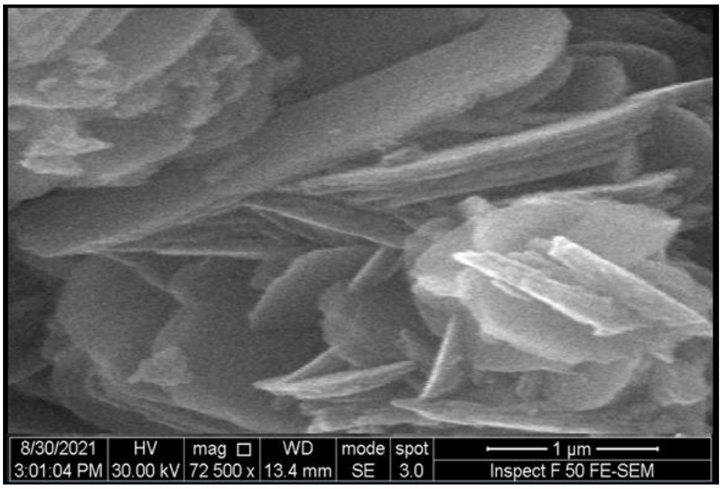

Figure (4.11): The SEM Images of WO_3 Powder Calcined at 800°C.

Element	Atomic %	Atomic % Error	Weight %	Weight % Error
O	75.3	0.6	21.0	0.2
W	24.7	0.2	79.0	0.5

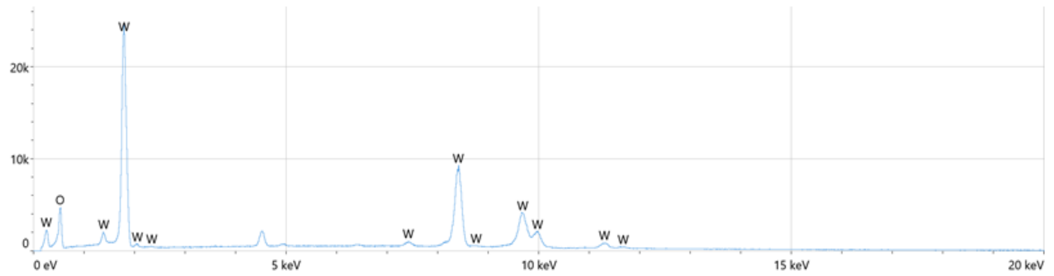

Figure (4.12): EDS of WO_3 Powder.

4.15 Particle Size Analysis for WO_3 Powder

The particles size WO_3 powder at 800°C has been analyzed. The results are shown in figures (4.13). It is clear that the WO_3 powder have an average particle size of 18.38 µm. Grain size of WO_3 powder is larger than that of tungstic acid powder, because when exposed to high temperatures, the particles will aggregate into larger particles.

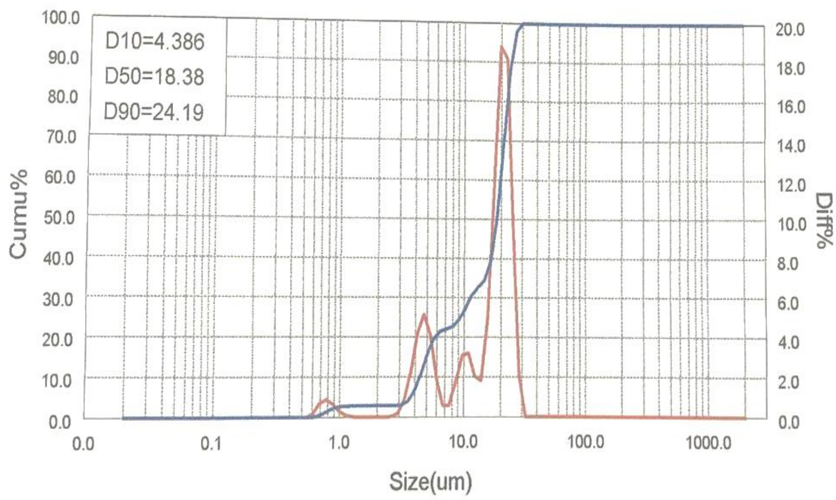

Diam um	Percent
0.100	0.00
0.200	0.00
0.500	0.00
1.000	2.58
2.000	2.80
5.000	15.52
10.000	26.80
20.000	62.28
45.000	100.00
75.000	100.00

Figure (4.13): Particle Size Analysis for WO_3 Powder.

4.16 Reduction of Tungsten Oxides powder Using Graphite

When tungsten oxide WO_3 is used for the production of WC, the efficiency of the synthesis depends on carburization processes and the highest degrees of transformation of $WO_3 \rightarrow WC$ are obtained with combinations of graphite and Argon atmospheres [60]. At the tube furnace system, reactions between mixtures of WO_3 powder and graphite powder in a 1:5 mole ratio took place at 900, 1100 and 1200°C in an argon stream. The starting temperature was 900°C as a lesser temperature indicated a lower rate of reduction. The reaction passes in two steps. The first step produce the products were $W_{20}O_{58}$, $W_{18}O_{49}$ and WO_2. As the temperature increased the rate of reaction was increased to pass through the second step to produce WC as reduction of $W_{20}O_{58}$ and $W_{18}O_{49}$, to WC seemed to occur in a single step [60].

4.17 Thermogravimetric Analysis (TGA)

Thermogravimetric Analysis is mainly used for understanding certain thermal events such as decomposition, oxidation, and reduction. Along with the prediction of thermal stability for specimen s, it is also possible to study the kinetics of chemical reactions under various conditions using TGA. The reaction of a 1:5 mole ratio mixture of WO_3 and graphite was studied in argon by heating the specimen at 3°C min^{-1} up to 925°C.The TG curve in figure (4.14) shows the mass decreases very slowly from 25 to 900°C, and starts decreasing more rapidly above 900°C. This indicates to the reduction of carbon and the reaction is start to transition of mixture of WO_3 and graphite to WC.

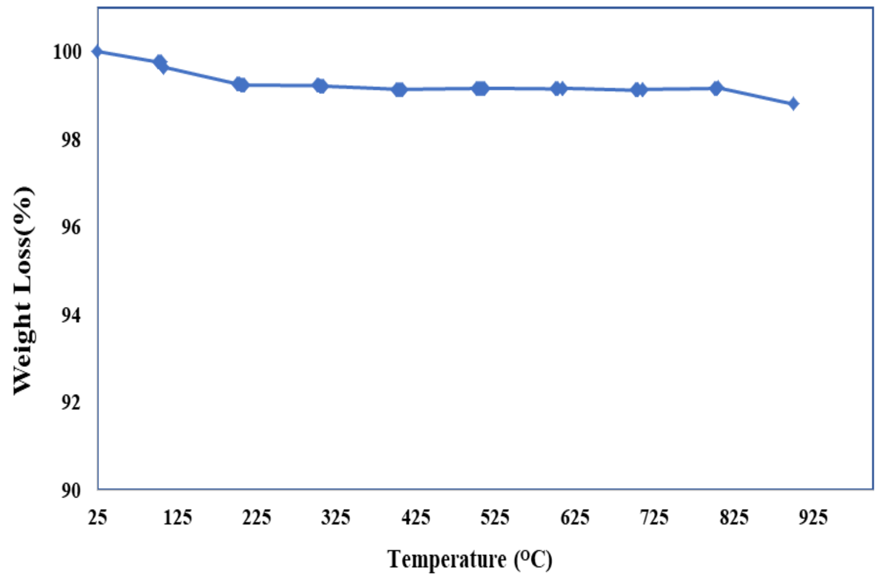

Figure (4.14): The TG Curve of (WO_3+ Graphite).

4.18 X-Ray Diffraction (XRD) for WC Powder

Figures (4.15), (4.16) and (4.17) show the XRD pattern of the reduction product test at 900°C with three different times 45min, 90min, and 135min respectively.

Figures (4.15) and (4.16) show WO_3 is the main phase, with significant amounts of intermediate product $W_{18}O_{49}$ ($WO_{2.72}$) and WO_2 present at this temperature. This result indicated that the time was insufficient and the temperature was lower compared to the required.

In Figure (4.17) WO_3 peaks has disappeared and the intermediate product $W_{18}O_{49}$ and WO_2 are still present, this indicated that the reduction reaction has started.

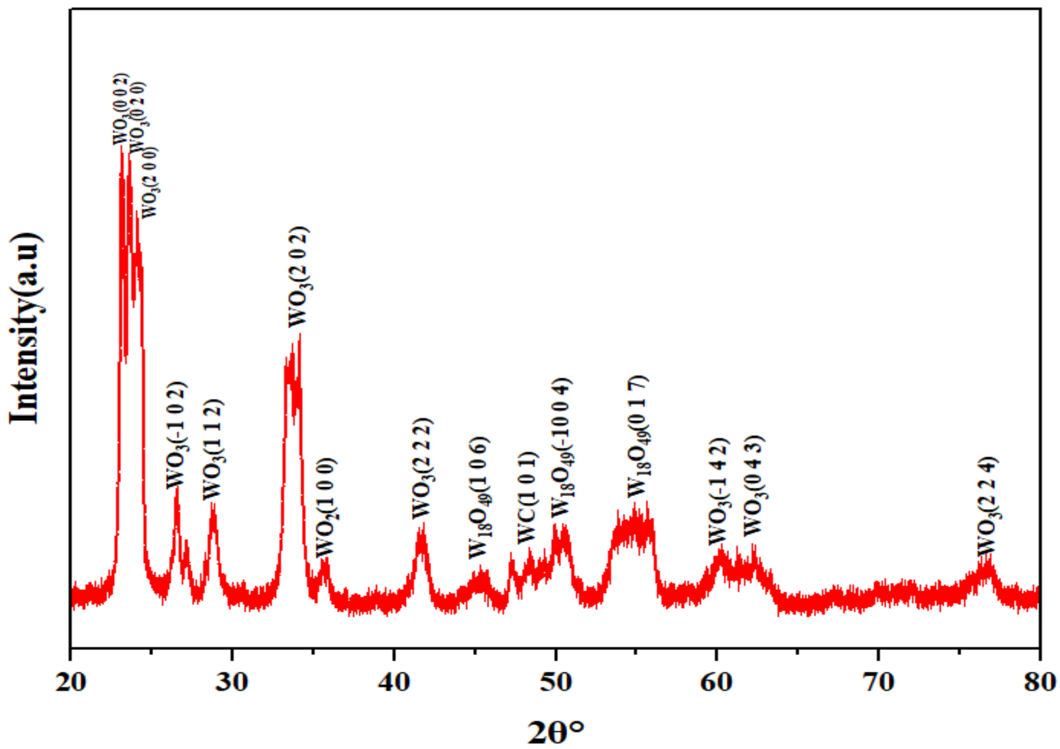

Figure (4.15): XRD Pattern for the powder that Carbothermal at 900°C and 45min.

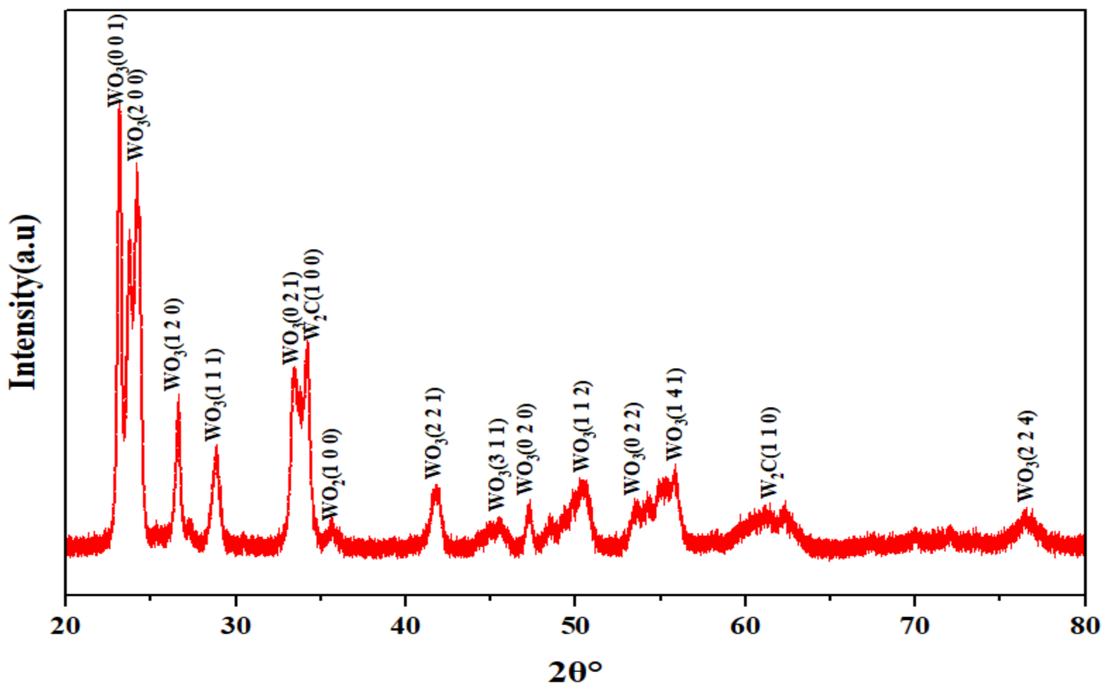

Figure (4.16): XRD Pattern for the powder that Carbothermal at $90^{O}C$ and 90min.

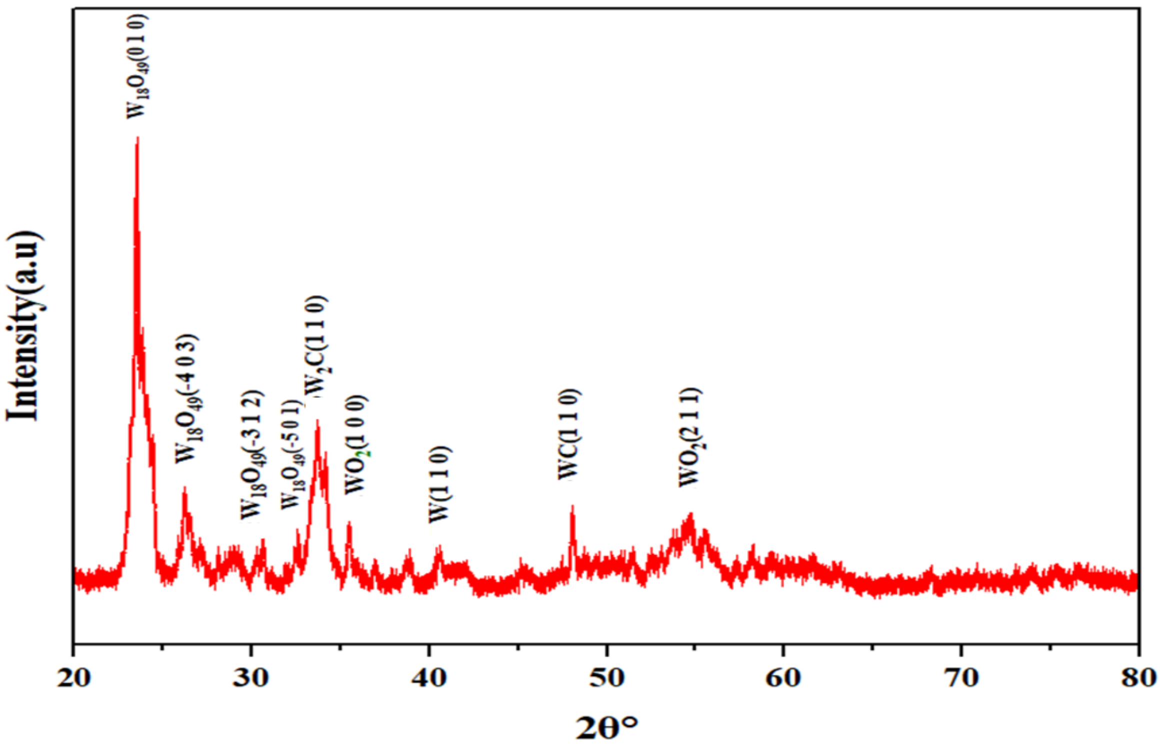

Figure (4.17): XRD Pattern for the powder that Carbothermal at $900^{O}C$ and 135min.

Figures (4.18) to (4.20) show the XRD pattern of the powder resulted from the reduction process at 1100°C with three different times 45min, 90 min, and 135 min respectively. Figure (4.18) shows WC appearance beginning to emerge with intermediates; it is interesting to notice the presence of W_2C already at this temperature that coexists with oxide phases. The reduction process is more efficient when increases time from 90 to 135 minutes as shown in figures (4.19) and (4.20) the WC is the main phase and no oxide phases are observed in the XRD patterns. The XRD patterns show a significant improvement in the carburization process and the complete reduction of the oxides phases at this temperatures.

.

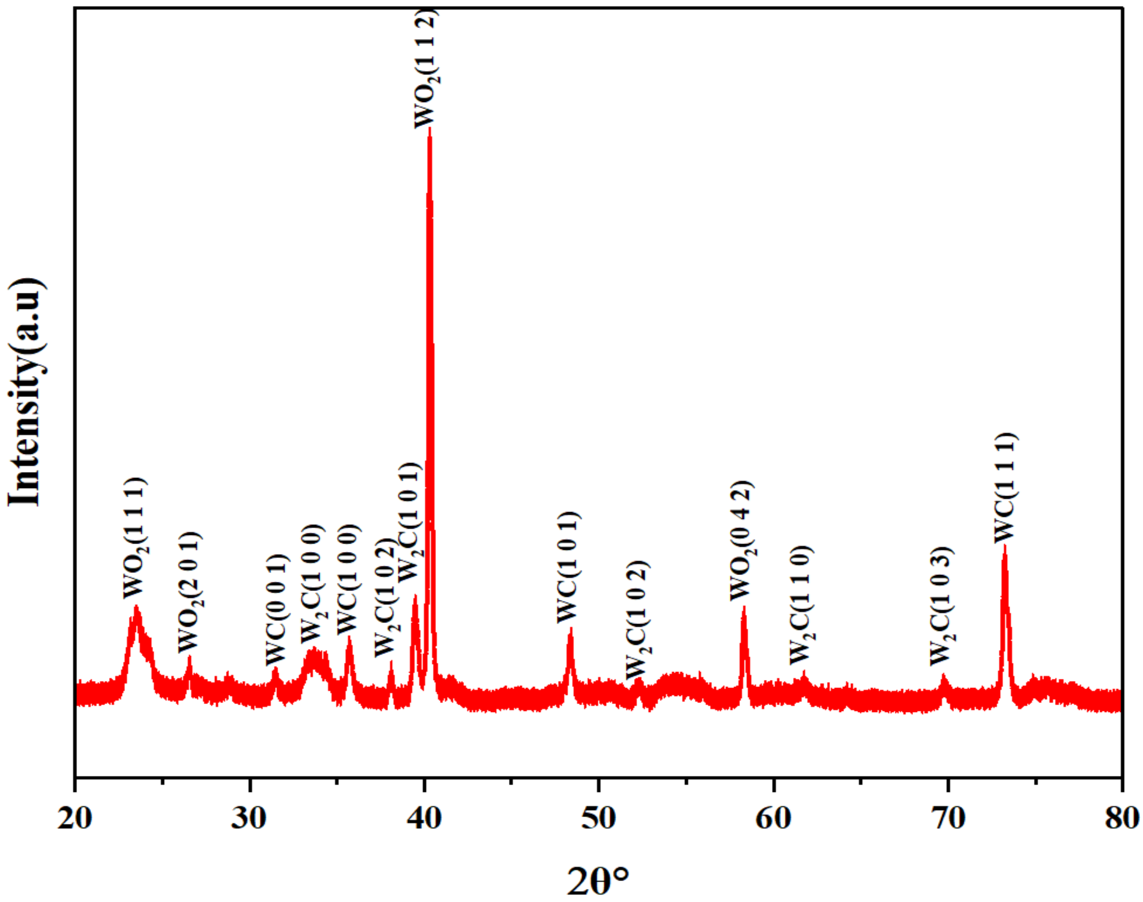

Figure (4.18): XRD Pattern for the powder that Carbothermal at 1100°C 45 min.

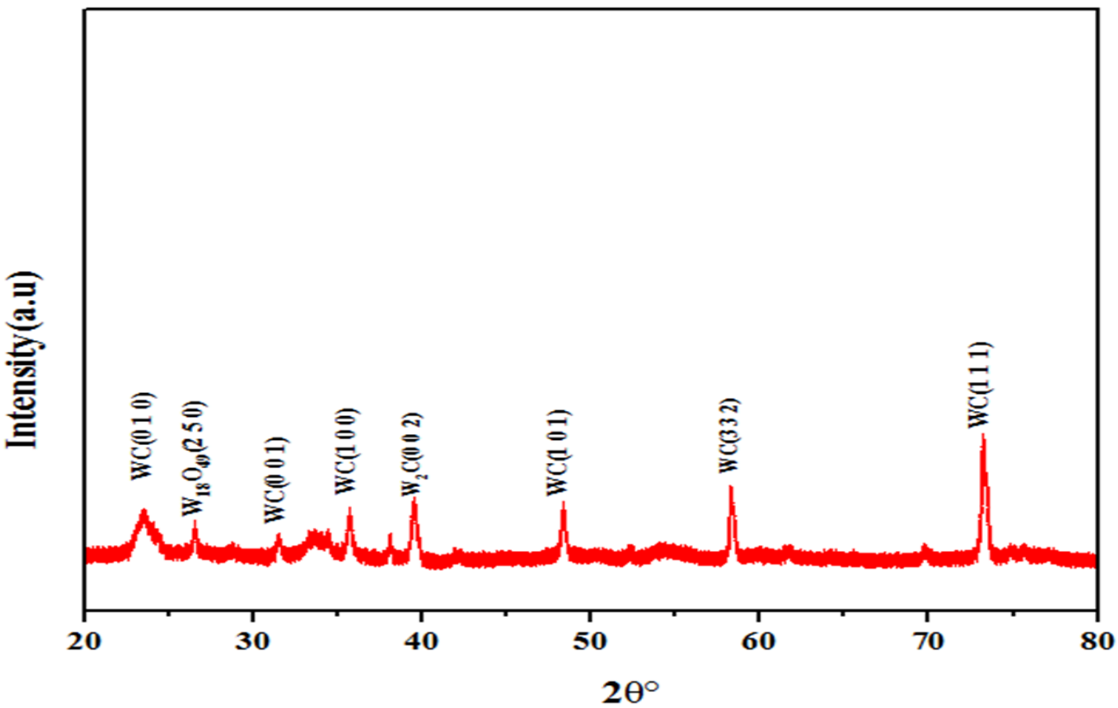

Figure (4.19): XRD Pattern for the powder that Carbothermal at 1100^{O}C and 90 min.

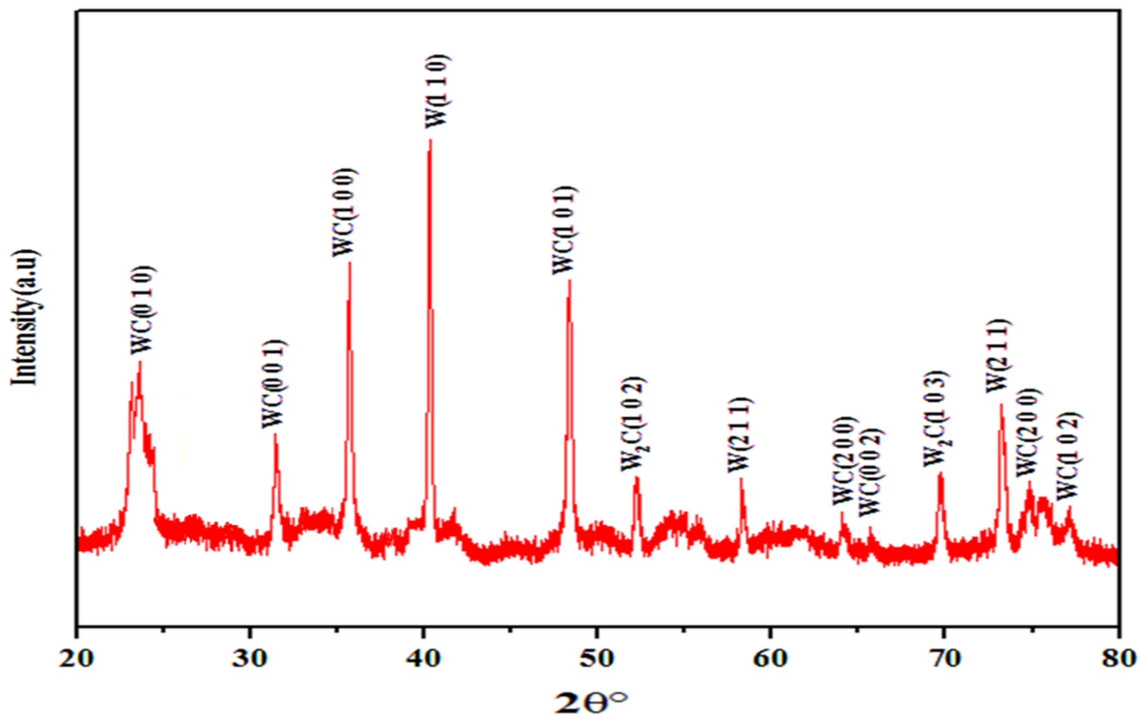

Figure (4.20): XRD Pattern for the powder that Carbothermal at 1100^{O}C and 135 min.

Figures (4.21) and (4.22) show the XRD pattern for the powder obtained by reduction at 1200°C for 45min and 90 min respectively. The disappearance of carbon and the non transformation of the tungsten oxide WO_3 are clearly noticed. Reactivity of the carbon with the atmosphere at this temperature can lead to a carbon deficiency rapidly that inhibits the complete transformation of WO_3 into WC.

It can be concluded that the best conditions for reduction process of WO_3 are: (1:5) mole ratio WO_3 to graphite powder at 1100°C and 135 min.

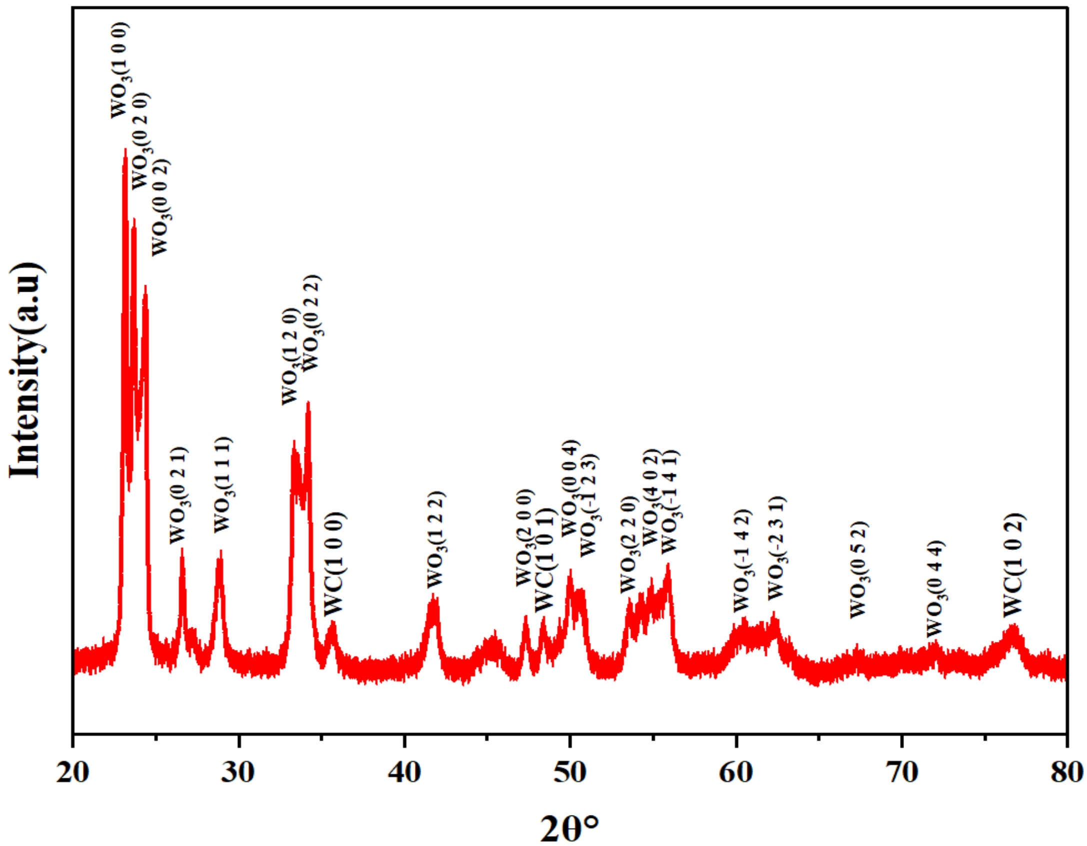

Figure (4.21): XRD Pattern for the Powder Obtained by Carbothermal at 1200°C and 45 min.

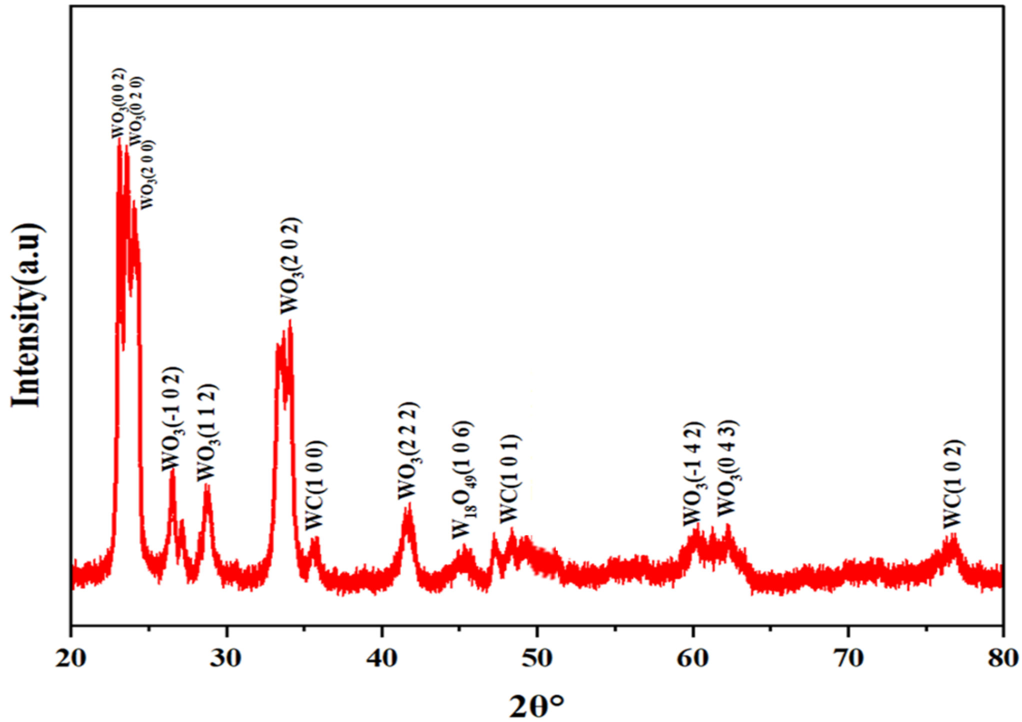

Figure (4.22): XRD Pattern for the Powder Obtained by Carbothermal at 1200°C and 90 min.

4.19 Particle Size Analysis of the produced WC Powder

The particles size of the produced WC powder by reduction of WO_3 at 1100°C for 135min has been analyzed. The results are shown in figure (4.23). It is clear that the WC powder have an average particle size of about 4.235 μm.

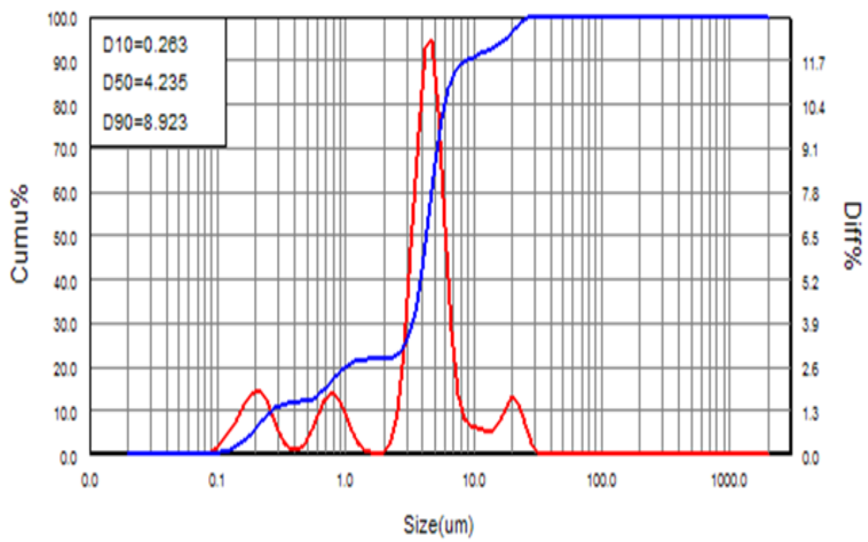

Diam um	Percent
0.100	0.16
0.200	6.14
0.500	12.19
1.000	19.90
2.000	21.66
5.000	67.01
10.000	90.84
20.000	96.44
45.000	100.00
75.000	100.00

Figure (4.23): Particle Size Analysis for WC Powder.

4.20 SEM and EDS Analysis of the produced WC powder

SEM and EDS image of the produced WC powder are shown in figures (4.24) and (4.25) respectively. The forms of all granulated powders are spherical. The EDS analysis indicates the purity of WC powder produced.

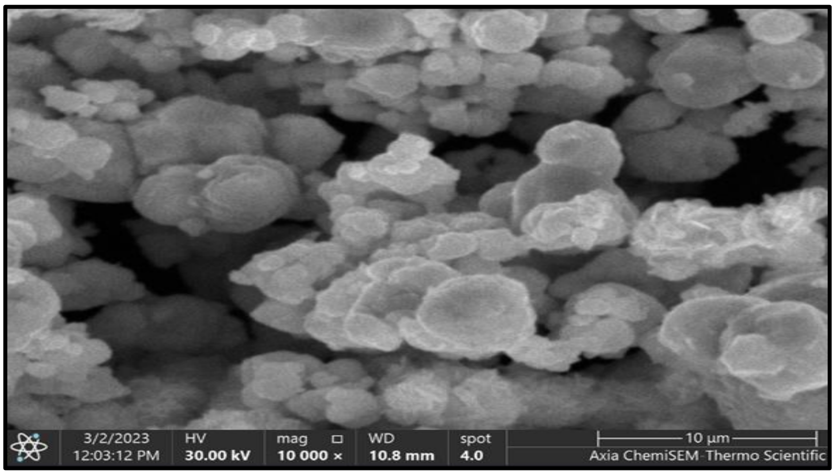

Figure (4.24): SEM for Tungsten Carbide Powder.

Total Number of Counts: 795 376
Average Count Rate: 17 773 cps
Acceleration Voltage: 30 kV
Total Acquisition Time: 46 seconds

Element	Atomic %	Atomic % Error	Weight %	Weight % Error
C	72.3	0.8	14.5	0.2
W	27.7	0.2	85.5	0.6

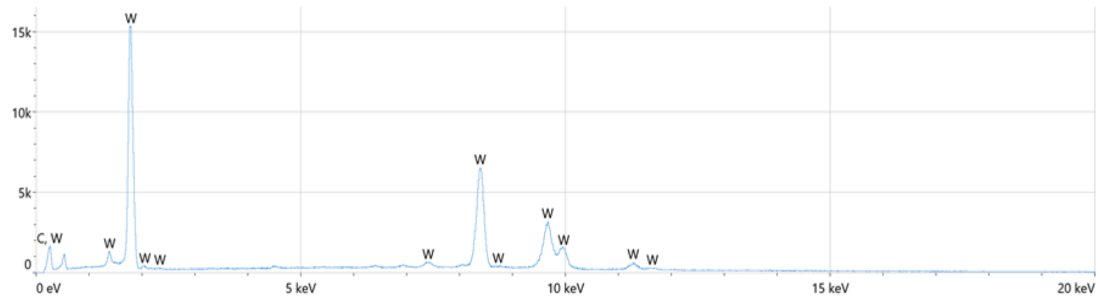

Figure (4.25): EDS for WC Powder.

4.21 Characteristics of WC-Co Coatings

The flame thermal spray method was used in this work. Figure (4.26) shows macro images of coated and uncoated specimens.

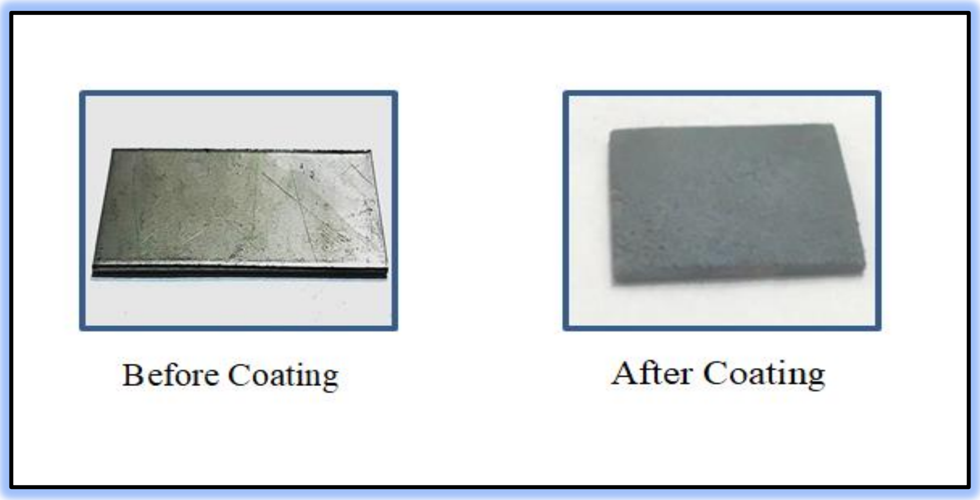

Figure (4.26): Macro Images of Coated and Uncoated Specimens.

4.21.1 XRD Characterization

X-ray for (WC-8%Co, WC-12%Co and WC-16%Co) powders are shown in figures (4.27-4.29) respectively. The feedstock powder primarily consists of the WC phase, Co phase and W_2C phase.

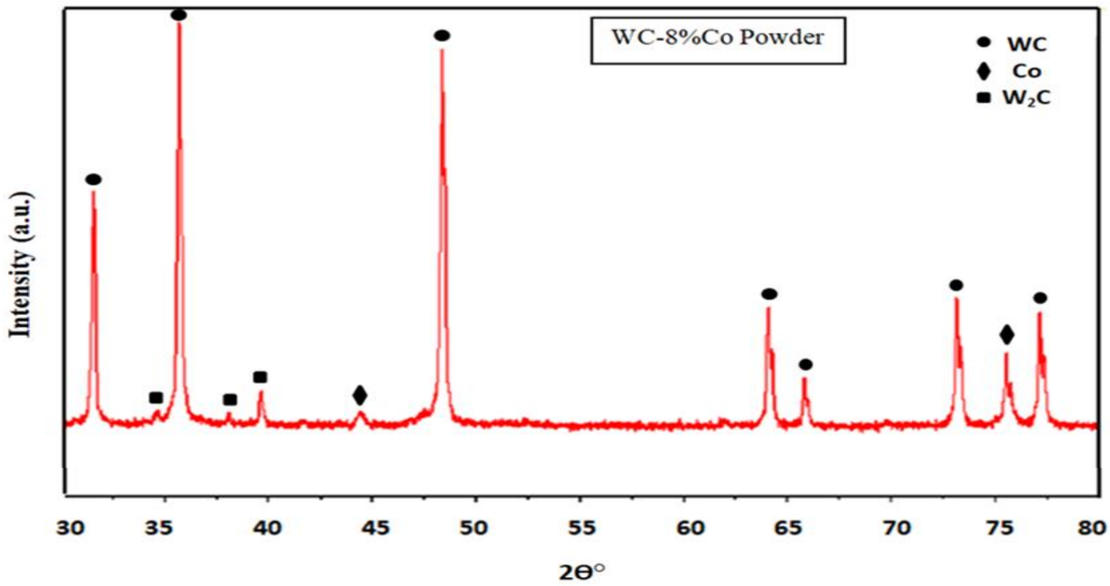

Figure (4.27): XRD Pattern for (WC-8%Co) Powder.

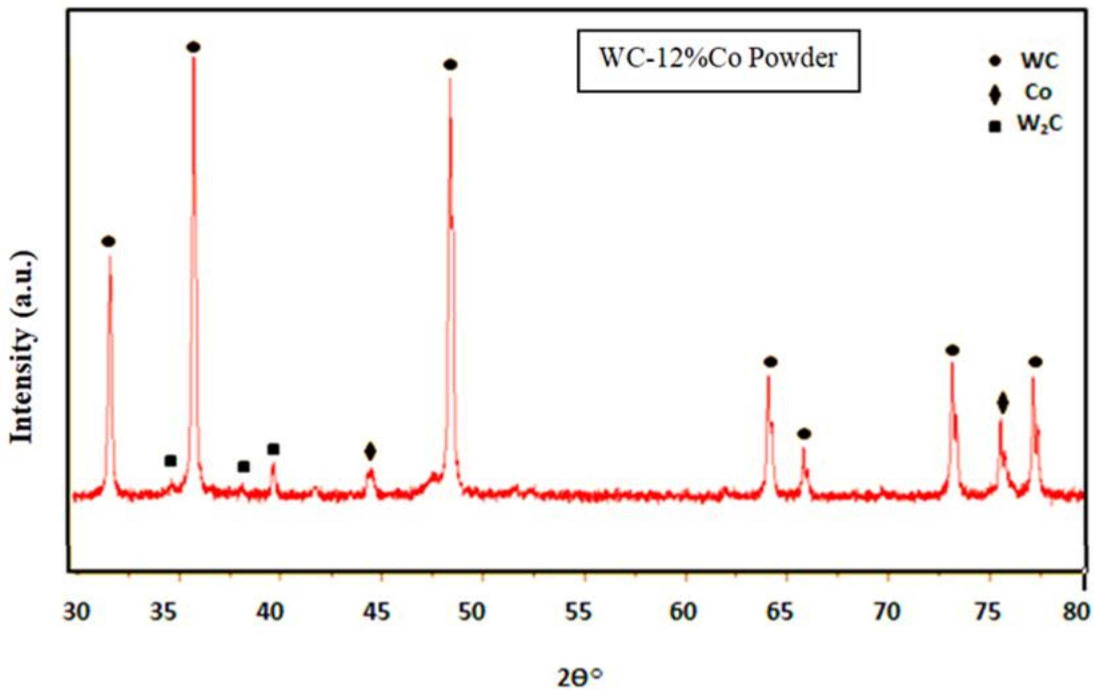

Figure (4.28): XRD Pattern for (WC-12%Co) Powder.

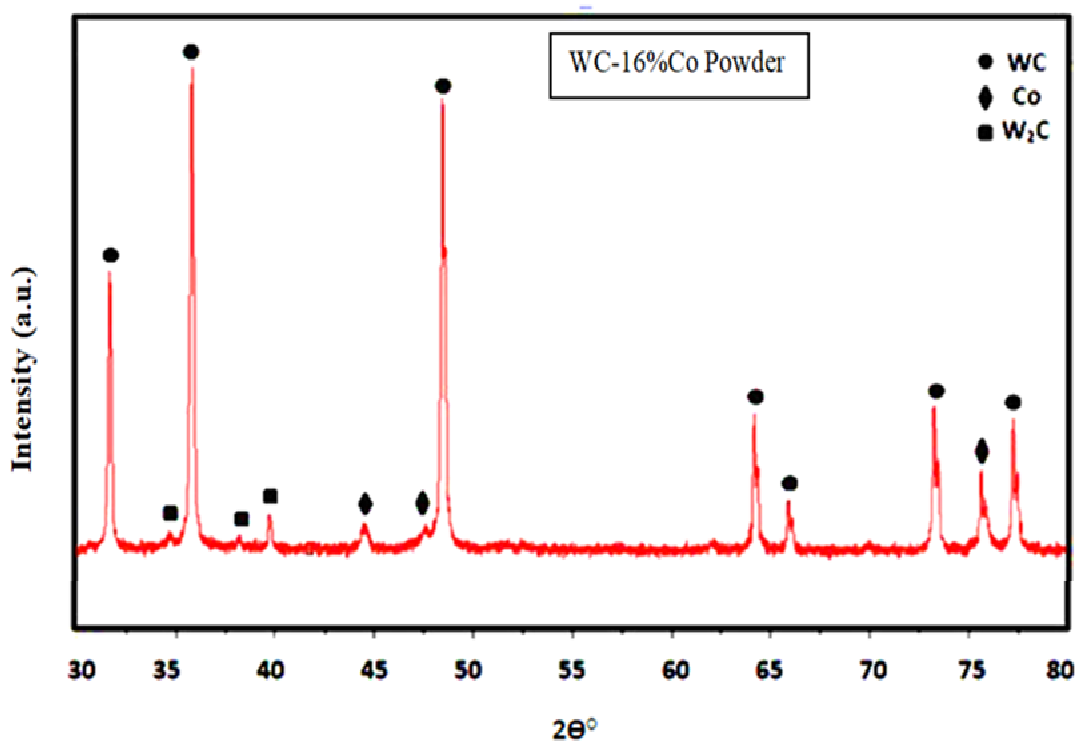

Figure (4.29): XRD Pattern for (WC-16%Co) Powder.

The XRD patterns of the coating layers deposited on the specimens (A1, B1, C1) are shown in Figures (4.30-4.32) respectively. X-ray diffraction indicated a substantial amount of WC, but did not reveal substantial amounts of cobalt-containing subcarbides glassy Co-W-C phases in the coatings that were sprayed, such as Co_6W_6C. The results of the (EDS) also showed that the coating included cobalt (as expected).

The pattern for the three coatings indicates that decarburisation of the WC phase has taken place, due to the formation of the deleterious brittle W_2C phase. Minimum decarburisation takes place in coating process because of lower flame temperature ≈3500°C and the flame velocity compared to other thermal coating methods. This is consistent with the research [117].

Due to the decarburization process occurring in the flame at high temperatures, the secondary phases (W and W_2C) appear. The metallic W phase and the brittle W_2C phase are the results of the coating degradation, which involves a carbon and W loss from the WC phase. There were two suggested mechanisms for the powder degradation [126].

$$2WC \longrightarrow W_2C + C \quad (4.2)$$

$$W_2C \longrightarrow 2W + C \quad (4.3)$$

The XRD spectra of the powder showed a crystalline structure, and WC, W_2C and Co phases. The XRD patterns for all the coatings showed WC, W_2C, W, Co and Co_6W_6C phases. During the spraying of WC-based powders different kinds of phase transformations occur that determine the microstructure and chemistry of the coatings. The decarburisation by oxidation of WC leads to the formation of W_2C and tungsten in the coatings, while the reaction of WC with the matrix leads to a solution of tungsten and carbide in the matrix and can cause the formation of mixed carbides. This is consistent with the research [117].

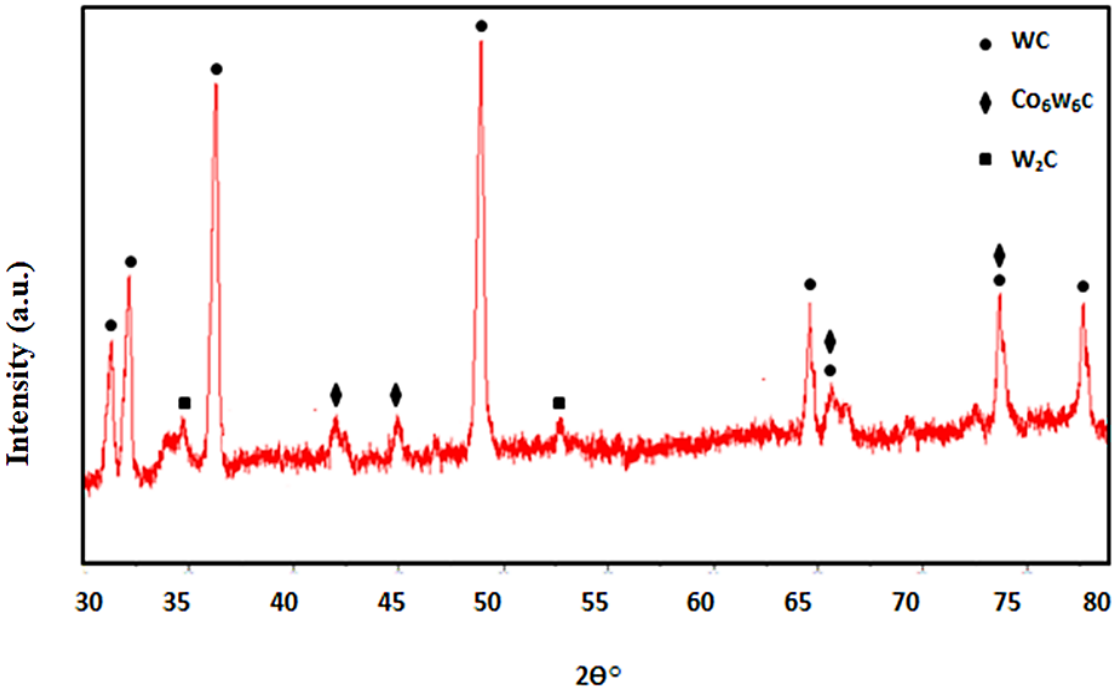

Figure (4.30): XRD Pattern for A1 specimen [WC-8%Co, velocity 300m/min].

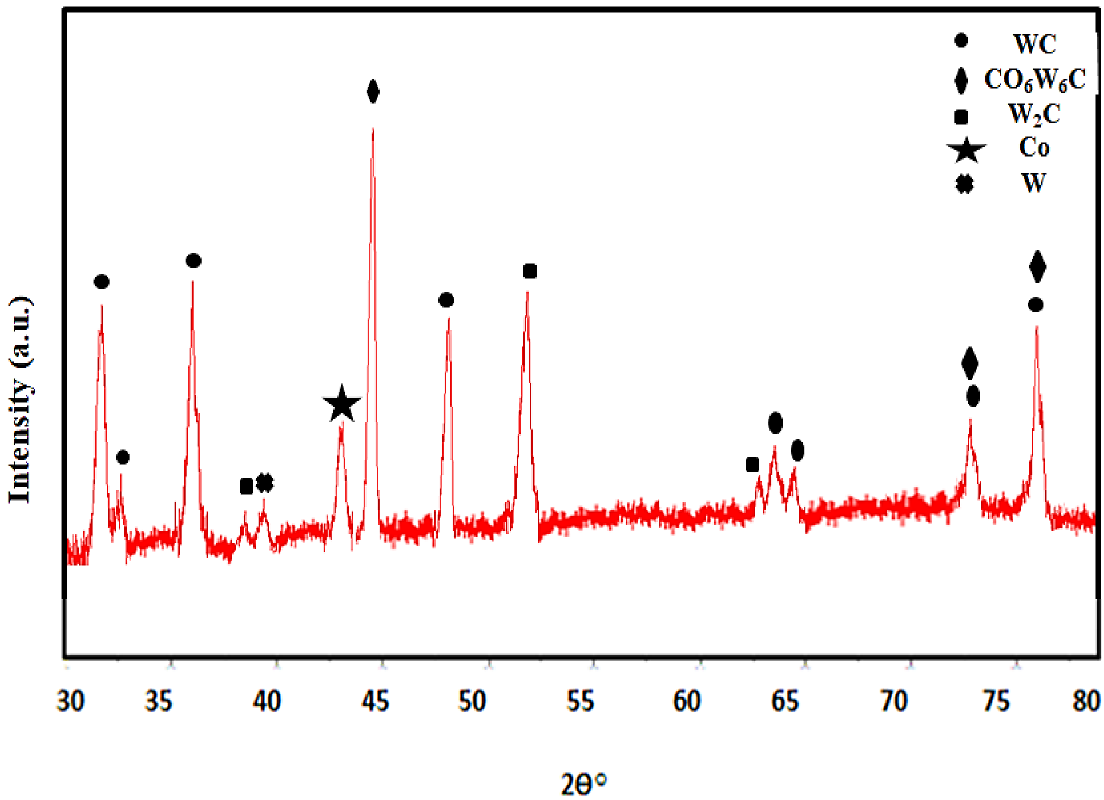

Figure (4.31): XRD Pattern for B1 specimen [WC-12%Co, velocity 300m/min].

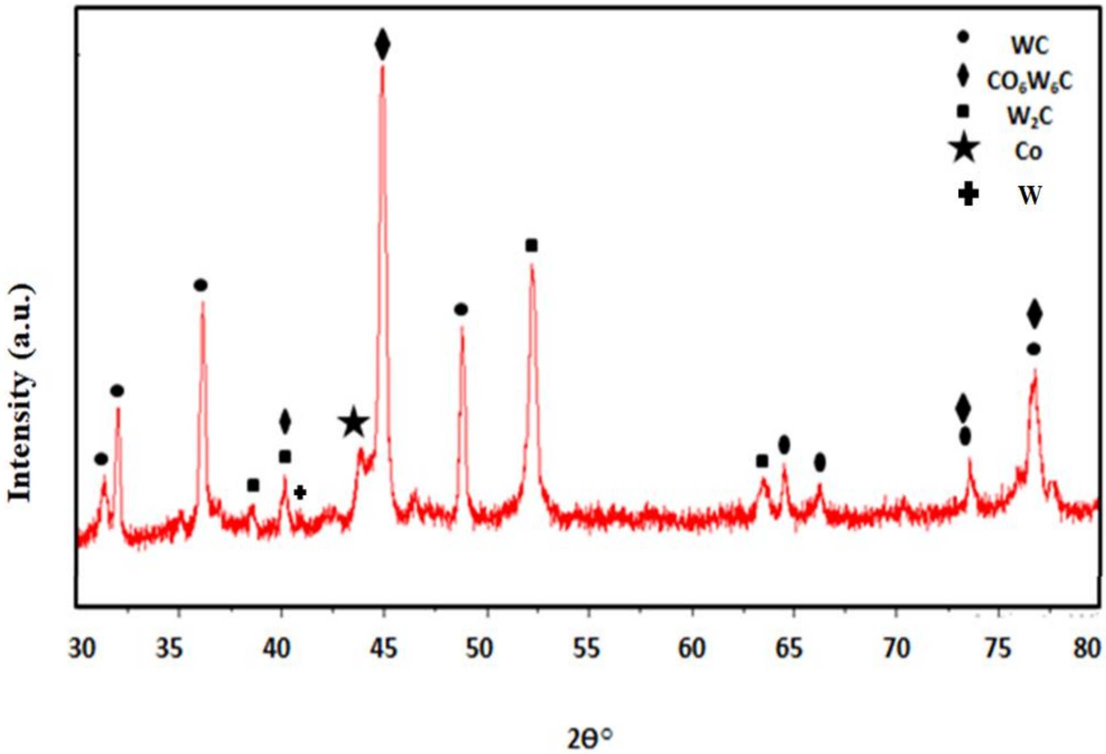

Figure (4.32): XRD Pattern for C1 specimen [WC-16%Co, velocity 300m/min].

4.21.2 Microstructural features of WC-Co coatings

Figures (4.33 through to 4.35) show the typical scanning electron microscope images of (WC-8%Co, WC-12%Co and WC-16%Co) powders respectively. Powders are of spherical shapes.

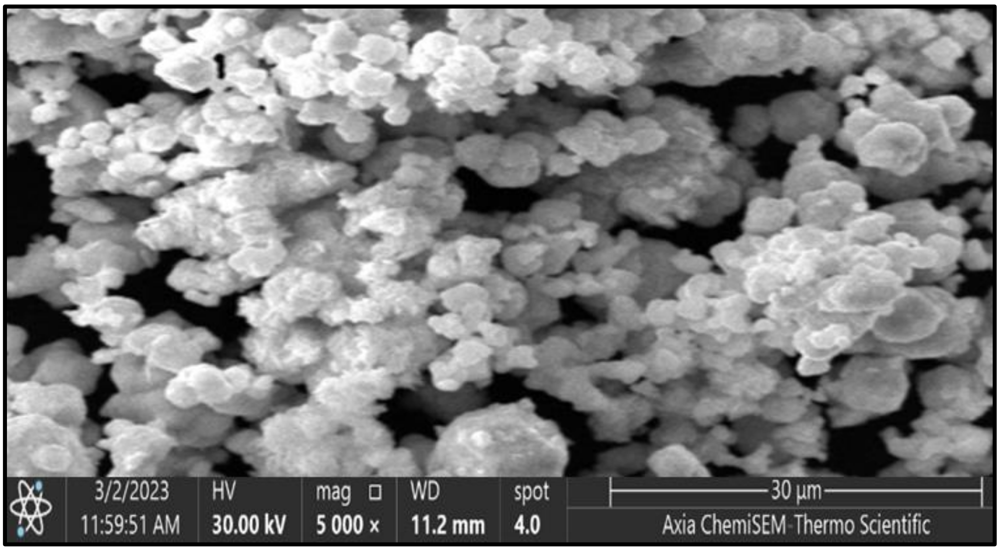

Figure (4.33): SEM for (WC-8%Co) Powder.

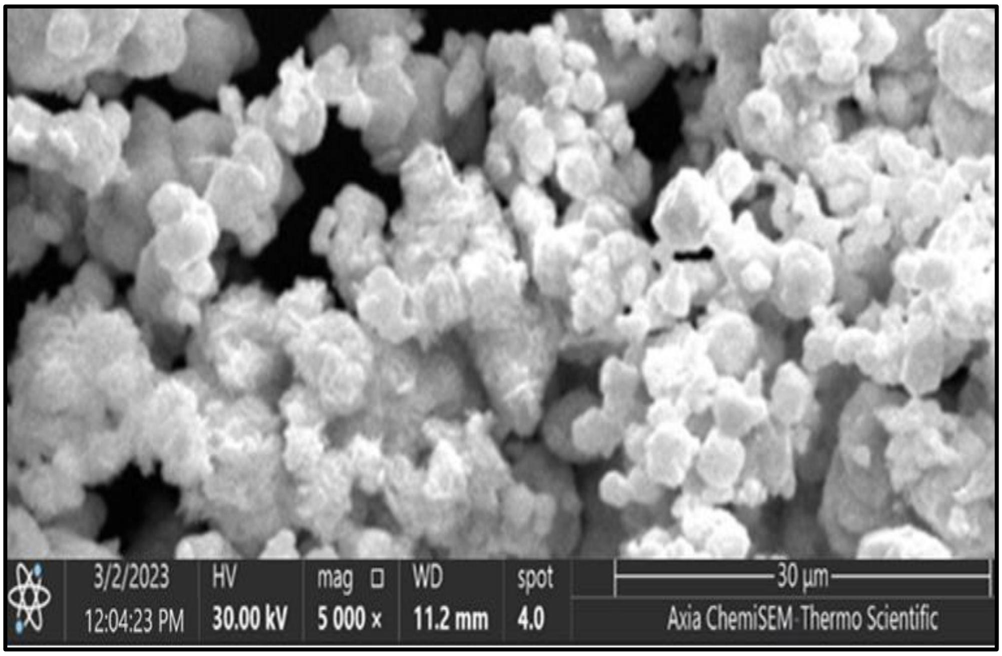

Figure (4.34): SEM for (WC-12%Co) Powder.

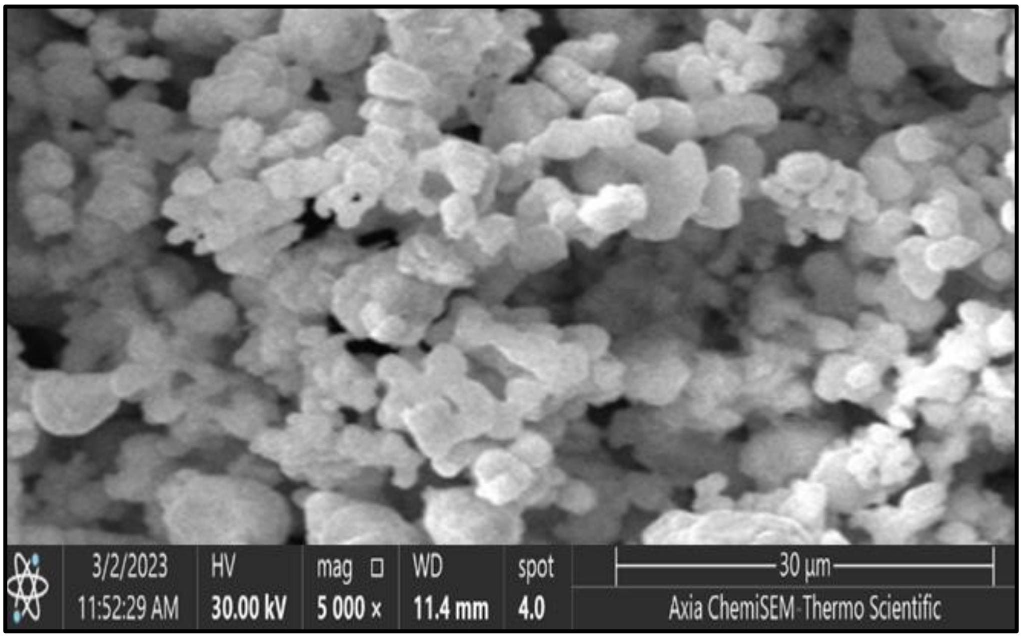

Figure (4.35): SEM for (WC-16%Co) Powder.

Figures (4.36 to 4.38) show the typical scanning electron microscope images for all specimens coating. In this image, the primary component: the white grains are represented by WC, while the light grey phase that surrounds WC is represented by Co.

As can be seen, on the surface of the coatings in figure (4.39) there were a small number of unmelted and semi molten particles, as well as porosity in the coating layer. A dark dissimilarity area indicates the presence of porosity. The microstructure reveals unmolten tungsten carbide grains, proving that the cobalt binder melted away while the tungsten carbide remained in its solid form. The coating may include partly melted particles because their speed is too slow. The coating consisted of randomly shaped WC particles dispersed throughout, with the metallic binder melting and spreading around them.

It was revealed in figures (4.40) that the (WC-Co), thermally sprayed coatings layer has homogeneous structure. The coating's surface morphology shows that the tungsten carbide granules were dissolved, resulting in a smoother finish. The low amounts of pores found in the coatings were promising as high protection against wear can be expected from such dense coatings. This indicates that the used velocity was perfect. In figures (4.41), the coating layer was not homogeneous due to the high speed, where the coating layer contained porosity and voids which reduces the tribological and mechanical properties of this layer.

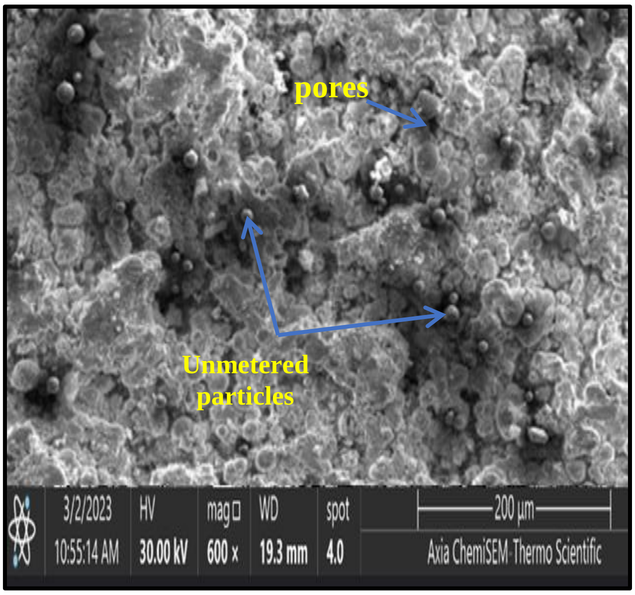

A1(WC-8%Co ,velocity 300m/min).

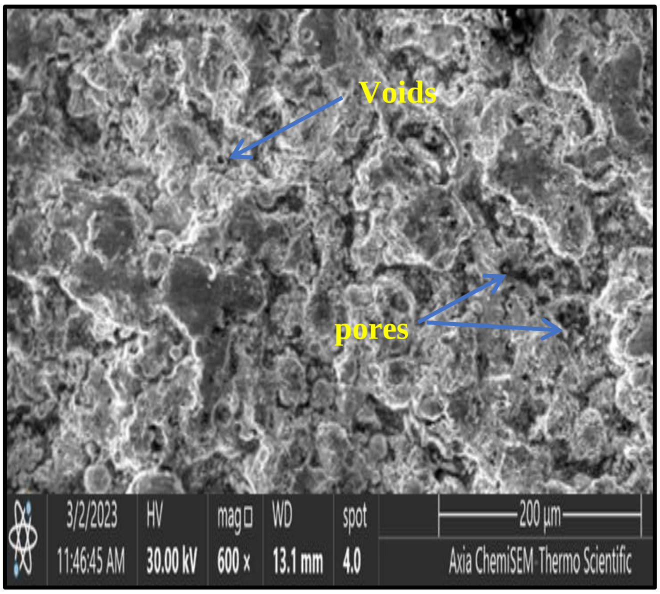

B1 (WC-12%Co, velocity 300 m/ min).

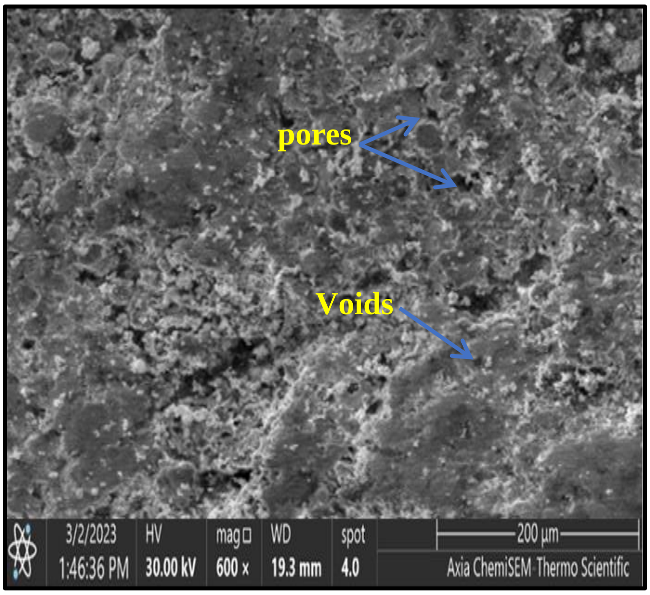

C1(WC-16%Co, velocity 300 m/ min).

Figure (4.36): SEM for (A1,B1 and C1) Specimens.

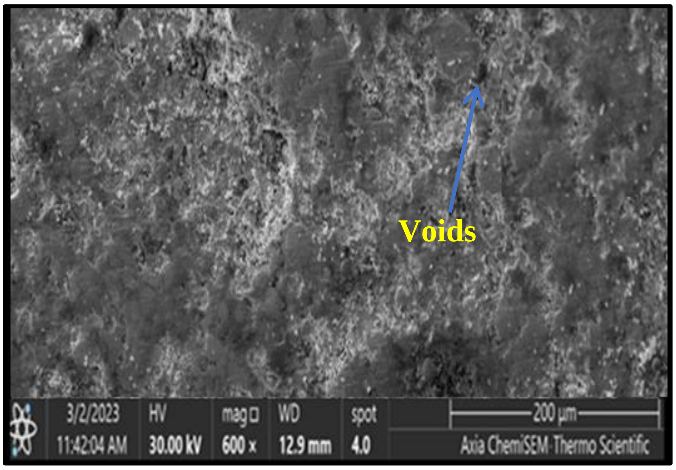

A2 (WC-8%Co, velocity 400 m/min).

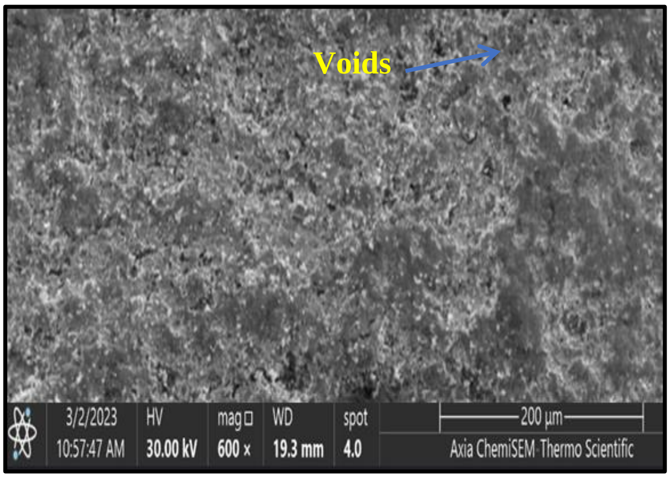

B2(WC-12%Co, velocity 400 m/min).

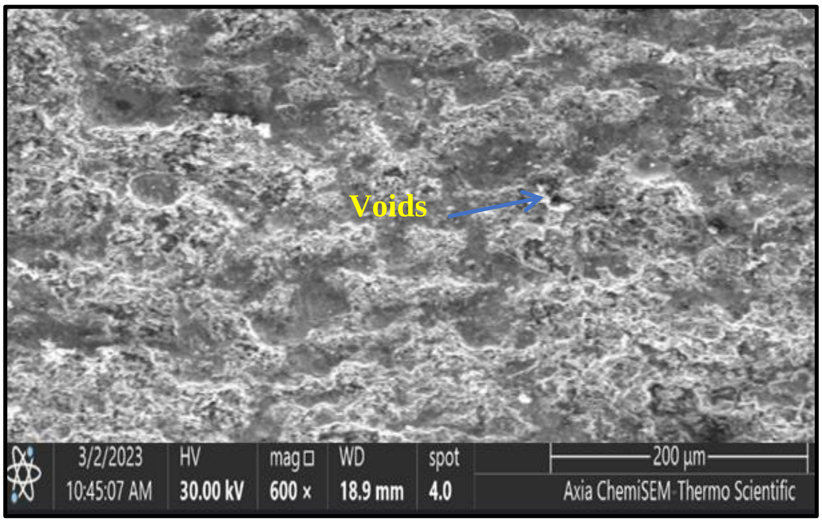

C2(WC-16%Co, velocity 400 m/min).

Figure (4.37): SEM for (A2,B2,C2) Specimens.

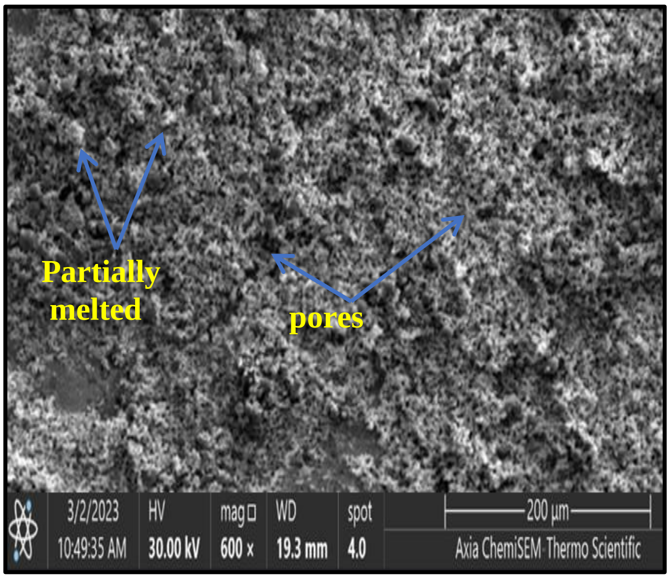

A3(WC-8%Co, velocity 500 m/min).

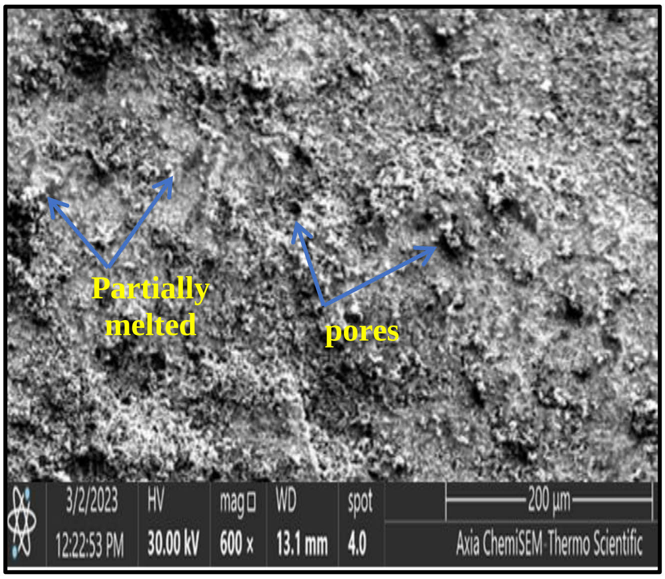

B3 (WC-12%Co, velocity 500 m/min).

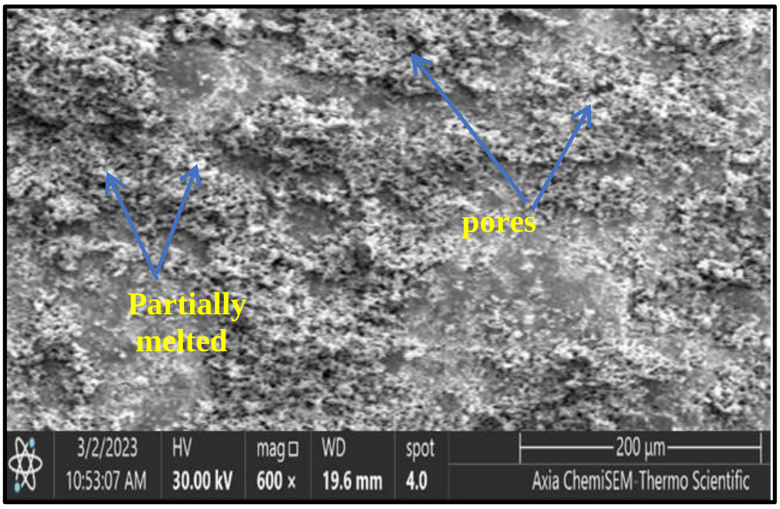

C3 (WC-16%Co, velocity 500 m/min).

Figure (4.38): SEM for (A3,B3 and C3) Specimens.

The investigation using energy dispersive spectroscopy discovered no oxygen and just tungsten, carbon, and cobalt as shown in figures (4.39-4.41). This means that the coating was deposited without forming an oxidation layer.

The spray powder was near-spherical in shape, and the tungsten carbide-cobalt coating was successfully prepared by thermal spraying technology. The tungsten carbide-cobalt coating and the substrate were clearly visible in a typical region of the polished cross-sections of the coating, Figures (4.39-4.41). Due to the presence of disseminated tungsten carbide particulates in the molten cobalt binder, the coating had a dense and homogeneous microstructure as well as a compact bonding to the substrate. The cross-sectional scanning electron microscopy image and the coating substrate interface confirm high interfacial adhesion integrity.

The formation of un-melt materials and voids is gradually minimized when the coating thickness increased, resulting in a reduction in residual stresses. Thickness must be within a certain range; it should not be too thin (doesn't provide appropriate protection) nor too thick (stresses generation and spalling may be occured). The measured thickness of the coated specimens is in the range that provides the proper protection without excessive generated stresses. The changes in thickness might be related to the influence of flame energy and powder velocity along with the amount of time they were exposed to the flame. The coating thickness was measured of (185-190) μm using FESEM at 400 m/min velocity of particle; this thickness is acceptable according the research [127].

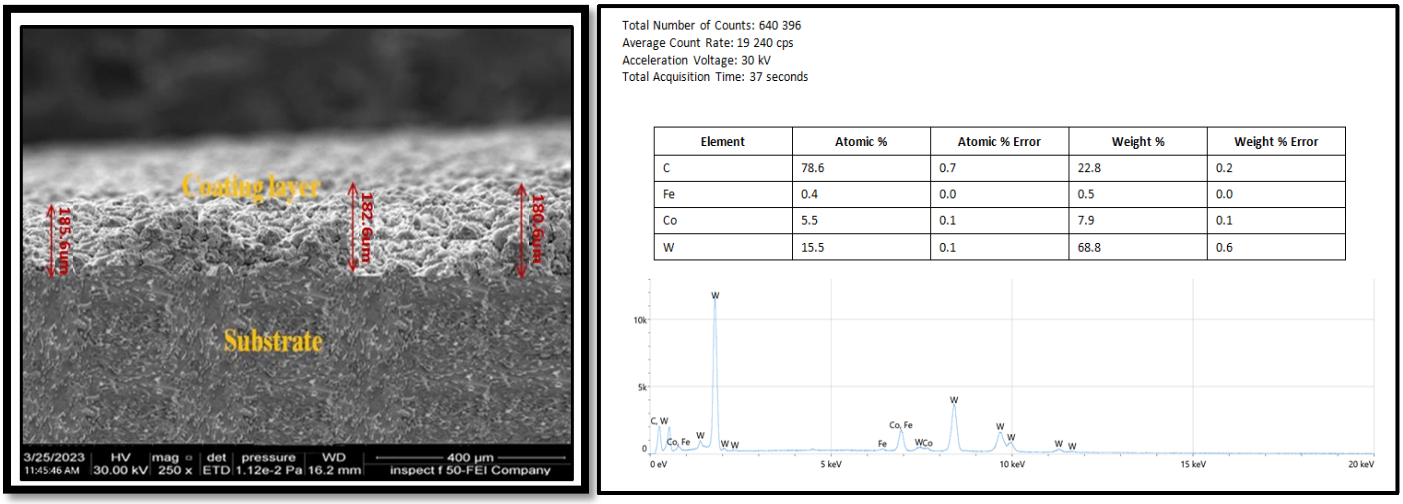

(A) (B)

Figures (4.39): A) Cross-section SEM images of specimens A2 (WC-8%Co, velocity 400 m/min) (B) EDS of specimens A2.

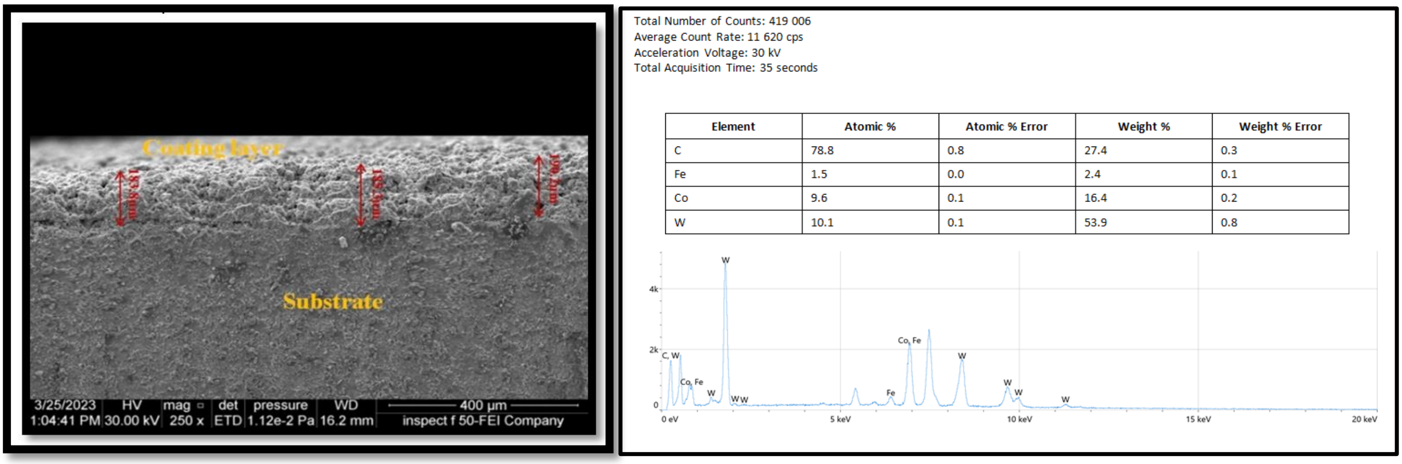

(A) (B)

Figures (4.40): A) Cross-section SEM images of specimens B2 (WC-12%Co, velocity 400 m/min) (B) EDS of specimens B2.

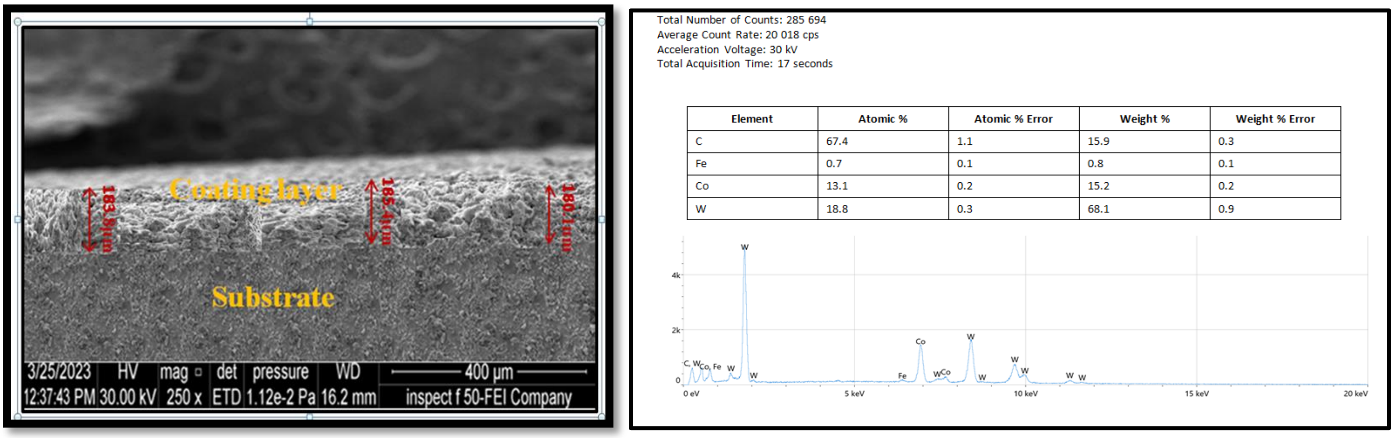

(A) (B)

Figures (4.41): A) Cross-section SEM images of specimens C2 (WC-16%Co, velocity 400 m/min) (B) EDS of specimens C2.

4.21.3 Microhardness of the Coatings

The surface micro hardness of the coating layers and substrate specimens is shown in Figure (4.42). These results can be attributed to the good adherence and uniform distribution of coating materials. It is noted that hardness decreases with the increase of Co content [128]. The smaller amount of tungsten carbide phase and the larger proportion of Co binder in WC-16%Co particles, result in a reduced hardness and greater ductility. Microhardness may have increased compared with substrate as a result of the formation of hard phases such as Co_6W_6C [128]. Because of the homogeneous structure of the samples A2, B2, C2 according to the SEM, they have the highest hardness per percentage of cobalt. This is consistent with the research [119].

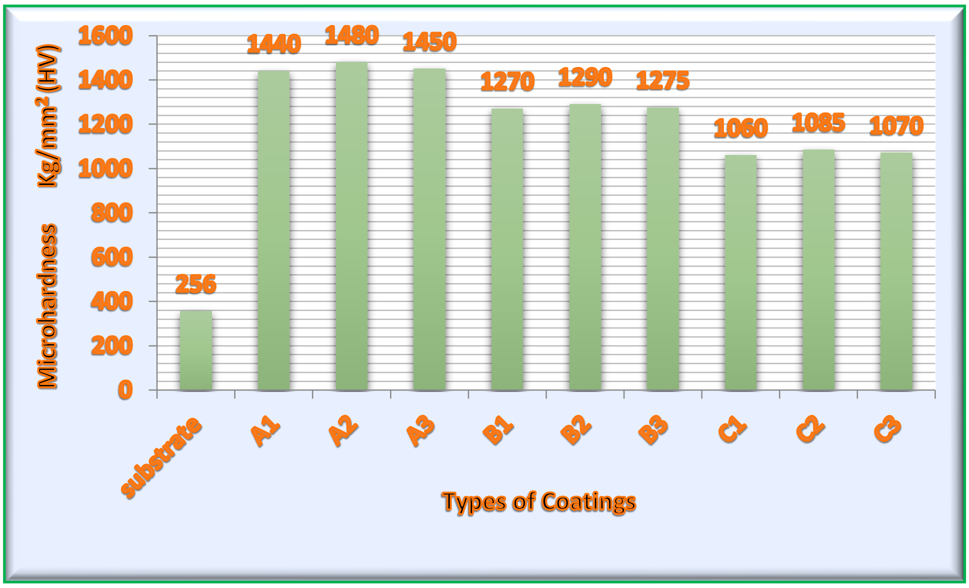

Figure (4.42): Microhardness of the Coatings.

4.21.4 Roughness Measurements

A surface's roughness is a gauge of its surface texture. The roughness of a surface may be described in a variety of ways. The roughness of the surface influences how it interacts with its surroundings. The most common way in the industry is to calculate the Ra value. Table (4.10) shows roughness of coatings, where (A2, B2, C2) is the smooth surface compared with other specimens because the condition of coating were best. To improve the mechanical and tribological properties, the roughness must be reduced to increase wear resistance and hardness. This is consistent with the research [116].

Table (4.10): Roughness of Coatings.

Specimens	Roughness(μm)
A1	3.2
A2	2
A3	3.5
B1	3.1
B2	1.9
B3	3.4
C1	3.3
C2	1.8
C3	3.6

4.21.5 Wear Test of WC-Co Coatings

Because of their high hardness and low wear coefficient, thermal sprayed WC-Co coatings are widely employed to enhance the sliding wear characteristics of various engineering components. Significant changes in wear behaviour have been seen across coating types when tested in dry sliding contact against a stationary ceramic ball. Figure (4.43-4.45) shows that wear rate of uncoated and coated specimens. Sliding wear behaviour of tungsten carbide based coatings may be affected by coating porosity, metal binder type and the amount of tungsten carbide phase. It revealed that thermal spray coating porosity was a major factor in the coatings' wear resistances during sliding. Under load (15N) for 25 minutes, the effect of the coating layer on the wear rate was studied. Due to the tungsten carbide particle dispersion in the ductile binder (Co) and lack of fragile phases or brittle, a very high slide resistance was attained for all coatings. Coated surfaces wear rate lower than uncoated surfaces. Due to the increased proportion of the ceramic phase in the specimen with low cobalt content (WC-8%Co), the wear resistance during testing was found to be higher. This is acceptable [116].

Due to high hardness for (A2,B2,C2) specimens and low roughness, these three layers have the lowest wear rate compared to uncoated and the remaining coated specimens. It is known that increasing hardness results in improved wear resistance. This is acceptable [116].

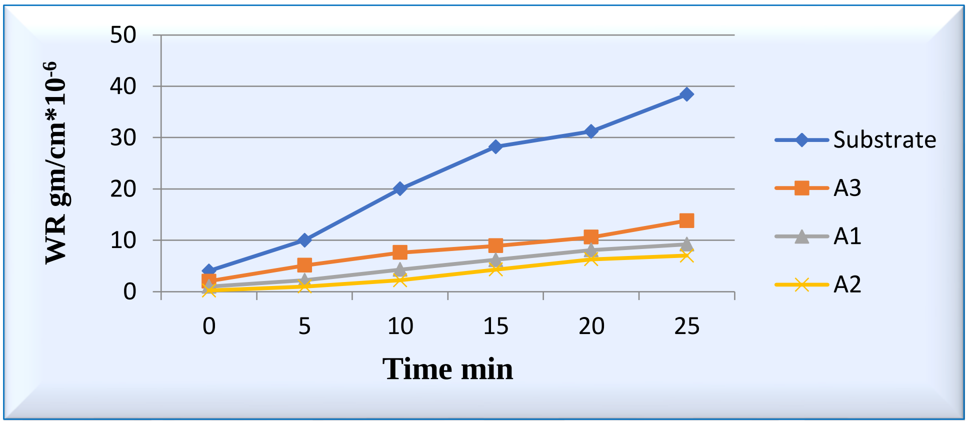

Figure (4.43): Wear Rate Test for Uncoated and Coated Specimens.

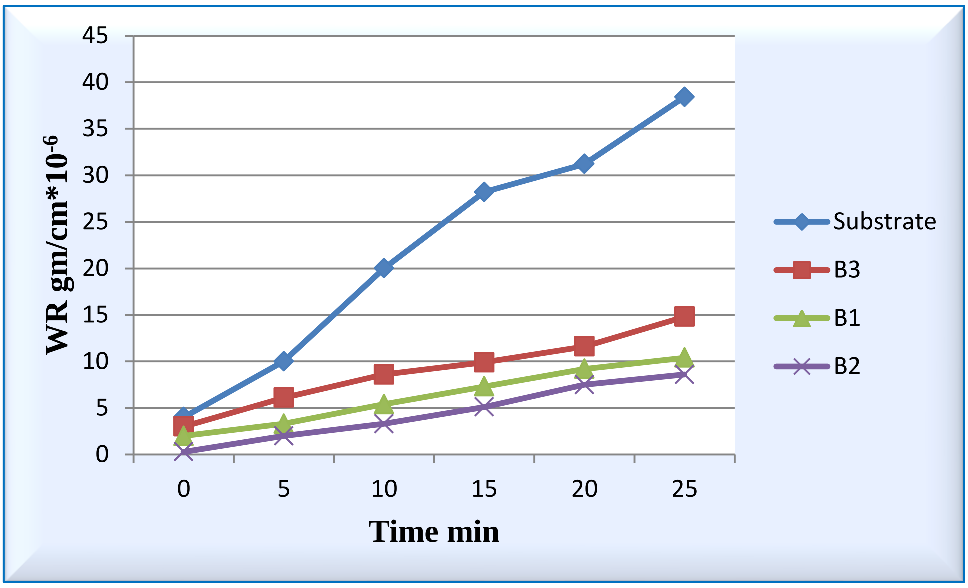

Figure (4.44): Wear Rate Test for Uncoated and Coated Specimens.

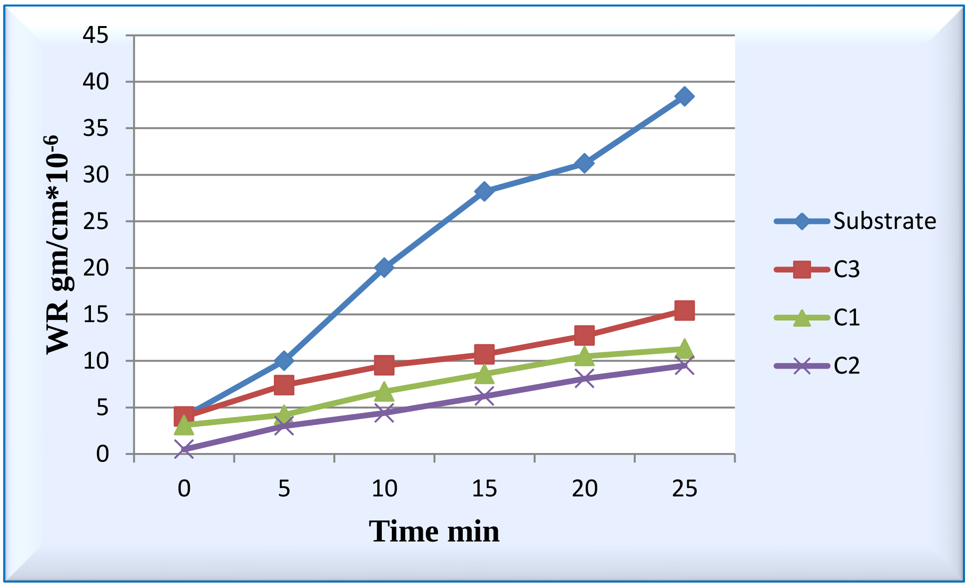

Figure (4.45): Wear Rate Test for Uncoated and Coated Specimens.

CHAPTER
Five
CONCLUSIONS AND RECOMMENDATIONS

Chapter Five

Conclusions and Recommendations

5.1 Conclusions

From the results of the present work, the following can be concluded:

1. Tungstic acid (H_2WO_4) can be obtained from scrap tungsten carbide cutting insert by an electrochemical method using nitric acid as the electrolyte. Maximum amount of this acid with minimum power consumption result from the optimum conditions (current density 4000 A/m^2, solution concentration 1.8 M, temperature 70°C and cathode electrode Al).
2. Tungsten carbide can be obtained by transformation the tungstic acid to WO_3 by heating at 800^{O}C and then, reduction of this oxide by graphite through heating at 1100^{O}C for 130 min.
3. The recovered WC can be applied for coating of stainless steel (316) by implementing the flame thermal spray process and using suitable parameters to produce a coating layer without crack and having high mechanical and metallurgical properties.
4. Among the different spray parameters varied, the velocity of particle had a great influence in the obtaining of a more metallurgical and mechanical properties.
5. It was determined that A2, B2 and C2 specimens are more resistant against wear. While the highest weight loss was seen in A3, B3 and C3 specimens. When wear values and hardness values are compared in experimental studies done, A2, B2 and C2 specimens, which has the highest hardness value, is the most resistant to wear. It was observed that wear resistance decreases by decreasing hardness in other specimens.

5.2 Recommendations for Further Work

1. Using low-voltage electrolysis route for recovery of (WC).
2. Using hydrogen gas in order to obtained WC at temperatures lower than those used in the work instead of the argon gas in carbothermal process.
3. Trying other parameters (feeding of powder and distance of spray) for flame thermal process and showing their effect on metallurgical and mechanical properties.
4. Adding other element like nickel to the coating layer with or without cobalt.

REFERENCES

References

1. Liu, B., Shi, A., Su, Q., Chen, G., Li, W., Zhang, L., & Yang, B. (2017). Recovery of tungsten carbides to prepare the ultrafine WC-Co composite powder by two-step reduction process. Powder Technology, 306, 113-119.
2. García, J., Ciprés, V. C., Blomqvist, A., & Kaplan, B. (2019). Cemented carbide microstructures: a review. International Journal of Refractory Metals and Hard Materials, 80, 40-68
3. Gaur, R.P.S., Modern hydrometallurgical production methods for tungsten. JOM, 2006. 58(9): p. 45-49.
4. Edtmaier, C., Schiesser, R., Meissl, C., Schubert, W. D., Bock, A., Schön, A., & Zeiler, B. (2005). Selective removal of the cobalt binder in WC/Co based hardmetal scraps by acetic acid leaching. Hydrometallurgy, 76(1-2), 63-71.
5. Zhang, Q., Xi, X., Nie, Z., Zhang, L., & Ma, L. (2019). Electrochemical dissolution of cemented carbide scrap and electrochemical preparation of tungsten and cobalt metals. International Journal of Refractory Metals and Hard Materials, 79, 145-153.
6. Lee, J. C., Kim, E. Y., Kim, J. H., Kim, W., Kim, B. S., & Pandey, B. D. (2011). Recycling of WC–Co hardmetal sludge by a new hydrometallurgical route. International Journal of Refractory Metals and Hard Materials, 29(3), 365-371.
7. Randhawa, N. S., Katiyar, P. K., Hait, J., Jana, R. K., Singh, K. K., & Mankhand, T. R. (2013). Anodic dissolution behaviour of tungsten carbide scraps in ammoniacal media.
8. Luković, J., Babić, B., Bučevac, D., Prekajski, M., Pantić, J., Baščarević, Z., & Matović, B. (2015). Synthesis and characterization

of tungsten carbide fine powders. Ceramics International, 41(1), 1271-1277.

9. Vats, A., Kumar, A., Patnaik, A., & Meena, M. L. (2021). Influence of deposition parameters on Tribological Performance of HVOF Coating: A review. In IOP Conference Series: Materials Science and Engineering (Vol. 1017, No. 1, p. 012015). IOP Publishing.
10. Iordanova, I., Surtchev, M., & Forcey, K. S. (2001). Metallographic and SEM investigation of the microstructure of thermally sprayed coatings on steel substrates. Surface and Coatings Technology, 139(2-3), 118-126
11. Raza, A., Ahmad, F., Badri, T. M., Raza, M. R., & Malik, K. (2022). An influence of oxygen flow rate and spray distance on the porosity of HVOF coating and its effects on corrosion—a review. Materials, 15(18), 6329.
12. Kumar, S., Kumar, R., Singh, S., Singh, H., & Handa, A. (2020). The role of thermal spray coating to combat hot corrosion of boiler tubes: a study. Journal of Xidian University, 14(5), 229-239.
13. Sunde, A. (2015). Properties of thermal sprayed coatings for internal use in pipes and bends (Master's thesis, NTNU).
14. Alam, M. S., & Das, A. K. (2022). Advancement in cermet based coating on steel substrate: A review. Materials Today: Proceedings.
15. Da Silva, F. S., Cinca, N., Dosta, S., Cano, I. G., Couto, M., Guilemany, J. M., & Benedetti, A. V. (2018). Corrosion behavior of WC-Co coatings deposited by cold gas spray onto AA 7075-T6. Corrosion Science, 136, 231-243.
16. Zhao, X. Q., Zhou, H. D., & Chen, J. M. (2006). Comparative study of the friction and wear behavior of plasma sprayed conventional and nanostructured WC–12% Co coatings on stainless steel. Materials Science and Engineering: A, 431(1-2), 290-297.

17. Groover, M. P. (2020). Fundamentals of modern manufacturing: materials, processes, and systems. John Wiley & Sons, USA, Seventh Edition: p. 1-1016.

18. Roulon, Z., Missiaen, J. M., & Lay, S. (2020). Carbide grain growth in cemented carbides sintered with alternative binders. International Journal of Refractory Metals and Hard Materials, 86, 105088.

19. Wu, Y. C., Yang, Y., Tan, X. Y., Luo, L., Zan, X., Zhu, X. Y., ... & Cheng, J. G. (2020). Preparation technology of ultra-fine tungsten carbide powders: an overview. Frontiers in Materials, 7, 94.

20. Smith, G. T. (2008). Cutting tool technology: industrial handbook (p. 600). London: Springer.

21. Mannesson, K., Borgh, I., Borgenstam, A., & Ågren, J. (2011). Abnormal grain growth in cemented carbides—Experiments and simulations. International Journal of Refractory Metals and Hard Materials, 29(4), 488-494.

22. Linder, D. (2020). Towards computational materials design and upscaling of alternative binder cemented carbides (Doctoral dissertation, KTH Royal Institute of Technology/ Materials Science and Engineering/ Stockholm).

23. Mari, D., Miguel, L., & Nebel, C. (Eds.). (2014). Comprehensive hard materials. Newnes, UK, volume 1: p.1-538.

24. Liu, C. (2014). Alternative binder phases for WC cemented carbides, master thesis, KTH Royal Institute of Technology/ Materials Science and Engineering/ Stockholm.

25. Rizzo, A., Goel, S., Luisa Grilli, M., Iglesias, R., Jaworska, L., Lapkovskis, V., ... & Valerini, D. (2020). The critical raw materials in cutting tools for machining applications: A review. Materials, 13(6), 1377.

26. Katiyar, P. K., & Randhawa, N. S. (2020). A comprehensive review

on recycling methods for cemented tungsten carbide scraps highlighting the electrochemical techniques. International Journal of Refractory Metals and Hard Materials, 90, 105251.

27. Kurlov, A. S., & Gusev, A. I. (2006). Tungsten carbides and WC phase diagram. Inorganic Materials, 42,p. 121-127.
28. Wright, E.M.T.P.K., (2000).Metal Cutting. Butterworth–Heinemann, UK, Fourth Edition: p.1-445.
29. Palei, B. B., Dash, T., & Biswal, S. K. (2020). Eutectoid Decomposition Of Tungsten Carbide By Thermal Arc Plasma Treatment. PalArch's Journal of Archaeology of Egypt/Egyptology, 17(7), 10133-10138.
30. Da Silva Fernandes, C. M. (2008). Sputtering on the Production of Tungsten Carbide Based Composites (Doctoral dissertation, Universidade of Aveiro/ Department of Ceramics and Glass Engineering /Portugal).
31. Upadhyaya, G. S. (1998). Cemented tungsten carbides: production, properties and testing. William Andrew.
32. Erdoğan, M., & Karakaya, İ. (2010). Electrochemical reduction of tungsten compounds to produce tungsten powder. Metallurgical and Materials Transactions B, 41, 798-804.
33. Lee, J., Lee, J., Kim, B., & Kim, Y. (2016). Leaching Behavior of Al, Co and W from the Al-alloying treated WC-Co tool as a new recycling process for WC hard scrap. Metals, 6(8), 174.
34. Shemi, A., Magumise, A., Ndlovu, S., & Sacks, N. (2018). Recycling of tungsten carbide scrap metal: A review of recycling methods and future prospects. Minerals Engineering, 122, 195-205.
35. Zeiler, B., Bartl, A., & Schubert, W. D. (2021). Recycling of tungsten: Current share, economic limitations, technologies and future potential. International Journal of Refractory Metals and Hard

Materials, 98, 105546.

36. Lassner, E., & Schubert, W. D. (1999). Tungsten: properties, chemistry, technology of the elements, alloys, and chemical compounds. Springer Science, New York: p.1-434.
37. Akcil, A. (Ed.). (2019). Critical and rare earth elements: recovery from secondary resources. CRC Press, USA: p. 1-384.
38. Retegan, M. W. K. I. T., Bru, K., Mennade, N., LGC, L. C., Sundqvist, L., Ye, G., ... & IMN, G. B.(2016). State of the art on the recovery of refractory metals from urban mines (Master's thesis, NTNU).
39. Chang, J. H. (2009). Modeling of an Electrochemical Cell, Master Thesis, University of Toronto/Department of Electrical and Computer Engineering.
40. Kelly, R. G., Scully, J. R., Shoesmith, D., & Buchheit, R. G. (2002). Electrochemical techniques in corrosion science and engineering. CRC Press, New York.
41. Sato, N. (1998). Electrochemistry at metal and semiconductor electrodes. Elsevier,USA, First Edition.
42. Bard, A. J., & Faulkner, L. R. (2001). Fundamentals and applications. Electrochemical methods, 2(482), p.580-632.
43. Perez, N. (Ed.). (2004). Electrochemistry and corrosion science. Boston, MA: Springer Us, pp 189–246.
44. Trivinho-Strixino, F., Santos, J. S., & Sikora, M. S. (2017). Electrochemical synthesis of nanostructured materials. William Andrew Publishing in Nanostructures (pp. 53-103).
45. Stansbury, E. E., & Buchanan, R. A. (2000). Fundamentals of electrochemical corrosion. ASM international,USA.
46. Bard, A. J., & Faulkner, L. R. (2002). Electrochemical Methods: Fundamentals and Applications. 2002: John Wiley & Sons, USA.

second edition.

47. Zoski, C. G. (Ed.). (2006). Handbook of electrochemistry. Elsevier, Holland.

48. Srivastava, R. R., Lee, J. C., Bae, M., & Kumar, V. (2019). Reclamation of tungsten from carbide scraps and spent materials. Journal of Materials Science, 54, 83-107.

49. Bhosale, S. N., Mookherjee, S., & Pardeshi, R. M. (1990). Current practices in tungsten extraction and recovery. High temperature materials and processes, 9(2-4), 147-162.

50. Lin, J.-C., J.-Y. Lin, and S.-L. Lee .(1995). Process for recovering tungsten carbide from cemented tungsten carbide scraps by selective electrolysis. Journal of Materials Science.

51. Randhawa, N. S., & Katiyar, P. K. (2020). Potentiodynamic polarization behavior and microscopic examination of tungsten carbide hard metal materials in supported ammoniacal medium. Journal of Materials Science.

52. Brown, M. E., Dollimore, D., & Galwey, A. K. (Eds.). (1980). Reactions in the solid state. Elsevier

53. Balázsi, C., & Pfeifer, J. (1999). Structure and morphology changes caused by wash treatment of tungstic acid precipitates. Solid State Ionics, 124(1-2),p. 73-81.

54. Ma, L., Zhou, X., Xu, L., Xu, X., Zhang, L., Ye, C., ... & Chen, W. (2015). Hydrothermal preparation and supercapacitive performance of flower-like WO3.H2O/reduced graphene oxide composite. Colloids and Surfaces A: Physicochemical and Engineering Aspects, 481, p.609-615.

55. Aslam, I., Farooq, M. H., Iqbal, M. W., Boddula, R., Abid, M., Ashfaq, M., & Ghani, U. (2019). Synthesis of WO3.H2O spherical particles for efficient photocatalytic properties under visible light

source. Materials Science for Energy Technologies, 2(2), p.187-193.

56. Liu, K. (Ed.). (2012). Tungsten carbide: processing and applications Elsevier, Holland.

57. Lu, Z. (2001). Synthesis of Nano-Structured Monoclinic WO3 Particles.

58. Suzuki, H., Tomita, O., Higashi, M., & Abe, R. (2017). Tungstic acids H2WO4 and H4WO5 as stable photocatalysts for water oxidation under visible light. Journal of Materials Chemistry A, 5(21), 10280-10288.

59. Hatel, R., & Baitoul, M. (2019, August). Nanostructured Tungsten Trioxide (WO3): synthesis, structural and morphological investigations. In Journal of Physics: Conference Series (Vol. 1292, No. 1, p. 012014). IOP Publishing.

60. Venables, D. S. (1995). Reduction of tungsten oxides with carbon and hydrogen (Doctoral dissertation, Rhodes University/ Grahamstown).

61. French, G. J. (1983). The Production of Tungsten Carbide and Tungsten Carbide/Cobalt Mixtures by Gas Phase Carburisation Reactions, United Kingdom).

62. Singh, H., Chatha, S. S., Sidhu, H. S., & Sharma, K. (2011). Hot-corrosion resistance of alloy and composite coatings: A review. In National Conference on Advancements and Futuristic Trends in Mechanical and Materials Engineering (Oct. 7-8, 2011).

63. Burakowski, T., & Wierzchon, T. (1998). Surface engineering of metals: principles, equipment, technologies. CRC press,USA.

64. Singla, M. K., Singh, H., & Chawla, V. (2011). Thermal sprayed CNT reinforced nanocomposite coatings–a review. J Miner Mater Charact Eng, 10(8), 726.

65. Wu, D., Yuan, Z., Liu, S., Zheng, J., Wei, X., & Zhang, C. (2020).

Recent development of corrosion factors and coating applications in biomass firing plants. Coatings, 10(10), 1001.

66. Padmavathi, G., Sarada, B. N., Shanmuganathan, S. P., Padmini, B. V., & Mohan, N. (2020). Effects of high velocity oxy fuel thermal spray coating on mechanical and tribological properties of materials–A review. Materials Today: Proceedings, 27, 2152-2157.

67. Joshi, S., & Nylen, P. (2019). Advanced coatings by thermal spray processes. Technologies, 7(4), 1-14.

68. Smith, M. F. (2007). The cold spray materials deposition process/ Woodhead Publishing, (pp. 43-61).

69. Vuoristo, P.(2014). Thermal spray coating processes, in comprehensive materials processing, 1st edition Volume 4: Coatings and films, Elsevier.

70. Zavareh, M. A., Sarhan, A. A. D. M., Zavareh, P. A., Razak, B. A., & Kakooei, S. (2017). Fundamentals and applications of thermal spray coating. Can. J. Basic Appl. Sci, 5, 1-11.

71. Curry, N. (2014). Design of thermal barrier coating systems (Doctoral dissertation, University West/ Konungariket Sverige).

72. Simunovic, K. (2010). Thermal spraying. Welding Engineering and Technology,Book Academic Collections.

73. Majumdar, J. D. (2015). Thermal and cold spraying technology in manufacturing. Handbook of Manufacturing Engineering and Technology, 2805-2850.

74. Babu, P. S., Madhavi, Y., Krishna, L. R., Sivakumar, G., Rao, D. S., & Padmanabham, G. (2020). Thermal Spray Coatings for Erosion–Corrosion Resistant Applications. Transactions of the Indian Institute of Metals, 73, 2141-2159.

75. Davis, J. R. (Ed.). (2004). Handbook of thermal spray technology.

ASM international / USA.

76. Thakare, J. G., Pandey, C., Mahapatra, M. M., & Mulik, R. S. (2021). Thermal barrier coatings—A state of the art review. Metals and Materials International, 27, 1947-1968.

77. Babiak, Z., Wenz, T., & Engl, L. (2006). Fundamentals of thermal spraying, flame and arc spraying. Modern Surface Technology, 119-136.

78. Aldosari, M. (2017). Comparative study of two nozzle assemblies for high velocity oxy fuel (HVOF) thermal spray coating process (Doctoral dissertation, Dublin City University/ Materials Science and Engineering / Ireland.).

79. Sadeghi, E., Markocsan, N., & Joshi, S. (2019). Advances in corrosion-resistant thermal spray coatings for renewable energy power plants. Part I: Effect of composition and microstructure. Journal of Thermal Spray Technology, 28, 1749-1788.

80. Kumar, R. and S. Kumar.(2018). thermal spray coating: a study. international journal of engineering sciences & research technology, 7, 2277-9655.

81. Yan, D.(2017).Application of Thermal Spray Techniques for Combatting High Temperature Corrosion of WTE Superheater Tubes, Master Thesis, Department of Earth and Environmental Engineering, Fu Foundation.

82. Kang, A. S., Singh, G., & Chawla, V. (2013). Some problems associated with thermal sprayed coatings: a review. Int J Surf Eng Mater Technol, 3(1), 10-14.

83. Fauchais, P. L., Heberlein, J. V., & Boulos, M. I. (2014). Thermal spray fundamentals: from powder to part. Springer Science & Business Media, 120-130.

84. Oksa, M., Turunen, E., Suhonen, T., Varis, T., & Hannula, S. P. (2011). Optimization and characterization of high velocity oxy-fuel sprayed coatings: techniques, materials, and applications. Coatings, 1(1), 17-52.

85. Stokes, J. (2003). Production of coated and free-standing engineering components using the HVOF (High Velocity Oxy-Fuel) process (Doctoral dissertation, Dublin City University/ Materials Science and Engineering/ Ireland).

86. Fanicchia, F., Maeder, X., Ast, J., Taylor, A. A., Guo, Y., Polyakov, M. N., ... & Axinte, D. A. (2018). Residual stress and adhesion of thermal spray coatings: Microscopic view by solidification and crystallisation analysis in the epitaxial CoNiCrAlY single splat. Materials & Design, 153, 36-46.

87. Marrocco, T. (2008). Development of improved cold spray and HVOF deposited coatings (Doctoral dissertation, University of Nottingham/UK).

88. Imeson, C. (2015). Erosion Resistance of High Velocity Oxy-Fuel WC-Co-Cr Thermal Spray Coatings/Master Thesis, University of Windsor/ Department of Mechanical, Automotive and Materials Engineering.

89. Planche, M. P., Normand, B., Liao, H., Rannou, G., & Coddet, C. (2002). Influence of HVOF spraying parameters on in-flight characteristics of Inconel 718 particles and correlation with the electrochemical behaviour of the coating. Surface and coatings technology, 157(2-3), 247-256.

90. Valarezo, A., Choi, W. B., Chi, W., Gouldstone, A., & Sampath, S. (2010). Process control and characterization of NiCr coatings by HVOF-DJ2700 system: A process map approach. Journal of thermal spray technology, 19, 852-865.

91. Verdian, M. M. (2017). finishing and post-treatment of thermal spray coatings, Springer Science, New York: 130-140.

92. Shrestha, S. K. (2000). Corrosion and erosion-corrosion of High Velocity Oxy-Fuel (HVOF) sprayed NiCrSiB coatings (Doctoral dissertation, University of Glasgow).

93. Fauchais, P., & Vardelle, A. (2001). Thermal spray coatings. Wiley Encyclopedia of Electrical and Electronics Engineering. John Wiley & Sons, USA, Fourth Edition: 220-244.

94. Fauchais, P. L., Heberlein, J. V., Boulos, M. I., Fauchais, P. L., Heberlein, J. V., & Boulos, M. I. (2014). Thermal Spray Fundamentals, John Wiley & Sons, USA, 17-72.

95. Pawlowski, L. (2008). The science and engineering of thermal spray coatings. John Wiley & Sons, USA.

96. Parker, D. S. (2003). Fracture and Residual-stress Characterization of Tungsten-carbide 17%-cobalt Thermal-spray Coatings Applied to High-strength Steel Fatigue Specimens (Doctoral dissertation, University of Florida).

97. Pratap, B., Bhatt, V., & Chaudhary, V. (2015). A review on thermal spray coating. Int J Sci Eng Res, 6(5), 53-59.

98. Krishnaiah, K., & Shahabudeen, P. (2012). Applied design of experiments and Taguchi methods. PHI Learning Pvt. Ltd..

99. Roy, R. K. (2001). Design of experiments using the Taguchi approach: 16 steps to product and process improvement. John Wiley & Sons

100. Hussain, M. Z., Khan, S., & Sarmah, P. (2020). Optimization of powder metallurgy processing parameters of Al2O3/Cu composite through Taguchi method with Grey relational analysis. Journal of King Saud University-Engineering Sciences, 32(4), 274-286.

101. Liu, S., & Forrest, J. Y. L. (2010). Grey systems: theory and applications. Springer Science & Business Media.

102. Liu, S., Yang, Y., & Forrest, J. Y. L. (2022). Grey Systems Analysis: Methods, Models and Applications. Springer

103. Haq, A. N., Marimuthu, P., & Jeyapaul, R. (2008). Multi response optimization of machining parameters of drilling Al/SiC metal matrix composite using grey relational analysis in the Taguchi method. The International Journal of Advanced Manufacturing Technology, 37, 250-255

104. Latha, T. M., & Venkatachalam, S. (1989). Electrolytic recovery of tungsten and cobalt from tungsten carbide scrap. Hydrometallurgy, 22(3), 353-361.

105. Ashrafizadeh, S. N., Bafghi, M. S., Shahbazi, R., & Hossein, M. R. (2003). Recovery of cobalt and tungsten from scrap carbide pieces through a hydrometallurgic route. Electrometallurgy and Environmental Hydrometallurgy, 2, 1605-1615.

106. Nogueira, H. I., Cavaleiro, A. M., Rocha, J., Trindade, T., & de Jesus, J. D. P. (2004). Synthesis and characterization of tungsten trioxide powders prepared from tungstic acids. Materials Research Bulletin, 39(4-5), 683-693.

107. Abdullaha, S. F., Radimanb, S., Hamidb, M. A., & Ibrahimb, N. B. (2007). Studies on the phase transitions and properties of tungsten (VI) oxide particles by X-Ray diffraction (XRD) and thermal analysis. Jurnal Fizik Malaysia, 28(1-2), 7-12.

108. Kumar, A., Singh, K., & Pandey, O. P. (2009). Reduction of WO3 to nano-WC by thermo-chemical reaction route. Physica E: Low-dimensional Systems and Nanostructures, 41(4), 677-684.

109. Ma, J., & Zhu, S. G. (2010). Direct solid-state synthesis of tungsten carbide nanoparticles from mechanically activated tungsten oxide

and graphite. International Journal of Refractory Metals and Hard Materials, 28(5), 623-627.

110. Katiyar, P. K., Randhawa, N. S., Hait, J., Jana, R. K., Singh, K. K., & Mankhand, T. R. (2014). An overview on different processes for recovery of valuable metals from tungsten carbide scrap. Hydrometallurgy, 20(2), 243-251.

111. Ahmadi, M., Sahoo, S., Younesi, R., Gaur, A. P., Katiyar, R. S., & Guinel, M. J. (2014). WO_3 nano-ribbons: their phase transformation from tungstite ($WO_3.H_2O$) to tungsten oxide (WO_3). Journal of Materials Science, 49, 5899-5909.

112. Wongsisa, S., Srichandr, P., & Poolthong, N. (2015). Development of manufacturing technology for direct recycling cemented carbide (WC-Co) tool scraps. Materials Transactions, 56(1), 70-77.

113. Xiao, X., Xi, X., Nie, Z., Zhang, L., & Ma, L. (2017). Direct electrochemical preparation of cobalt, tungsten, and tungsten carbide from cemented carbide scrap. Metallurgical and Materials Transactions B, 48, 692-700.

114. Behnami, A. K., Hoseinpur, A., Sakaki, M., Bafghi, M. S., & Yanagisawa, K. (2017). Synthesis of WC powder through microwave heating of WO_3–C mixture. International Journal of Minerals, Metallurgy, and Materials, 24, 202-207.

115. Sun, F., Chen, X., & Zhao, Z. (2018). Anodic passivation on the recycling of cemented carbide scrap by selective electro-dissolution. Waste Management, 80, 285-291.

116. Kahraman, N., & Gülenç, B. (2002). Abrasive wear behaviour of powder flame sprayed coatings on steel substrates. Materials & design, 23(8), 721-725

117. Krishna, B. V., Misra, V. N., Mukherjee, P. S., & Sharma, P. (2002). Microstructure and properties of flame sprayed tungsten carbide

coatings. International Journal of Refractory Metals and Hard Materials, 20(5-6), 355-374.

118. Nahvi, S. M., & Jafari, M. (2016). Microstructural and mechanical properties of advanced HVOF-sprayed WC-based cermet coatings. Surface and Coatings Technology, 286, 95-102.

119. Kıratlı, N. (2017). Investigation of the Wear and Hardness Behavior of ST 37 Steel Coated by the Powder Flame Spraying Method. American Scientific Research Journal for Engineering, Technology, and Sciences (ASRJETS), 31(1), 101-108.

120. Ferrer, M., Peña, G., & Rodríguez, L. F. (2019). Obtaining and characterizing of WC-Co coatings obtained from thermal spray by flame. In Journal of Physics: Conference Series (Vol. 1386, No. 1, p. 012023). IOP Publishing.

121. Matthews, S., Ansbro, J., Berndt, C. C., & Ang, A. S. M. (2021). Carbide dissolution in WC-17Co thermal spray coatings: Part 1-project concept and as-sprayed coatings. Journal of Alloys and Compounds, 856, 157464.

122. Govande, A. R., Chandak, A., Sunil, B. R., & Dumpala, R. (2022). Carbide-based thermal spray coatings: A review on performance characteristics and post-treatment. International Journal of Refractory Metals and Hard Materials, 103, 105772.

123. Bayer, R. J. (2004). Mechanical Wear Fundamentals and Testing, revised and expanded, Second Edition. CRC Press,USA,P.P:1-347.

124. Herrmann, K. (Ed.). (2011). Hardness testing: principles and applications. ASM international,USA,P.P:1-255

125. Paul, A., Laurila, T., Vuorinen, V., & Divinski, S. V. (2014). Thermodynamics, diffusion and the Kirkendall effect in solids (pp. 115-139). Cham: Springer International Publishing.

126. Magnani, M., Suegama, P. H., Espallargas, N., Dosta, S., Fugivara,

C. S., Guilemany, J. M., & Benedetti, A. V. (2008). Influence of HVOF parameters on the corrosion and wear resistance of WC-Co coatings sprayed on AA7050 T7. Surface and Coatings Technology, 202(19), 4746-4757.

127. Alam, M. S., & Das, A. K. (2022). Advancement in cermet based coating on steel substrate: A review. Materials Today: Proceedings.

128. Baik, K. H., Kim, J. H., & Seong, B. G. (2007). Improvements in hardness and wear resistance of thermally sprayed WC-Co nanocomposite coatings. Materials Science and Engineering: A, 449, 846-849.

الخلاصة

استخدمت الصناعات المعدنية الصلبة على نطاق واسع كربيد التنجستن لتصنيع لقم القطع والأجزاء عالية المقاومة للتآكل. عندما تتحول هذه الادوات والاجزاء الى سكراب ، يتم تجميعها وإعادة تدويرها. في هذه الدراسة تم إعادة تدوير لقم القطع الكاربيدية من نوع P10 للحصول على مسحوق كربيد التنجستن. تم ترسيب المسحوق الناتج كطبقة طلاء على سطح الفولاذ المقاوم للصدأ من النوع 316 لتحسين مقاومة البلى. تم تنفيذ عملية إعادة التدوير في ثلاث خطوات. الخطوة الاولى تكون عن طريق استخدام العملية الكهروكيميائية حيث تم الحصول على حمض التنكستك النقي (H_2WO_4) بهذه العملية. تمت دراسة تأثير أربع متغيرات في هذه العملية. هذه المتغيرات هي نوع الكاثود (لوح من الجرافيت والألومنيوم) ، تركيز المحلول الالكتروليتي (حمض النيتريك) ، كثافة التيار ودرجة حرارة الخلية. تم الحصول على القيم المثلى لهذه المتغيرات باستخدام تحليل ال (GRA) بناءً على طريقة Taguchi باستخدام برنامج mintab17. كانت هذه القيم كثافة تيار 4000 أمبير/ م^2، تركيز المحلول 1.8مولاري ، درجة حرارة الخلية تساوي 70 درجة مئوية وقطب الكاثود من الالمنيوم. وفقًا لهذه الحالة المثلى ، كانت النتيجة استهلاك طاقة تساوي 3.702 كيلوواط.ساعه\كغم، و فقدان الوزن\الساعة يساوي 1.350 غم\ساعة ، من حمض التنكستك (H_2WO_4) بحجم حبيبي يبلغ 11.11ميكرومتر. تم التحقق من الحمض باستخدام XRD و SEM. في الخطوة الثانية ، تم تحويل مسحوق حمض التنكستك إلى مسحوق أوكسيد التنكستن (WO_3) بحجم حبيبي يبلغ 18.38 ميكرومتر عن طريق الكلسنة عند 800 درجة مئوية. بعد ذلك ، في الخطوة الثالثة ، تم إجراء عملية الكربنة للحصول على مسحوق WC عن طريق اختزال مخلوط WO_3 مع الجرافيت بنسبة (1: 5) مول باستخدام فرن مفرغ بوجود الأركون عند درجات حرارة مختلفة (900 ، 1100 و 1200 درجة مئوية) بأوقات مختلفة (45 ، 90 ، 130 دقيقة). لإنتاج كميات نقية من كربيد التنكستن كان أفضل وقت ودرجة حرارة (1100 درجة مئويه و 135 دقيقة) على التوالي.

في هذا العمل، تم استخدام عملية الرش الحراري لترسيب خليط من كربيد التنكستن المعاد تدويره مع نسبة معروفة من الكوبالت النقي على سطح الفولاذ المقاوم للصدأ (SS316). تم الأخذ بعين الاعتبار ثلاث نسب وزنيه من الكوبالت (8 ، 12 ، 16٪) ، لكل منها ثلاث سرعات للرش (300 ، 400 و 500 م / دقيقة). تم دراسة الخصائص والسلوك الترايبولوجي لطبقة الطلاء. أشار حيود الأشعة السينية إلى وجود كمية كبيرة من كربيد التنكستن ، لكنه لم يكشف عن كميات كبيرة من أطوار (Co-W-C) الزجاجية المحتوية على الكوبالت

في الطلاءات المرشوشة ، مثل Co_6W_6C. يشير نمط الحيود أيضًا إلى حدوث الحد الأدنى من نزع الكربنة في عملية الطلاء.

طلاء الرش الحراري، الرش الحراري باللهب بشكل استثنائي، يحسن الصلادة ومقاومه البلى للمعدن. تلعب متغيرات الطلاء دورًا حيويًا في خصائص الطلاء. يمكن زيادة جودة الطلاء عن طريق اختيار متغيرات الطلاء المناسبة. المتغير الأكثر أهمية هي سرعة الجسيمات التي تؤثر بشكل مباشر على صلادة وخشونة ومقاومة البلى للطلاء. نتيجة الرش عند سرعة جسيمات (400 م/دقيقة) مع نسبة وزنية من الكوبالت تساوي (8 ، 12 و 16٪) كان للطلاء بنية متجانسة جيدة ولم تتشكل طبقة أكسدة. تتميز هذه الطبقات الثلاث بصلادة عالية (1290،1480 و 1085 كجم /ملم^2 HV) على التوالي ، وخشونة السطح (2 ، 1.9 و 1.8 ميكرومتر) على التوالي ، ولها معدل بلى أقل. تنخفض معدلات البلى المحددة للطلاءات تدريجياً مع زيادة صلادة الطلاء.

وزاره التعليم العالي والبحث العلمي

جامعة بابل

كلية هندسة المواد

قسم هندسه المعادن

تأثير مسحوق كربيد التنكستن المعاد بالعملية الكهروكيميائية على كفاءة الطلاء للتطبيقات الترايبولوجية

اطروحة

مقدمة الى قسم هندسة المعادن في كلية هندسه المواد/جامعة بابل كجزء من متطلبات نيل درجه الدكتوراه فلسفة في هندسه المواد/المعادن

من قبل

لبنى منير هادي قدوري

(بكالوريوس هندسة مواد 2012)

(ماجستير هندسة مواد 2015)

بإشراف

أ.د . حيدر عبد الحسن العذاري

2023 م　　　　1444 هـ